Control of Self-Assembly Using Multiple Modified Amyloid Peptides for Functionalized Nanowires and Nanocircuitry

Laboratory of Biological Chemistry,
Graduate School of Chemical Sciences and Engineering,
Hokkaido University

Hiroki Sakai

2013

Contents

Abbreviations

iii

Abbreviations:

AFM: atomic force microscopy

ATD: arrival time distribution

BSPP: bis(*p*-sulfonatophenyl)phenylphosphine

CD: circular dichroism

DCM: dichloromethane

DIEA: *N,N*-diisopropylethylamine

DMF: *N,N*-dimethylformamide

EDX: energy dispersive X-ray spectroscopy

EDT: ethanedithiol

ESI-MS: electrospray ionization

Fmoc: 9-fluorenylmethoxycarbonyl

HBTU: 2-(1H-benzotriazole-1-yl)-1,1,3,3-tetramethyluronium hexafluorophosphate

HFIP: 1,1,1,3,3,3-hexafluoro-2-propanol

HOBt: 1-hydroxybenzotriazole

HPLC: high performance liquid chromatography

IM-MS: ion mobility-mass spectrometry

IMS: ion mobility spectrometry

LB: Langmuir–Blodgett

LED: laser emitting diode

MALDI   matrix-assisted laser desorption/ionization

MS: mass spectrometry

NHS: *N*-hydroxysuccinimidyl ester

NMP: *N*-methyl-2-pyrrolidone

PLL: poly-L-lysine

SCAP: Structure-Controllable Amyloid Peptide

TEM: transmission electron microscopy

TFA: trifluoroacetic acid

ThT: thioflavin T

THPTA: tris(3-hydroxypropyltriazolylmethyl)amine

TIS: triisopropylsilane

TMR: tetramethylrhodamine

TOF: time-of-flight

TTR: transthyretin fragment (105-115) peptide

VLS: vapor-liquid-solid

WSCI: water soluble carbodiimide

1. General Introduction

1.1. Functionalized Nanowires

Research focus on functionalized nanowires has been exponentially increasing over the past decade because of their tremendous potential for a wide range of applications in the fields of nanotechnology, biotechnology, chemistry, physics, the life sciences, and medicine. This is because their nanosized one-dimensional geometry affords them a variety of unique and intriguing properties, for example, exceptional electrical properties (1-5), very high sensitivity (6-11), excellent catalytic activity (12-14), mutifunctionality (15-18), unprecedented integration (19-21), efficient drug delivery (22,23), and controlled cell culture (24,25). These properties make functionalized nanowires key materials for the design of devices, systems, and biological tools with novel functions.

Bottom-up approach has been a great focus for preparing functionalized nanowires since it allows assembling a wide variety of materials ranging from inorganic atoms to biomolecules into nanowire structure with divers properties (26-29). One successful bottom-up method reported to date is vapor-liquid-solid (VLS) nanowire growth, whereby nanowire crystals can be formed from a nanodroplet catalyst through a chemical vapor deposition process, yielding single-crystalline nanowires composed of metal and inorganic materials (30,31). Based on this method, Lieber and colleagues have developed strategies to create various nanowire-based devices such as field-effect transistors (32,33), *p-n* diodes (33-36), light-emitting diodes (LEDs) (37-39), and nanosensors (40). Molecular self-assembly has widely been investigated to achieve mild and cost-effective preparation of functionalized nanowires (26,27). Researchers have

1

employed organic and biomolecular building blocks containing pentacene (41,42), hexabenzocoronene (43-46), cyclic peptides (47,48), peptide amphiphiles (49,50), and amyloid peptides (51,52). Although self-assembly-based methods have successfully yielded conductive and semiconductive nanowires and nanotubes, light-harvesting nanowires, and nanowire templates for biominerals and cells, challenges remain regarding the diversity of function and, more importantly, in the control of the supramolecular architecture of the functionalized nanowires because modification of building blocks with a particular molecule for functionalization seriously alters their self-assembly. Therefore, methodologies to control the self-assembly of modified building blocks are highly required.

The bottom-up approach has also attracted attention for future manufacturing of commercial device. This is because top-down method, which includes a nanolithography process creating patterns of small objects from bulk materials to construct integrated functional systems and fabricate commercially available devices, have faced to physical and economical problems (53). A key goal for the bottom-up strategy, for this objective, is to integrate preformed nanowires into designed hierarchical structures. And, creating nanowire patterns, which provides functional nanosystems working within a device, is the first step to achieve this goal. Researchers have approached nanowire patterning by using physical and chemical forces such as hydrophilic/hydrophobic, electric, dielectric, magnetic, and fluidic forces (40,54-59). Although these approaches have been successful to some extent, they still have limitations because the array highly depends on the nanowire's ability to respond the applied forces, and the methods employed often require special instruments and setup. These limitations make it challenging and costly to assemble bottom-up nanowires into

nanodevices.

1.2. Amyloids

Amyloids are highly organized aggregates that result from self-assembly of proteins and peptides (51,60). The common feature of these biomolecular aggregates is their nanofibrillar architecture, referred to as 'amyloid fibrils', typically with micrometers long and approximately 10 nm wide (61,62). Amyloid formation and deposition of normally soluble proteins on the extracellular matrices of organs or tissues are referred as amyloidosis, which is related to numerous protein misfolding disorders such as Alzheimer's disease, prion diseases, type II diabetes, and dialysis-related amyloidosis (60,63). Thus, amyloids are among the most important therapeutic targets. In contrast, *in vitro* studies have revealed that sequentially unrelated proteins or even artificial peptides have a substantial property to form amyloid fibrils under appropriate conditions (51,52,64). Therefore, the amyloid state is thought to be a thermodynamically favorable state that all polypeptide molecules inherently possess. The supramolecular structure of the fibrils comprises a cross-β conformation in which intermolecular β sheets are aligned along the fibril axis, with the β strands oriented perpendicularly to the fibril axis through formation of a backbone hydrogen-bonding network (62). Methods based on X-ray and solid-state NMR have demonstrated an inter-strand separation of 4.7 Å and a distance between stacked β-sheets of approximately 10 Å (65). This β-sheet-rich structure with extensive intermolecular hydrogen bonds affords the fibrils high stability and mechanical strength (66-70). These attractive properties in conjunction with the availability of synthetic peptides (amyloid peptides) *in vitro* make amyloid fibrils promising materials to create functionalized

nanowires. Therefore, understanding of the mechanism of amyloid fibrillation is of great interest to identify effective approaches for the development of nanomaterials and for therapeutic strategies.

A prevailing model of amyloid self-assembly is shown in Figure 1-1 and consists of two phases: nucleation, and elongation. Elongation and maturation usually concurrently take place and are indistinguishable by traditional kinetic assays such as ThT. Thus, these two steps are often considered as a single step, i.e., only the elongation step). Nucleation is a rate-determining step, before which monomer and globular oligomers containing a variable number of peptides coexist in equilibrium. Some oligomers can be present as stable soluble species and have been hypothesized to convert into the nucleus of amyloid fibril formation; for example, the Aβ(1-42) peptide forms a stable dodecamer that would be a terminal species towards nucleation (71,72). The elongation phase starts when a critical number of nuclei form. In this phase the nucleus serves as a template onto which monomer peptides accrete by undergoing a conformational transition with subsequent exposure of the interactive domains for fibril growth. Successive addition of monomers takes place for assembly into a 'protofibril', which is metastable prefibrillar intermediate with a short and flexible filamentous morphology and a typical length of a few hundred nanometers. This intermediate species has been demonstrated to adopt a partially unfolded β conformation (73). Accumulating evidence suggests that the stable globular oligomers and protofibrils are primary cytotoxic species that cause cellular damage or cell death (74,75). The protofibrils subsequently assemble into 'mature fibril' by associating with one another and through further addition of monomers. The mature fibril is a terminal species of fibrillation and has a relatively straight and twisted structure. Some morphological
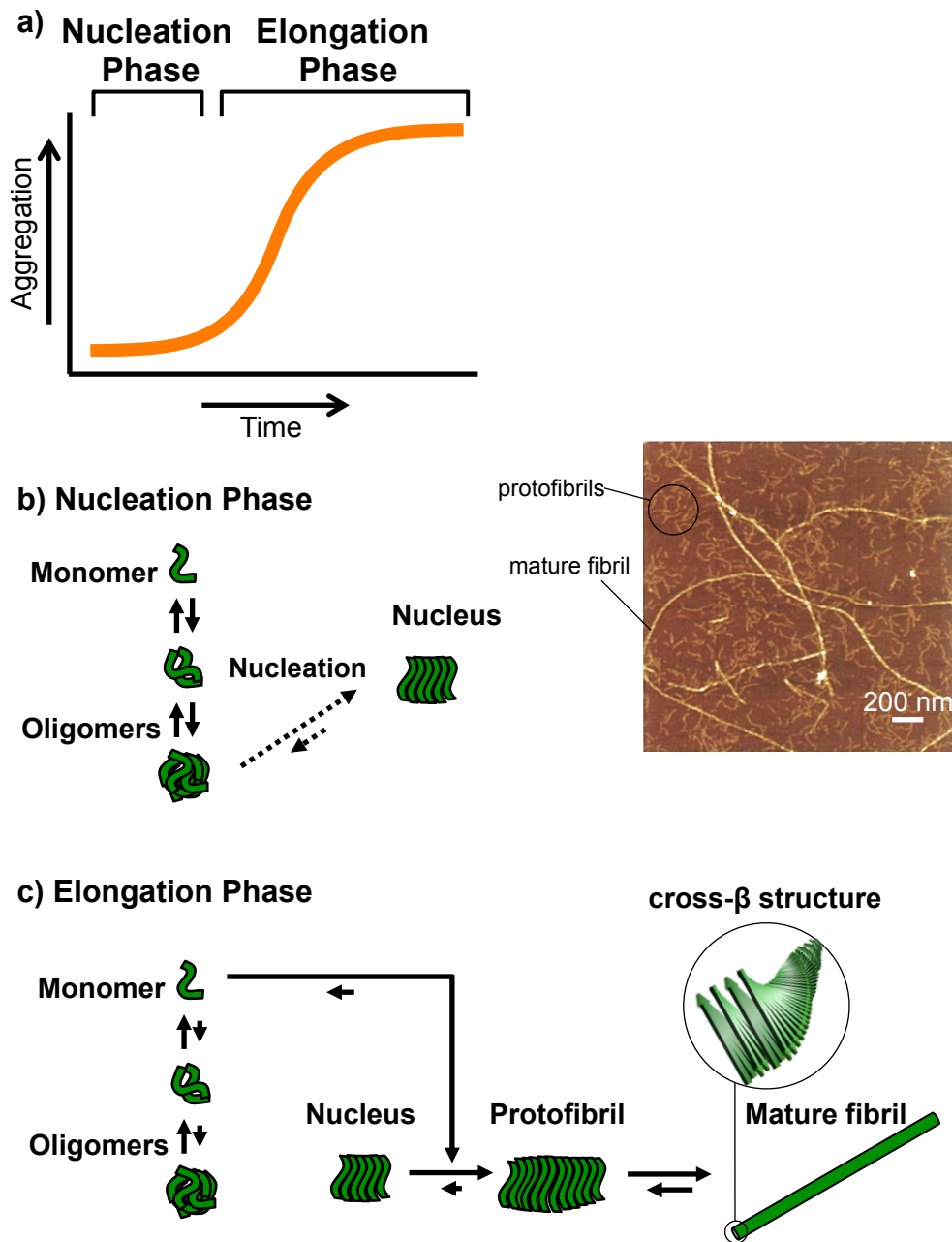
Figure 1-1. General model of amyloid fibrillation comprising two phases: nucleation and elongation (a). In the nucleation phase (b), peptide monomers are in equilibrium with their oligomers with globular structure, wherein certain oligomers can exist in a stable conformation. Elongation phase (c) starts coincident with the emergence of a certain number of nuclei. In this phase, the peptide monomer, not oligomer, assemble into protofibrils by addition to the nucleus and the growing protofibril ends. The protofibrils then further assemble into mature fibril through continuous monomer addition and tangling together with conformational rearrangement to form a characteristic cross-β structure. (inset) An AFM image of protofibrils and mature fibrils formed from Aβ(1-40) peptide (76).

5

differences, such as periodicity and the number of filaments comprising a single fibril, are normally observed; this variability is termed as polymorphism (61,76).

Although many cases can be explained using this model, emerging evidence suggests that some fibrillation systems involve other additional pathways such as secondary nucleation (77,78), which is a process where assembly-dependent nucleation takes place because of the creation of additional reaction sites for monomer addition based on the interaction of monomers with the fibril surface (surface-catalyzed nucleation) or fibril breakage (79). Therefore, it is still challenging to understand amyloid self-assembly and control fibril architecture.

1.3. Ion Mobility-Mass Spectrometry

Ion mobility-mass spectrometry (IM-MS) is an analytical technique allowing simultaneous measurements of the mass and shape of analytes based on mass spectrometry coupled to ion mobility spectrometry, which enables shape-dependent separation of ions. This hybrid method was first introduced by Kebarle and Hogg in 1965 (80,81) and has been developed over the past 40 years. In addition to the progress of soft ionization techniques, the quadrupole-coupled ion mobility instrument developed by Wyttenbach, Kemper, and Bowers (82) has opened up enormous opportunities to structurally study an impressive range of biomolecules and biomolecular complexes including self-assembling peptides (72,83-87).

Figure 1-2 represents an overview of the IM-MS instrument, which is mainly composed of a nanoESI source, an ion storage component, a drift cell, a quadrupole mass analyzer, and a detector (82). Peptide or protein samples are first electrosprayed from the nanoESI capillary under mild conditions in which peptide or protein ions can
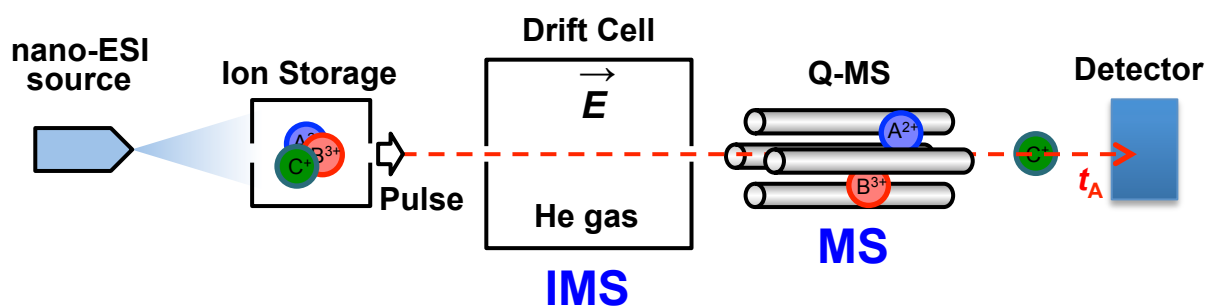
Figure 1-2. Schematic illustration of a general IM-MS instrument (82). Ions electrosprayed from the nano-ESI capillary are stored and pulsed into the drift cell for ion mobility spectrometry (IMS) and subsequently selected by mass in the quadrupole for detection of the arrival time (t_A) of particular ions.

retain their solution structure even in the gas phase (88). The ions are subsequently pulsed from the ion storage component into the drift cell, into which a buffer gas (normally helium) is injected and a weak electric field is applied. Thus, the ions experience both acceleration from the electric field and deceleration due to collisions with the buffer gas, and they consequently pass through the cell with a constant velocity determined by the balance of these two forces. Ions with the same mass-to-charge ratio but different structure can be separated according to drift time based only on collision frequency. The size of the ions is quantitatively described according to the collision cross section between the ion and the buffer gas, which is proportional to the drift time. The quadrupole mass filter enables the selection of ions with a particular mass-to-charge ratio and detection of drift time for mass-selected species. This equipment allows a selective structural analysis of particular species in solution, even if they are present at a very low level, which makes IM-MS a powerful tool to study self-assembly.

Employing IM-MS, Bowers and coworkers have successfully characterized the oligomerization process of various amyloid peptides including amyloid β, human IAPP, and prion fragments over the last five years (83,85,89-92). Furthermore, the ability of IM-MS to identify specific inhibitors for amyloid formation of these peptides (93) demonstrates that oligomerization properties revealed by IM-MS are actually related to the bulk fibrillation features.

1.4. Biomineralization

Biomineralization is the process by which living organisms produce minerals in tissues in a well-controlled and selective manner (94-96). This process is generally controlled by the primary sequence and/or three-dimensional structure of proteins,

which possess a crystallographic recognition capability that defines the composition, order, and direction of the inorganic materials produced. Recent phage display-based studies have successfully identified a series of peptide sequences with high affinity to specific inorganic materials (Table 1-1) (97), which has opened up new strategies to control and design the nanostructure of inorganic nanoparticles (98,99). Given its peptidic nature and compatibility with various chemical and synthetic procedures, biomineralization could be a practical approach to control nanoparticle shape and also hierarchical 1D, 2D, and 3D nanostructures.

1.5. Aims

In the current study, I aimed to 1) develop a methodology to control the self-assembly of amyloid peptides that allows not only modulation of the fibril architecture but also effective formation of modified amyloid fibrils for use as functionalized nanowires, 2) determine the structure-modulation mechanism based on studies of oligomerization and fibrillation using IM-MS and AFM, and 3) develop approaches to construct nanowire patterns. Throughout the study I employed the mixtures of our designed amyloid peptides, termed as structure-controllable amyloid peptides (SCAPs), which have a three-amino-acid-residue unit at the N-terminus to control or modulate fibrillation and fibril architecture. The combination of fibril modification with biomineralization could expand the application of our strategy to inorganic nanowire systems, such as nanoelectronics. The straightforward functionalization, control mechanism, and nanowire patterning would shed new light on the field of bottom-up functionalized nanowires and nanomaterials.

Table 1-1. Specific biomineralization sequences for inorganic materials reported in (97).

Mater.	Sequence	Mater.	Sequence	Mater.	Sequence
Au	MHGKTQATSGTIQS		AYSSGAPPMPPF	ZnO	YDSRSMRPH
		Ag	NPSSLFRYLPSD		
	DRTSTWR		SLATQPPRTPPV	CaCO$_3$	HTQNMRMYEPWF
Pt	QSVTSTK				DVFSSFNLKHMR
	SSSHLNK		MSPHPHPRHHHT		
		SiO$_2$	RGRRRLSCRLL	Cr$_2$O$_3$	VVRPKAATN
	SVTQNKY		KPSHHHHHTGAN		RIRHRLVGQ
Pd	SPHPGPY				
	HAPTPML		AQNPSDNNTHTH	Fe$_2$O$_3$	RRTVKHHVN
		GaAs	RLELAIPLQGSG		
Zeolites	MDHGKYRQKQATPG		TPPRPIQYNHTS	ZnS	NNPMHQN

10

2. Formation of Functionalized Nanowires Based on Control of Self-Assembly Using Structure-Controllable Amyloid Peptides

2.1. Abstract

Amyloid peptides have great potential as building blocks in the creation of functional nanowires because of their natural ability to self-assemble into nanofibrillar structures and because they can be easily modified with various functional groups. However, extensive modification of an amyloid peptide generally alters its self-assembly property, making it difficult to construct functionalized fibrils with a desired structure and function. In this study, we demonstrate an effective method to overcome this problem by using our structure-controllable amyloid peptides (SCAPs) terminated with a three-amino-acid-residue cap. The method consists of mixing two or more structurally related amyloid peptides with a fraction of modified SCAPs that co-assemble into a fibril. This SCAP-mixing method provides remarkable control of self-assembly and reproducibly forms extremely long and homogeneous fibrils regardless of the presence of modified amyloid peptides. Furthermore, we show that the modified peptides embedded in the resulting fibril can subsequently be functionalized to generate nanowires with the desired properties, thus highlighting the importance of our SCAP method for nanotechnology applications.

11

2.2. Introduction

Functionalized nanowires possess unique properties that make them valuable materials for the design of next-generation devices but also systems with never before seen functions. Adding functional groups to nanowires allows mixing of the structural and electrical properties of nanowires with the recognition or catalytic properties of biomolecules. These added properties give these materials great potential in nanoelectronic applications as novel sensors, field-effect transistors, photodiodes, and LEDs (1-7), creating a high demand for this nanoscale material.

One practical approach to create these functionalized nanowires is to use the bottom-up strategy, which consists of assembling molecular building blocks into a variety of functionalized nanostructures. Several materials such as peptide amphiphiles, carbon, and DNA have been identified as building block candidates to make nanowires (5-9). However, despite their ability to successfully form fibrils, these materials are very limited in the type of functional nanowires they can form, or they require complicated synthetic procedures. Therefore, attention has been focused on the use of amyloid peptides as building blocks since, not only they can naturally self-assemble into uni-dimensional fibrils of exceptional stability and mechanical strength (10-20), but given their peptidic nature, it is easy to assign them various functionalities with rather simple engineering techniques.

The most common problem when making fibrils from amyloid peptide building blocks is the difficulty in controlling the structure of the resulting fibrils (for example the length, height, and homogeneity of the ensemble), especially when functionalized amyloid building blocks are employed because the modification of amyloid peptides seriously alters their self-assembling property (21). This fact highlights the importance

of developing effective methodologies to control the self-assembly of modified amyloid building blocks.

Recently, we demonstrated that the attachment of a three-amino-acid-residue unit to the N-terminus of amyloid peptides drastically affects their self-assembly (22). These peptides can accelerate fibril formation but also can yield fibrils with various architectures depending on the properties of attached amino acids. Therefore, the added N-terminus of the SCAPs offers an additional binding interface that helps to stabilize self-assembly. Furthermore, in natural systems, interactions among multiple amino acid residues support folding or stabilization of protein structures, which suggests that employing two or more SCAPs as a mixture would allow effective control of fibril formation and structure. This would also make it possible to introduce functional molecules to the building blocks without any disruption of fibril formation.

In this study, we describe an efficient and straightforward way to control the self-assembly of peptides by mixing multiple SCAPs and also present a method to make functionalized nanowires (shown schematically in Figure 2-1) (23). Mixing of multiple SCAPs allowed effective control of fibril formation. We also show that modification of one of the SCAPs in the mixture does not disrupt the structure or the self-assembly of the fibrils and yields modified nanowires containing functional or probe molecules. We were further able to functionalize the probed nanowires with probe-specific nanomaterials.
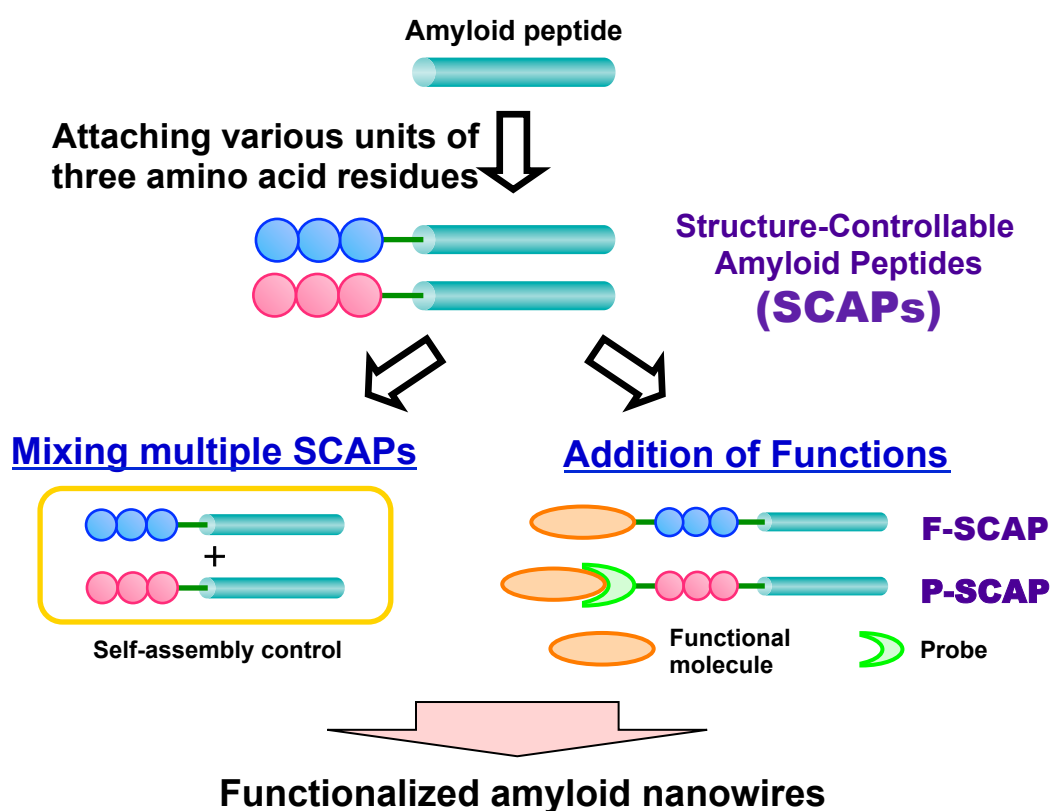
Figure 2-1. Schematic picture of our strategy for forming a wide variety of functionalized amyloid nanowires. Mixing multiple SCAPs containing two different units controls the self-assembly of amyloid peptides. When functionalized SCAPs (F-SCAP) or probed SCAPs (P-SCAPs), which have a functional or probe moiety, respectively, at the N-terminus, are added to the SCAP mixture, nanowires form with the attached molecules embedded. Many types of molecules can be incorporated into the fibrils. The probed nanowires can be subsequently functionalized by associating the corresponding functional materials with the nanowires via specific interaction with the probe.

2.3. Experimental Procedures

Peptide Synthesis

Peptides (Table 2-1) were synthesized with a standard Fmoc-chemistry on Rink amide resin automatically with an Applied Biosystems 433A peptide synthesizer (Applied Biosystems Inc., Foster City, CA) or manually. All N-terminal modifications, biotin, α-lipoic acid, maleimide, azide, tetramethylrhodamine, fluorescein, and aminomethylcoumarine, were carried out on the resins. Biotin or α-lipoic acid was coupled by the use of 10 eq. D-Biotin (Sigma) or DL-α-lipoic acid (Watanabe Chem.), 10 eq. HBTU/HOBt, and 20 eq. DIEA in NMP for 1 h or 30 min, respectively. Maleimide coupling was performed with a mixture of 2 eq. 3-maleimidopropionic acid (*N*-maleoyl-β-alanine, Aldrich), and 1 eq. WSCI in DMF/DCM = 1/1, for 1 h. The azide group was conjugated with a mixture containing 4 eq. 5-azidopentanoic acid (Aldrich), 4 eq. HBTU and HOBt, and 8 eq. DIEA in NMP for 2 h. For fluorescent modifications, the N-terminal-free peptide resins were washed once using 2 M DIEA in NMP and twice with NMP prior to coupling. Fluorescein and tetramethylrhodamine were coupled with 1.2 eq. NHS-Fluorescein (Pierce) and NHS-Rhodamine (Pierce) for 12 h, respectively. The conjugation of aminomethylcoumarine was conducted using a mixture of 1.2 eq. 7-amino-4-methyl-3-coumarinylacetic acid (Aldrich), 1.2 eq. HBTU/HOBt and 2.4 eq. DIEA for 30 min. The peptides, except for maleimide-, azide- and alkyne-containing peptides, were then deprotected and cleaved with reagent K (TFA/H$_2$O/phenol/thioanisole/ethaneditiol = 82.5/5/5/5/2.5) over two-hour incubation to yield crude peptide materials. The cleavage of maleimide-, azide- and alkyne-modified peptides were performed treated with TFA/H$_2$O = 95/5 for 2 h, TFA/H$_2$O/EDT =

95/2.5/2.5 for 2 h, and TFA/phenol/TIS = 85/10/5 for 90 min, respectively. All crude materials were subsequently purified using a reverse-phase HPLC (SCL-10A, SPD-10A, DGU-12A, LC-6AD, Shimadzu) with a C-8 column (22 x 250 mm, Cat. No. 208TP1022, Vydac) eluted with a linear gradient of water and acetonitrile containing 0.05 or 0.04% TFA, respectively. The peptides were obtained in ≥95% purity determined by reverse-phase HPLC (PU-980, UV-970, HG-980-31, DG-980-50, Jasco) with a C8 column (4.6 x 250 mm, Cat. No. 208TP104, Vydac), and were identified by MALDI-TOF-MS (voyager System 6171, Applied Biosystems, in Stractural Chemistry Laboratory or at the OPEN FACILITY in Sousei Hall) (Table 2-2). To obtain a cyclic peptide with a disulfide link, the purified peptide was incubated in 20% DMSO/H_2O for 1 day, followed by lyophilized and further purified by HPLC. The cyclic peptide was finally obtained with >99% purity assessed by HPLC and Ellman's reagent.

Fibril Formation

All peptides were initially dissolved at a concentration of 8 mM into HFIP to make stock solutions. The stock solution of each peptide mixture was prepared by mixing the stock solutions of respective single peptides. To initiate fibril formation, each stock solution was diluted by a factor of 40 in aqueous solution at pH 2.0 (adjusted with a small amount of hydrochloric acid), and incubated in plastic tubes at 37 °C. To observe the fibril formation 5 μl aliquots of samples incubated for 1, 2, and 4 days were deposited on fleshly cleaved mica (Cat. No. 990066, Nilako) for 5 min, followed by washed three times with 1 mL of water, dried in air and subsequently observed by AFM. Samples that showed no fibril formation after 4-day incubation were incubated further (8 and 16 days).

Table 2-1. Peptide Sequences

Peptide	Sequence
TTR(105−115)	H-YTIAALLSPYS-NH$_2$
E$_3$-TTR	H-EEE-GG-YTIAALLSPYS-NH$_2$
K$_3$-TTR	H-KKK-GG-YTIAALLSPYS-NH$_2$
TMR-E$_3$-TTR	*TAMRA*-GG-EEE-GG-YTIAALLSPYS-NH$_2$
Bio-E$_3$-TTR	Biotin-(ε-Aca)$_2$-EEE-GG-YTIAALLSPYS-NH$_2$
Lip-E$_3$-TTR	α-Lipoyl-EEE-GG-YTIAALLSPYS-NH$_2$
Lip-K$_3$-TTR	α-Lipoyl-KKK-GG-YTIAALLSPYS-NH$_2$
Mal-E$_3$-TTR	Maleimide-(CH$_2$)$_2$-CO-EEE-GG-YTIAALLSPYS-NH$_2$
Azd-E$_3$-TTR	Azide-(CH$_2$)$_4$-CO-EEE-GG-YTIAALLSPYS-NH$_2$
F-TBP-Cys	*FAM*-G-RKLPDA-GG-C-NH$_2$
AMC-cCN225-Alk	*AMCA*-GG-CGPRHTDGLRRIAARPGC-GGG(propargyl)-NH$_2$

Table 2-2. Identification of peptides by MALDI TOF-MS.

Peptide	Theoretical	Observed
TTR(105−115)	1197.7 [M+H]$^+$	1197.9
E$_3$-TTR	1698.8 [M+H]$^+$	1698.9
K$_3$-TTR	1696.0 [M+H]$^+$	1696.9
TMR-E$_3$-TTR	2226.4 [M]$^+$	2225.6
Bio-E$_3$-TTR	2173.1 [M+Na]$^+$	2172.8
Lip-E$_3$-TTR	1911.2 [M+Na]$^+$	1910.7
Lip-K$_3$-TTR	1885.0 [M+H]$^+$	1885.6
Mal-E$_3$-TTR	1873.0 [M+Na]$^+$	1873.2
Azd-E$_3$-TTR	1845.9 [M+Na]$^+$	1846.0
F-TBP-Cys	1330.6 [M+H]$^+$	1331.6
AMC-cCN225-Alk	2472.8 [M+H]$^+$	2472.9

Arrangement of Functional Materials onto Probed Nanowires

Probed fibrils were first adsorbed on a substrate surface of mica or cover glass (Micro Cover Glass 22 × 32 mm, Matsunami Glass, Osaka, Japan) by incubating 10 μl of 20-fold diluted samples, followed by washing (1 mL x 3 water). All surface were dried in air except for biotin-probed samples. 10 μl of reaction mixture containing 5-fold diluted avidin magnetic beads (MACS, Cat. No. 130-048-102, Miltenyi Biotec), 5-fold concentrated gold nanoparticles (Colloidal gold/SC ϕ = 15 nm, Lot No. A070515-2C, Tanaka Kikinzoku Kogyo, Japan), and 10 μM F-TBP-Cys with 10 mM phosphate (pH 7.4) was subsequently incubated on the surface for 15, 1, and 10 min, respectively. Modification of biotin-probed nanowires was carried out on a shaker. After incubation, the surface was washed three times with 1 mL of ultra-pure water and dried in air. The functionalization of azide-probed nanowires through click chemistry was initiated by mixing equivolume fibril suspension and a solutions of peptide alkyne, yielding a final concentration of 10 μM AMC-cCN225-Alk, 100 μM CuI (Wako), 500 μM THPTA (Aldrich), 5 mM HCl, in a plastic tube. After incubated for an hour, the reaction mixture was diluted 20-fold with 10 mM HCl, then dropped on a cover glass for 5 min. The surface was subsequently washed by immersing the glass in 0.1 mM HCl (pH 4) for 15 sec, followed by rinsing three times with 1 mL of water.

Biomineralization on Fibrils

For titania biomineralization, a polymer-coated Cu grid (High resolution carbon substrate, carbon thickness <15 nm, STEM 100-Cu grids, Okenshoji, Tokyo, Japan), on which F-TBP-Cys-conjugated fibrils had been deposited, was immersed in a solution of

20 mM K_2TiF_6 containing 10 mM sodium phosphate (pH 7.4) for 2 h. After mineralization, the grid was washed by immersing in ultra-pure water for 30 sec.

Atomic Force Microscopy

AFM measurements were performed in the tapping mode in air using a Nanoscope IIIa system (Digital Instruments, Santa Barbara, CA) or PicoScan 2500 (Molecular Imaging) with a standard silicon cantilever (OMCL-AC240TS, Olympus). Images were acquired at 512 × 512 pixel resolution at a standard scan rate of 0.25 Hz with a typical condition of 60-80 kHz of drive frequency, and 1.6-1.8 V of amplitude set point.

Fluorescence Microscopy

Fluorescence microscopy was performed using a BIOREVO BZ-9000 confocal microscope (Keyence) with a DAPI-BP filter (excitation, 360±40 nm; emission, 467.5±50 nm; dichroic, 409 nm long pass), a GFP-BP filter (excitation, 470±40 nm; emission, 520±35 nm; dichroic, 495 nm long pass), or a TRITC filter (excitation, 540±25 nm; emission, 605±55 nm; dichroic, 565 nm long pass). Shutter speed was set at 5.0 sec for blue, 3.5 sec for green, and 1.0 sec for red fluorescence.

Electron Microscopy

Transmission electron microscopy equipped with energy dispersive X-ray spectroscopy was conducted using an HD-2000 ultra-thin film evaluation system (Hitachi, at the OPEN FACILITY, Sousei Hall).

2.4. Results

2.4.1. Fibril Formation of Individual TTR(105-115)-Based SCAPs

Two types of SCAPs were synthesized by adding three amino acids to the N-terminus of the TTR(105–115) amyloidogenic fragment of transthyretin (24,25): one with a triple lysine (K_3-TTR) and the other with a triple glutamic acid (E_3-TTR). When these two SCAPs and the unmodified TTR(105–115) peptide were incubated individually in acidic water at pH 2.0 as described elsewhere (25-27), only E_3-TTR was able to form fibrils of several micrometers long with a height of 4.56 ± 0.45 nm, which is typical of amyloid fibrils (Figure 2-2). This enhanced fibrillation of E_3-SCAP was also observed previously for another amyloidogenic sequence, Aβ(10–35) (22). Therefore, addition of three-amino-acid residue units functions similarly for different amyloid peptides, thus showing the versatility of our SCAP strategy.

2.4.2. Extremely Long Nanofibrils Formed by Mixing Multiple SCAPs

Interestingly, mixing of K_3-TTR and E_3-TTR at a 1:1 molar ratio resulted in the formation of extremely long fibrils well over 40 μm long and 5.11 ± 0.69 nm high (Figure 2-3a). These very long fibrils, to my knowledge, have the highest aspect ratio (length/thickness >8,000) to date, and therefore can be useful as nanowire templates. This dramatic difference in fibrillation suggests that mixing SCAPs can provide particular self-assembling properties to peptides. Another mixture of 1:9 K_3-TTR and E_3-TTR also formed very long fibrils (Figure 2-3b), which demonstrates that simple mixing of K_3-TTR with E_3-TTR allows the fibrillation of peptides to be controlled. A 9:1 mixture, in contrast, did not form any fibrils (Figure 2-3c), presumably because of
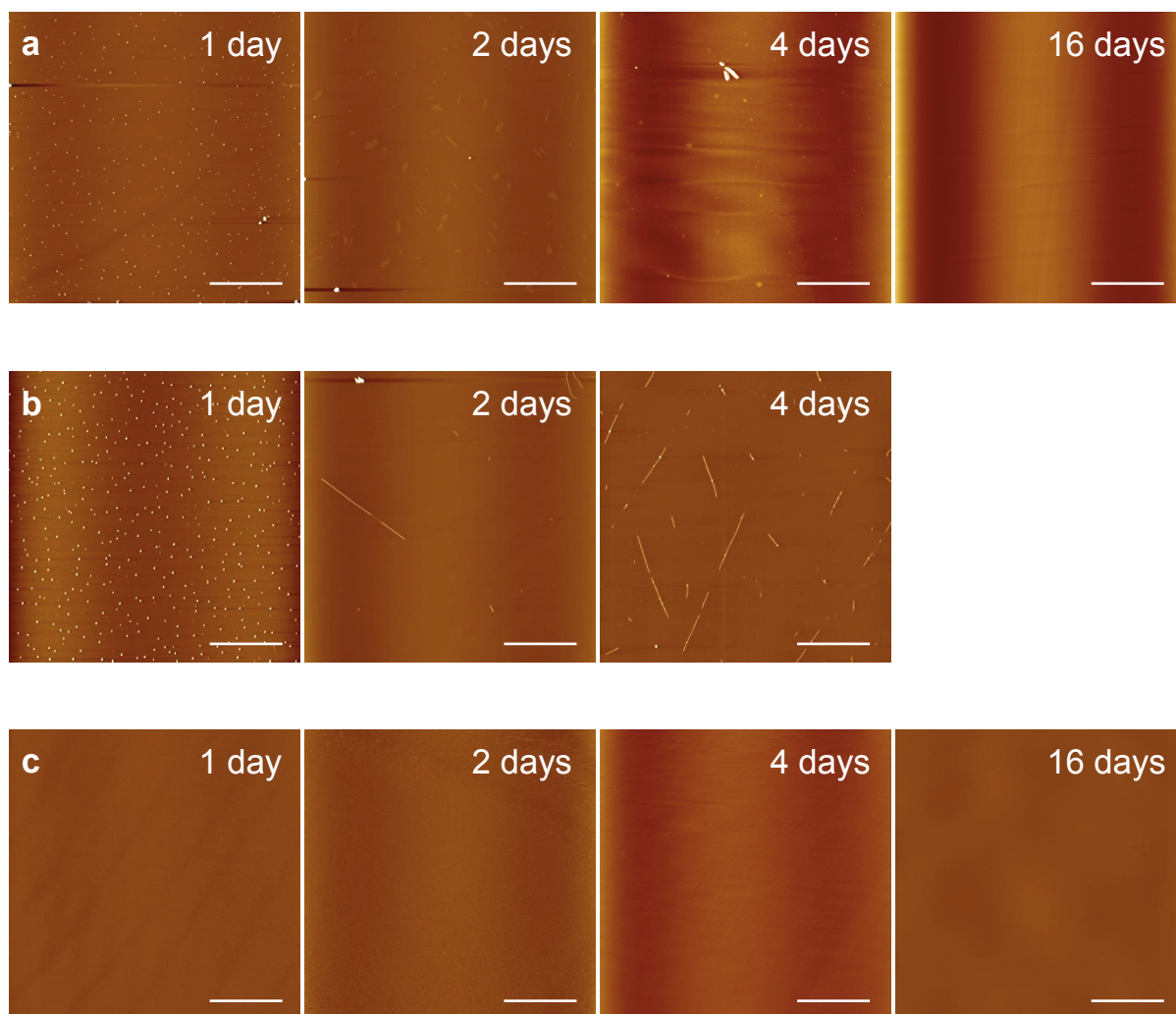
Figure 2-2. AFM images of fibril formation of (a) native TTR(105-115) peptide and TTR-based SCAPs, (b) E_3-TTR and (c) K_3-TTR. Scale bar represents 5 μm.
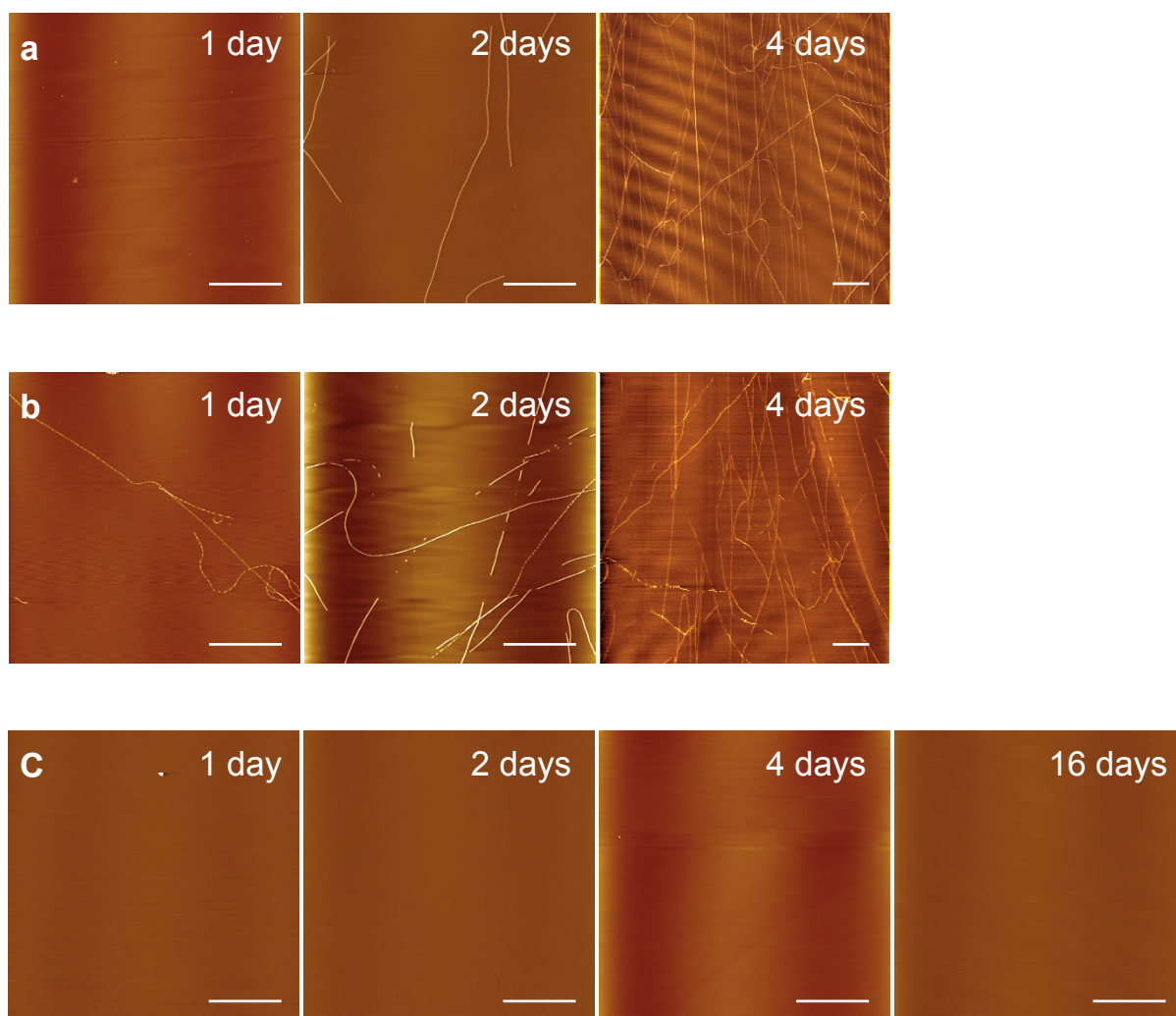
Figure 2-3. Fibril formation of mixed SCAPs, (a) 1:1, (b) 1:9 and (c) 9:1 mixtures of K$_3$-TTR:E$_3$-TTR. Scale bar shows 5 μm.

the small population of E_3-TTR species that is required for nucleation (Figure 2-2).

2.4.3. Control of the Formation of Modified Amyloid Fibrils with Various Molecules Using Functionalized/Probed SCAPs

Control of the self-assembly of modified amyloid building blocks using a functional molecule is of great interest. Mixing SCAPs during self-assembly would allow control of fibril formation in the presence of modified peptides. We synthesized two types of functionally modified SCAPs: one was functionalized SCAP (F-SCAP) terminated with a functional molecule for direct assembly of functionalized nanowires (Figure 2-4a). The other type of SCAP was probed SCAP (P-SCAP) capped at the N-terminus with a probe molecule that has the ability to specifically recruit functional nanomaterials (Figure 2-4b). The use of P-SCAPs enables the formation of probed nanowires that can be functionalized after fibrillization. We here synthesized one F-SCAP and four P-SCAPs with tetramethylrhodamine, biotin, α-lipoyl, maleimide, and azide groups (Figure 2-4). These probes have specific binding properties to avidin protein, gold, thiol, and alkyne materials, respectively. These modified SCAPs were termed as TMR-E_3-TTR, Bio-E_3-TTR, Lip-K_3-TTR, Mal-E_3-TTR, and Azd-E_3-TTR, respectively (Table 2-1).

A series of fibril formation using Bio-E_3-TTR can be seen in Figure 2-5. Bio-E_3-TTR formed no fibrils by itself or even under mixing with E_3-TTR at a ratio of Bio-E_3-TTR:E_3-TTR = 1:9 (Figure 2-5 a and b), which demonstrates the serious inhibitory effect of the biotin moiety on fibrillation. As expected, however, the addition of K_3-TTR at a ratio of K_3-TTR:Bio-E_3-TTR:E_3-TTR = 5:1:4 (yielding a ratio of K_3:E_3 = 1:1) allowed fibril formation (Figure 2-5c). Fibrils were also formed from a mixture

a) F-SCAP

Functional molecule

> *Functional molecule*
>
> **tetramethylrhodamine**
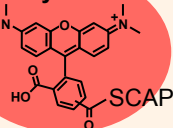
b) P-SCAP

Functional material   **Probe**
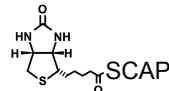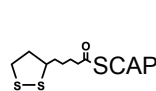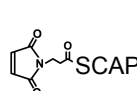
> *Probes*
>
> **biotin**   **α-lipoic acid**   **maleimide**   **azide**
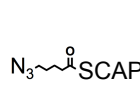
Specificity

> *Functional materials*
>
> **avidin protein**   **gold**   **thiol**   **alkyne**
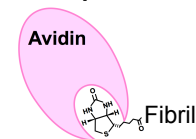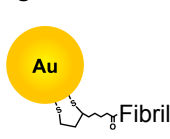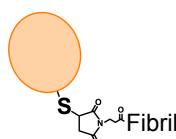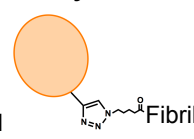
Figure 2-4. Schematic illustration of (a) F-SCAP and (b) P-SCAP. Various molecules, i.e. tetramethylrhodamine as a functional molecule and biotin, α-lipoic acid, maleimide, and azide as probes, were coupled to the N-terminus of SCAP to yield the F/P-SCAPs.
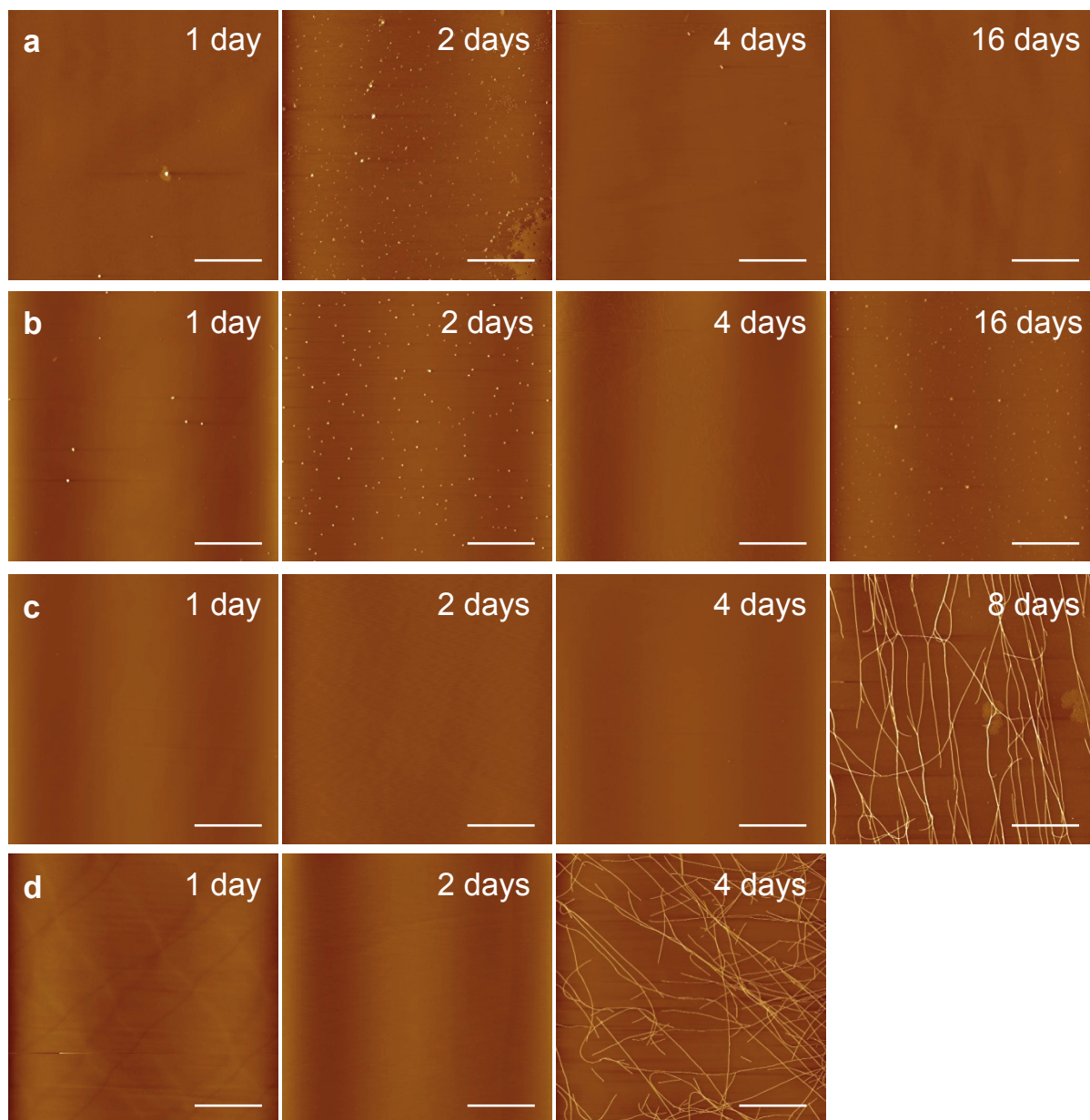
Figure 2-5. Formation of biotin-probed nanowires by mixing SCAPs. (a) Bio-E$_3$-TTR, (b) Bio-E$_3$-TTR:E$_3$-TTR = 1:9, (c) K$_3$-TTR:Bio-E$_3$-TTR:E$_3$-TTR = 5:1:4, and (d) K$_3$-TTR:Bio-E$_3$-TTR:E$_3$-TTR = 1:1:8. Scale bar represents 5 μm.

of K_3-TTR:Bio-E_3-TTR:E_3-TTR = 1:1:8 (to give a 1:9 ratio for K_3 to E_3) (Figure 2-5d).

These results clearly show that mixing multiple SCAPs provides fine control for the

self-assembly of modified amyloid peptides. In addition, these fibrils possessed a

similar morphology to that of fibrils of mixtures without Bio-E_3-TTR (Figure 2-3).

Therefore, the same major control mechanism must underlie the fibrillation of both

probed and probe-free fibrils, which could be a consequence of K_3-E_3 interaction.

When F-SCAP and other P-SCAPs were utilized, mixing of multiple SCAPs also

resulted in effective fibril formation. Long fibrils were observed in all samples of

K_3-TTR:TMR-E_3-TTR:E_3-TTR = 1:1:8, K_3-TTR:Lip-K_3-TTR:E_3-TTR = 1:1:2,

K_3-TTR:Mal-E_3-TTR:E_3-TTR = 5:1:4, K_3-TTR:Azd-E_3-TTR:E_3-TTR = 5:1:4, and

(Figures 2-6), although these F/P-SCAPs themselves formed seriously disrupted fibrils

(Figure 2-7a) or no fibrils (Figures 2-7 b-d). Therefore, our SCAP-mixing method has

wide versatility for assembling modified amyloid nanowires.

Figure 2-8 summarizes the formation of functionalized/probed nanowires at

various mixing ratios for F/P-SCAPs with a K_3 or E_3 unit. A ratio of K_3:E_3 = 1:1

allowed nanowire formation at the highest proportion (50%) of F/P-SCAPs displayed as

green area. Thus, an overall ratio of K_3:E_3 = 1:1 is a simple but the best condition to

yield functionalized/probed nanowires.

2.4.4. Straightforward Formation of Functionalized Nanowires

The F-SCAP-based nanowires functionalized directly with tetramethylrhodamine

showed characteristic red fluorescence under fluorescence microscopy (Figure 2-9a).

The fluorescence showed uniform distribution on the nanowires. Thus, the

TMR-E_3-TTR had actually and constantly been coassembled with K_3-TTR and E_3-TTR.
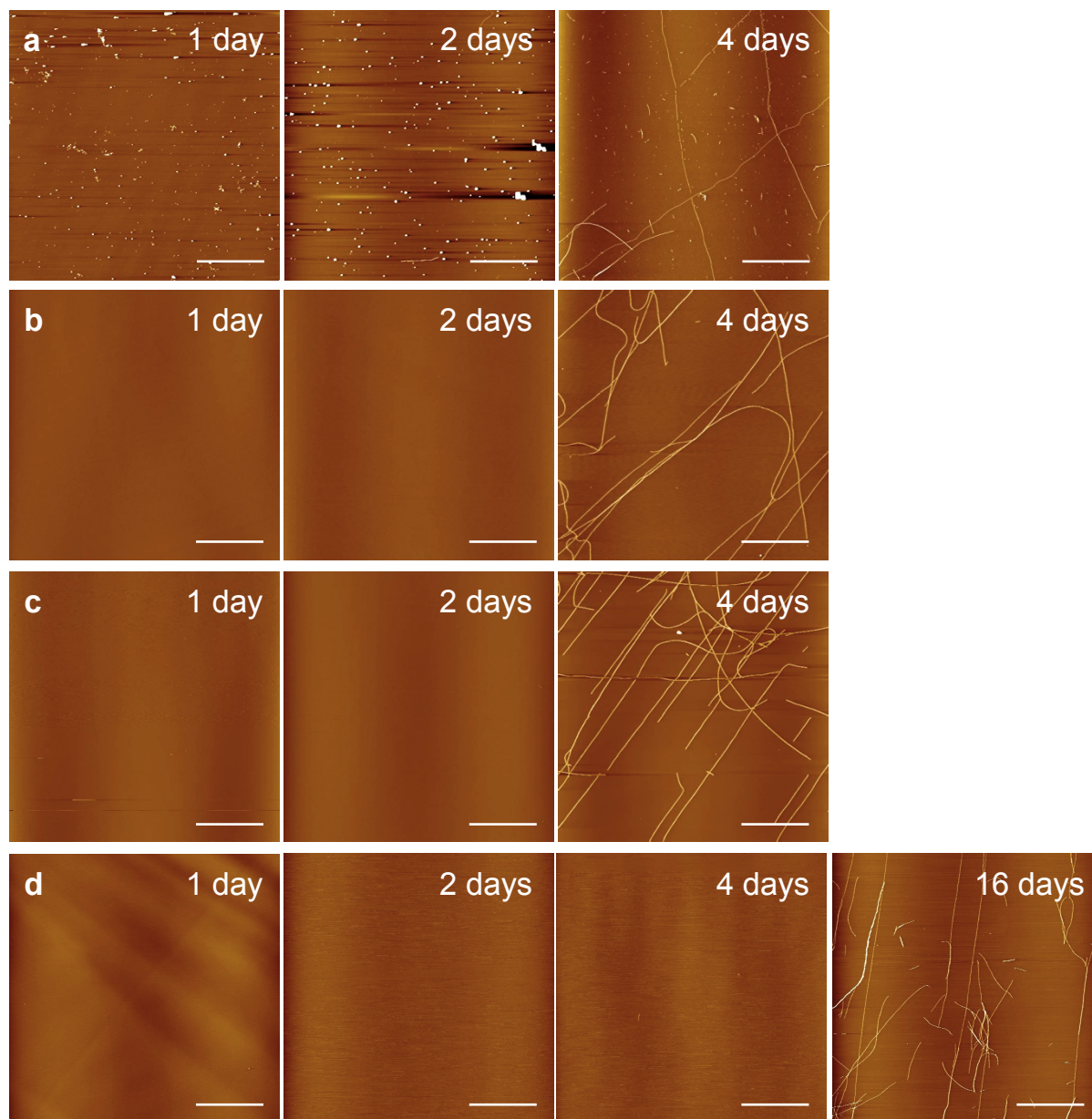
Figure 2-6. Formation of functionalized and probed nanowires by mixing F/P-SCAP with multiple SCAPs. (a) K_3-TTR:TMR-E_3-TTR:E_3-TTR = 1:1:8, (b) K_3-TTR:Lip-K_3-TTR:E_3-TTR = 1:1:2, (c) K_3-TTR:Mal-E_3-TTR:E_3-TTR = 5:1:4, and (d) K_3-TTR:Azd-E_3-TTR:E_3-TTR = 5:1:4. The scale bars are 5 μm.
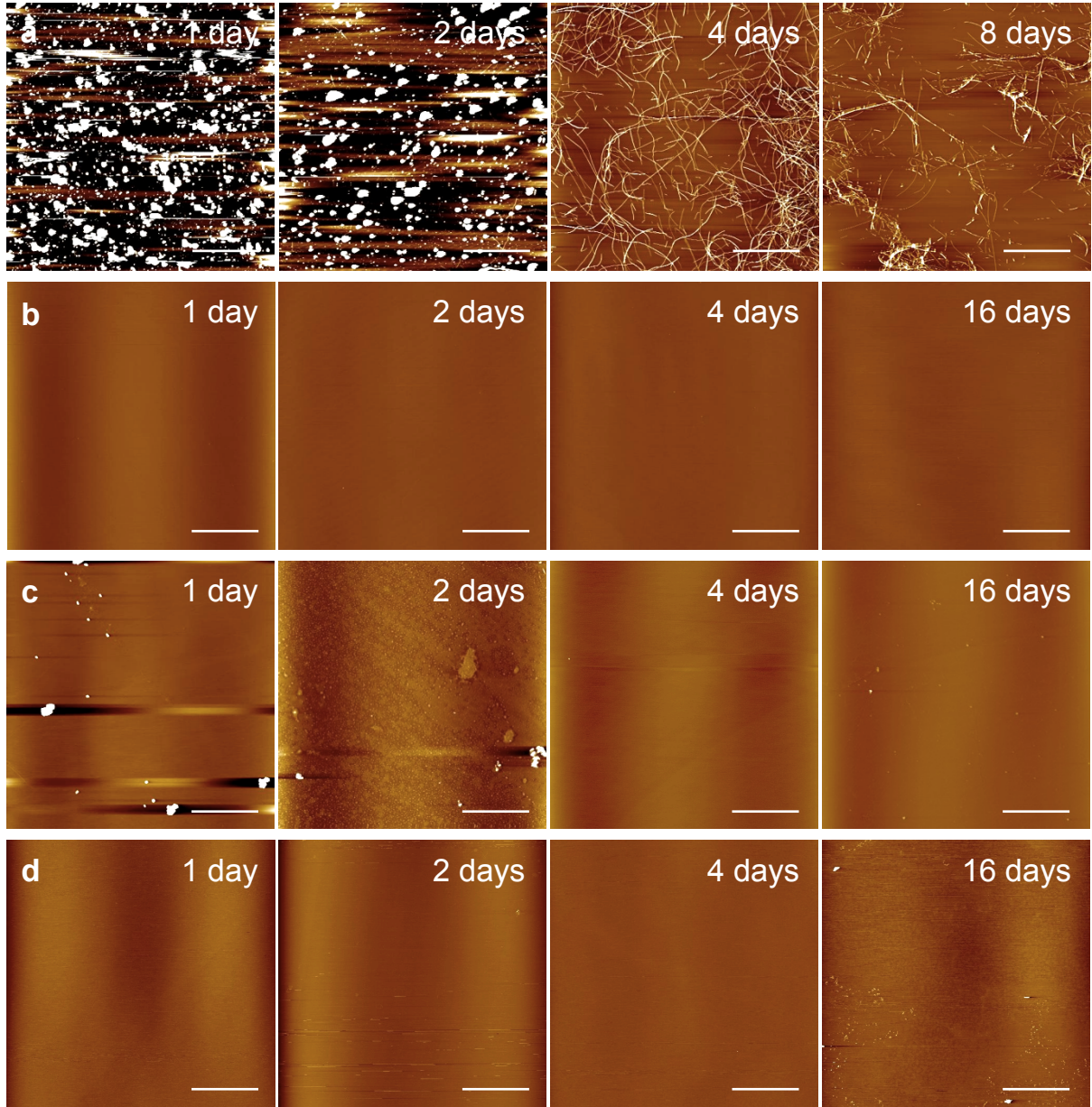
Figure 2-7. Incubation of F/P-SCAPs under fibrillation conditions. (a) TMR-E$_3$-TTR, (b) Lip-K$_3$-TTR, (c) Mal-E$_3$-TTR, and (d) Azd-E$_3$-TTR. Scale bar is 5 μm.
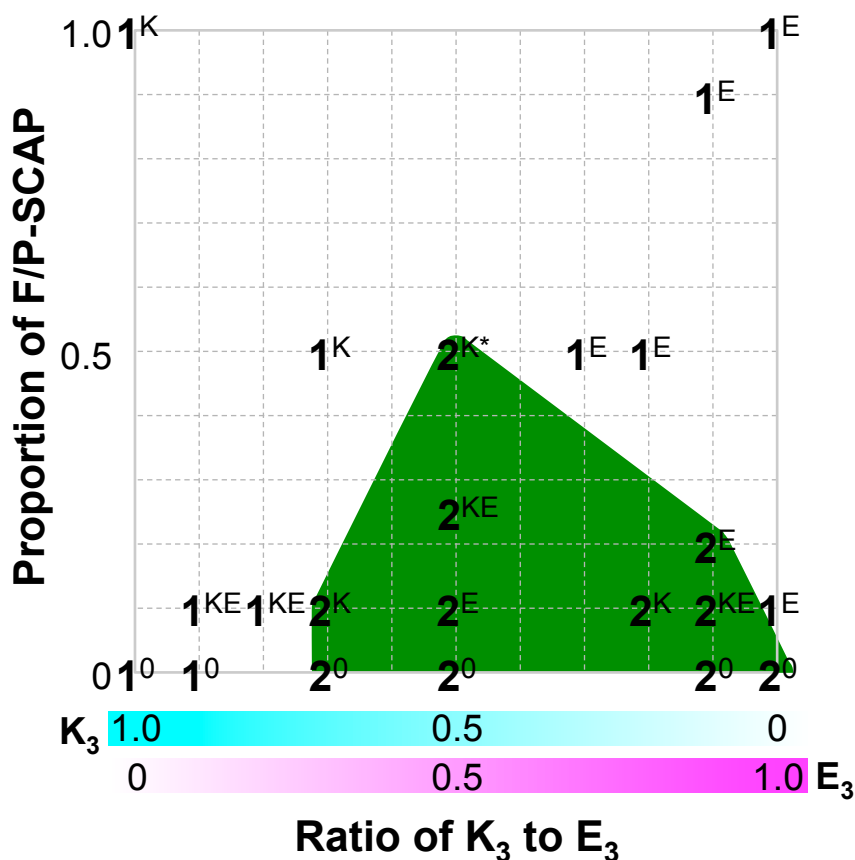
Figure 2-8. A summary of nanowire formation for various peptide mixtures with or without F/P-SCAPs, which contain a unit of either K_3 or E_3. Fibril formation was checked at several dozen mixing ratios shown on the graph. Each label shows that fibrils were either 1^0: not formed without F/P-SCAPs, 1^K: not formed with K_3-based F/P-SCAPs, 1^E: not formed with E_3-based F/P-SCAPs, 1^{KE}: formed by neither K_3- nor E_3-based F/P-SCAPs, 2^0: formed without F/P-SCAPs, 2^K: formed with K_3-based F/P-SCAPs, 2^E: formed with E_3-based F/P-SCAPs, 2^{KE}: formed with both K_3- and E_3-based F/P-SCAPs, 2^{K*}: formed with K_3- but not with E_3-based F/P-SCAPs. In the absence (0%) of F/P-SCAPs, fibrils were formed when E_3-TTR presented at 30% or more of the total peptide concentration. When F/P-SCAPs were employed, effective fibril formation was observed within the mixing range indicated by the green area. A total K_3:E_3 ratio of 1:1 enabled highest (50%) introduction of attached functional or probe molecules.
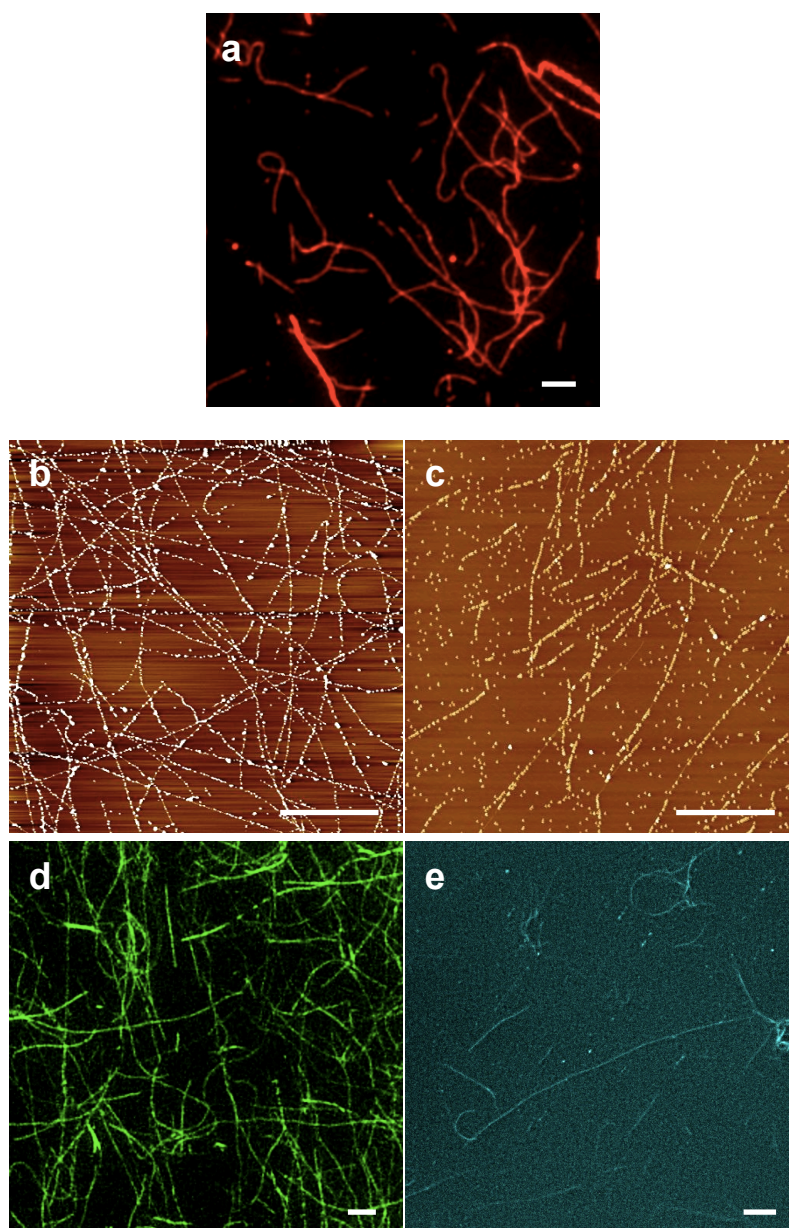
Figure 2-9. Functionalized nanowires prepared using (a) F-SCAP and (c-e) P-SCAPs. (a) A fluorescence image of tetramethylrhodamine-containing nanowires. (c-e) Arrangements of (b) avidin magnetic beads, (c) gold nanoparticles, (d) F-TBP-Cys, and (e) AMC-cCN225-Alk on biotinylated, α-lipoyl, maleimide and azide nanowires, respectively. The scale bars show 5 μm.

This result also suggests that the P-SCAP-based probed nanowires presumably contain the probe molecules on the fibril surface.

Then, the probed nanowires were functionalized by targeting specific nanomaterials with responsive moieties to the probe. In the present study, the following four functional nanomaterials were employed: avidin magnetic beads, gold nanoparticles, and designed multi-functional peptides with a cysteine residue and an alkyne group at the C-termini, which were termed as F-TBP-Cys and AMC-cCN225-Alk (Table 2-1), respectively. These peptides contain two functional moieties: a fluorophore at the N-terminus and a biomineralization sequence in the middle. Aqueous solutions of these functional materials, except for AMC-cCN225-Alk, were incubated with the corresponding probed nanowires on a mica or glass surface. Consequently, the probed nanowires were readily functionalized with specific materials, as demonstrated by AFM and fluorescence microscopy observation of avidin magnetic beads, gold nanoparticle arrays, and unambiguous green fluorescent fibrils (Figure 2-9 b-d). AMC-cCN225-Alk was conjugated to azide-probed nanowires in bulk solution through Cu(I)-catalyzed azide-alkyne cycloaddition (click chemistry), which yielded blue fluorescent fibrils observed under fluorescence microscopy (Figure 2-9e). In contrast, no fluorescence or arrangement of the materials was observed after incubation with probe-free fibrils (Figure 2-10), which confirms that all probes were definitely incorporated into nanowires, and that the functional materials were successfully arranged through their specific binding ability to the probes. These results in conjunction with the F-SCAP-based functionalization clearly demonstrate the great usefulness of our SCAP-mixing method for creating a wide variety of functionalized nanowires.
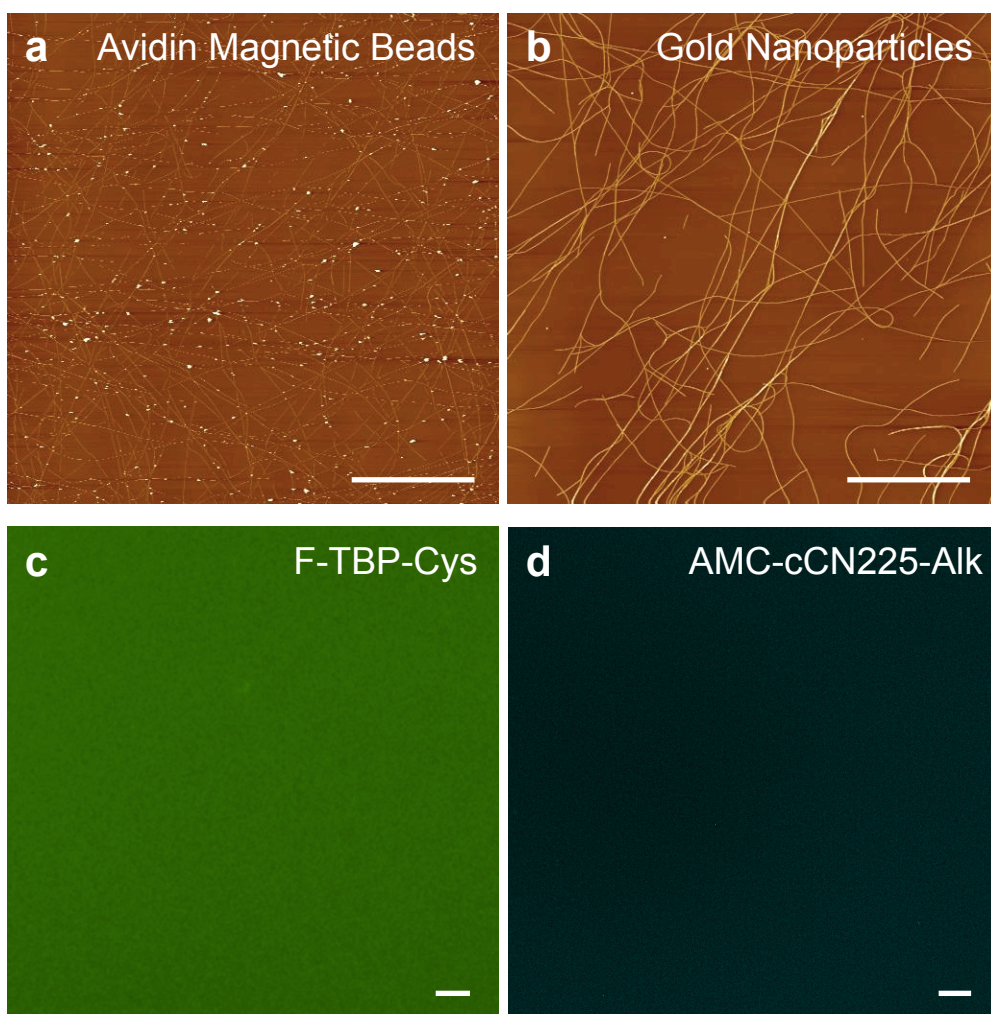
Figure 2-10. Incubation of functional materials with probe-free fibrils. (a) Avidin magnetic beads, (b) gold nanoparticles, (c) F-TBP-Cys and (d) AMC-cCN225-Alk. The scale bars show 5 μm.

2.4.5. Creating Inorganic Nanowires through Biomineralization on Fibrils

F-TBP-Cys contains a biomineralization sequence derived from minTBP-1 (RKLPDA) that can promote specific formation of titania, silver, and silica nanowires (28,29). Thus, this biomineralization peptide enables us to transform fibrils modified with F-TBP-Cys into inorganic nanowires via biomineralization on the fibrils. We let titania mineralize onto the nanowires by applying a K_2TiF_6 solution at neutral pH for 2 h. After incubation, titania nanowires were successfully observed by TEM and identified by EDX spectroscopy (Figures 2-11), which suggests that the F-TBP-Cys conjugated onto the fibrils was actually able to perform its function. These results demonstrate the substantial potential of our SCAP method for practical use in creating various classes of inorganic nanowires that can be a component of nanoelectronic devices.
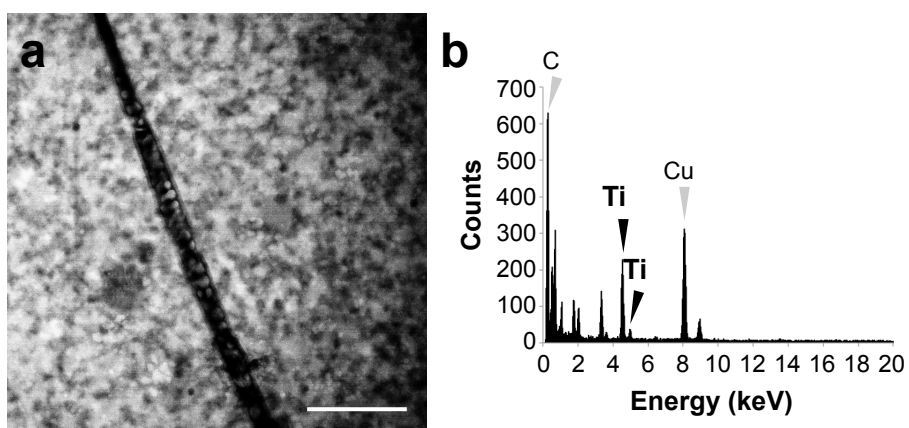
Figure 2-11. (a) A transmission electron micrograph of a titania nanowire formed after biomineralization with K_2TiF_6 and F-TBP-Cys-conjugated nanowires. (b) Energy dispersive X-ray spectrum obtained from the titania nanowire shown in (a). Two peaks attributed to titanium were observed. The carbon and copper peaks are derived from the grid. The scale bar represents 200 nm.

2.5. Discussion

In the present study we have developed an effective method for creating various functionalized amyloid nanowires by control of self-assembly using our SCAPs. The extremely long nanowires formed by simple mixing of multiple SCAPs (and F/P-SCAPs) with different K_3 and E_3 units demonstrates the ability of our method to control amyloid self-assembly. Fabrication of functionalized nanowires was successful both in direct assembly of functionalized nanowires with a F-SCAP and in the post-fibrillation functionalization of the probed nanowires formed with P-SCAPs. The probed nanowires could be modified with various materials such as avidin magnetic beads, gold nanoparticles, and biomineralization peptides. Furthermore, the F-TBP-Cys-conjugated fibrils were transformed into titania nanowires, demonstrating the versatility of our method for application in inorganic-nanowire-based nanodevices.

Fibrils grown under mixed-SCAP conditions reached great lengths well over 40 μm, which is approximately ten times as long as typical amyloid fibrils. The fibril structure possessed the highest aspect ratio of length/height observed to date (>8,000), which could be useful in nanotechnological application, such as large-scale nanowire patterning. These remarkably long fibrils were reproducibly observed under a total K_3:E_3 ratio of 1:1 and 1:9, even in the presence of F/P-SCAPs. Therefore, the fibril architecture should primarily be determined by the interaction of the K_3 and E_3 units through provision of particular binding modes among peptides present in fibrils. Electrostatic interaction, which has been known to promote fibril formation (20,30), may contribute to the observed great length. However, other interactions must be taken into account to determine the mechanism of long fibril formation, as under the condition

employed (pH 2 aqueous water) the electrostatic interaction of K_3-E_3 units should theoretically provide small attraction forces resulting from the protonation of the carboxyl groups of the Glu residue. It is noteworthy that the biotinylated fibrils formed efficiently under mixing multiple SCAPs with different units of K_3 and E_3. The condition containing E_3-TTR and Bio-E_3-TTR with an identical E_3 unit resulted in no fibril formation, which indicates the inhibitory effect of the biotinyl group on fibrillization. Therefore, mixing SCAPs can effectively work on the nucleation step in addition to the process of fibril elongation. Certain microenvironments formed under mixed-SCAP conditions in the starting solution, such as assembly states of oligomers, may be involved in the observed efficient nucleation. The effect of mixing SCAPs on both the nucleation and elongation steps has to be elucidated to determine the control mechanism.

The density of modification of the fibril surface is important for the properties of functionalized nanowires. Three groups have reported a similar approach to ours, where a fraction of modified peptides was co-assembled with unmodified peptides (31-33). However, only a maximum of approximately 1% of the modified peptides could be co-assembled with the amyloid-forming peptide. In contrast, our method allowed the assembly of probed/functionalized nanowires with 10% P/F-SCAP, which should provide a 1–2 nm distribution of functional/probe molecules on the surface based on the reported TTR(105-115) fibril structure, in which four peptides exist in each 4.7 Å unit (27). The contents of the embedded molecules can be further tuned, if required, just by adjusting the mixing ratios.

Limited types of functionalization to amyloid fibrils have been reported to date because most previous studies focused on the arrangement of metal nanoparticles bound

to cysteine residues (34-36) or of fluorophore-containing amyloid peptides (31,33,37-40). Our method of incorporating functional molecules or probes attached to F/P-SCAPs embedded in the fibril allows functionalization of the fibrils with various materials. The successful modification of probed nanowires with specific materials further indicates the great ability of our method to produce functional nanowires. The probed nanowires can also be used to yield nanowires functionalized with gold-, avidin protein- and alkyne-containing materials, respectively. Therefore, our method can confer any type of function to the fibrils regardless of the size or properties of the molecules employed. The only limitation is that a responsive group must be introduced to the molecules, but such groups can be attached normally through simple chemical procedures. Hence, our method will introduce great opportunities to produce nanowires with various practical functions such as light-harvesting nanowires, conductive nanowires, and nanowires modified with proteins, catalytic compounds, or biomineralization peptides.

Many biomineralization sequences with specificity for various inorganic elements have recently been identified (41-43). This fact makes our method more important because the use of such specific biomineralization peptides could enable the fabrication of a variety of inorganic nanowires suitable for nano-electro devices. Previous studies have shown that it is feasible to grow fibrils composed of a certain amyloid peptide from a seed fibril prepared with a different type of peptide (44,45). Combining that technique with our technique may allow the fabrication of patterned functional nanowires, which would have many applications in nanotechnology.

3. Novel Mechanism of Mixing SCAPs for Enhancement of Fibril Length Controlled by a Unique Oligomerization Property

3.1. Abstract

Amyloid formation is a self-assembly process of misfolded protein and peptides that produces a very stable nanofibrillar structure, called amyloid fibrils, associated with various neurodegenerative diseases including Alzheimer's disease. Materials scientists have focused on the morphological and mechanical properties of amyloid fibrils to create functionalized nanowires. However, it is still difficult to control fibril structure because of the complexity of the self-assembly mechanism, which becomes more elaborate when modified peptides are employed to functionalize the fibril surface. Our SCAP-mixing method has attracted attention because it can not only induce fibril growth to a great length but also reproducibly yield long fibrils even in the presence of modification. Here, I present the impressive fibril-growth mechanism underlying our mixed-SCAP system. Ion mobility-mass spectrometry (IM-MS) demonstrated a unique structural evolution of peptides at a small oligomer level, wherein mixed SCAPs produced an extended fibrillar arrangement through heterooligomer formation. Structural analysis of fibrillation by AFM showed that, during elongation phase, no protofibrils were detected in mixed SCAPs and all the fibrils took the mature structure. The data therefore suggest that the unique oligomerization property of mixed SCAPs could accelerate the maturation process but also allow addition of soluble peptides to the fibril end as oligomer unit with extended structure. These two aspects may contribute to the formation of extremely long fibrils.

3.2. Introduction

Amyloid fibrils have a highly ordered nanostructure with an average width of approximately 10 nm and a typical length of several micrometers (1-3). This nanostructure is a consequence of the self-assembly of misfolded proteins or synthetic peptides, in which the constituent proteins/peptides are aligned perpendicular to the fibril axis in a cross-β conformation (2,3). Amyloid fibrils have been associated with a wide-range of protein misfolding diseases, such as Alzheimer's disease, transmissible spongiform encephalophathies, prion disease, and systemic senile amyloidosis (4,5). However, the high stability and mechanical strength of amyloid fibrils also makes them a promising material in the area of nanotechnology (6-11). Researchers have reported the application of amyloid fibrils to form conductive nanowires (12-14), coaxial metal nanocables (15), catalytic nanofibers (16), and biocompatible hydrogels (17-19). For practical use of amyloid fibrils, the nanostructure of the fibrils (length, width, and homogeneity of the ensemble) has to be highly controlled (14,20,21). However, the very complicated system of amyloid fibrillation, in which various kinetic and thermodynamic pathways are possible depending on the primary peptide sequence and fibrillation conditions (22,23), makes it difficult to elucidate the self-assembly mechanism and to control self-assembly. This difficulty highlights the importance of a mechanistic study of our mixed-SCAP system that allows control of fibril length and homogeneity as described in Chapter 2.

Several mechanistic studies of amyloid fibrillation have characterized the structural evolution of fibrils using various techniques including AFM (24-29) and IM-MS (30-32). AFM has long been utilized to evaluate self-assembly processes

through detection of transient oligomers and protofibrils in addition to stable mature fibrils. IM-MS is a powerful tool to study oligomer structure because it allows quantitative measurement of the size of mass-selected oligomers, which are not necessarily the cytotoxic oligomers observed in other systems as described in Chapter 1. A lower or higher number of oligomers present at very small numbers can be detected. Given this analysis capability, IM-MS has been used to successfully characterize the self-assembly of peptides at the very small oligomer level. For example, a difference in oligomer distribution between Aβ(1-40) and Aβ(1-42) has been revealed (30); Aβ(1-42), which is an aggregation-prone species and strongly cytotoxic (33), shows dimers and tetramers but also hexamers and dodecamers with globular structures, which were the species detected in other studies (34). By contrast, in Aβ(1-40), which possesses lower aggregation propensity and less cytotoxicity (33), only dimers and tetramers appeared. The data were correlated with actual fibrillation and therefore demonstrate the usefulness of IM-MS for characterizing oligomer self-assembly.

Here, I demonstrate a novel fibrillation mechanism underlying our mixed-SCAP system. Analysis of oligomerization by IM-MS presented an extended fibrillar conformation of very small oligomers induced by mixing of SCAPs. Detailed observation of the fibrillation processes by AFM showed that oligomerization to form the extended structure plays a key role growing the fibrils to a great length. Therefore, mixing of SCAPs provides remarkable control over the self-assembly process of very small oligomers to form macroscopic fibrils.

3.3. Experimental Procedures

Peptide Synthesis

Peptides were synthesized with a standard Fmoc-chemistry on Rink amide resin automatically with an Applied Biosystems 433A peptide synthesizer (Applied Biosystems Inc., Foster City, CA) or manually. All peptides were then deprotected and cleaved from the resins with reagent K (a 82.5/5/5/5/2.5 mixture of TFA/H_2O/phenol/thioanisole/ethanediitol) over two-hour incubation to yield crude peptide materials. The crudes were purified using a reverse-phase HPLC (SCL-10A, SPD-10A, DGU-12A, LC-6AD, Shimadzu) with a C-8 column (22 x 250 mm, Cat. No. 208TP1022, Vydac) eluted with a linear gradient of water and acetonitrile containing 0.05 or 0.04% TFA, respectively. The peptides were obtained in ≥95% purity determined by reverse-phase HPLC (PU-980, UV-970, HG-980-31, DG-980-50, Jasco) with a C8 column (4.6 x 250 mm, Cat. No. 208TP104, Vydac), and were identified by MALDI-TOF-MS (voyager System 6171, Applied Biosystems, at the OPEN FACILITY in Sousei Hall).

Ion Mobility-Mass Spectrometry

All IM-MS experiments were carried out on a home-built instrument developed in Bowers' Group at University of California, Santa Barbara (35). Peptides were first dissolved in HFIP at a concentration of 8 mM as a stock solution. The concentration was adjusted by UV absorption of the peptides measured by UV 3600 UV-Vis-NIR spectrometer (Shimadzu). The extinction coefficient of $\varepsilon_{276} = 2900$ M^{-1}cm^{-1}, derived from the two tyrosine residues at 100 mM sodium phosphate (pH 7.0) in the presence of

6 M guanidine hydrochloride (36), were used for calculation. The samples for IM-MS were prepared by diluting the HFIP stock solution with acidic water (pH 2.0 adjusted by hydrochloride) to 200, 400, or 800 μM, followed by loaded into nano-ESI gold-coated borosilicate capillaries (0.1 mm od/0.78 mm id), which had been purchased from Proxeon (Germany) and pulled to a fine point on a tip puller (Sutter Instrument Co., Novato, CA). The samples were subsequently sprayed in the electrospray source of the IM-MS instrument at a voltage of <1 kV (Refs). Ions generated in the spray were focused and stored in an ion funnel and then pulsed into a drift tube filled with ~3 torr of helium gas for the IMS measurement. The ions passed through the drift tube with constant velocity under the influence of a weak electric field. The velocity (v_D) is determined by the balance between the force of the electric field (E) and the retarding force of friction, thus v_D is proportional to E with the proportionality constant (K) termed the ion mobility:

$$v_D = KE \tag{1}$$

After exiting the drift cell, ions of a particular oligomeric state are selected by mass in a quadrupole mass filer and detected as a function of their arrival time. From the position t_A of a peak in these arrival time distributions (ATDs) the respective ion mobility or ion-He collision cross section (σ) can be evaluated (37,38) using the relationship

$$\sigma = 1.3 \left(\frac{q^2 E^2 T}{\mu k_B p^2 N^2 l^2} \right)^{\frac{1}{2}} (t_A - t_0) \tag{2}$$

where q is the charge of the ion, T the temperature, μ the reduced mass of the ion-He collision, k_B the Boltzmann constant, p the He gas pressure, N the He number density at STP, l the drift cell length, and t_0 the time the ion spends outside of the drift cell. All of the quantities in eq 2 are either known or measured for each experiment; therefore σ can be accurately determined for each species. An additional mass spectrometer, a Q-TOF instrument with higher mass resolution (Waters, UK) equipped with a nano-ESI source, was used to measure the ^{13}C isotope separation (39). However, no IMS data were obtained on this instrument.

Fibril Formation

The 8 mM stock solutions of each peptide and mixture were diluted by a factor of 40 in aqueous solution at pH 2.0 (adjusted by HCl), and incubated in plastic tubes at 37 °C. UVmini-1240 spectrophotometer (Shimadzu) was utilized for measurements of stock solution concentration.

Atomic Force Microscopy

5 µl aliquots of samples incubated were deposited on fleshly prepared mica (Cat. No. 990066, Nilako) for 5 min, followed by washed three times with 1 mL of water, dried and subsequently observed by tapping mode AFM in air. AFM measurements were performed using a Nanoscope IIIa system (Digital Instruments, Santa Barbara, CA) with a standard silicon cantilever (OMCL-AC240TS, Olympus). Images were captured at 512 × 512 pixel resolution at a scan rate of 0.25 Hz with a typical condition of 60-80 kHz of drive frequency, and 1.6-1.8 V of amplitude set point.

Thioflavin T Assay

10 μl of sample solutions were diluted 50-fold with buffer containing ThT at final concentrations of 4 μM peptide, 10 μM ThT, 50 mM phosphate (pH 7.5) and 100 mM NaCl. The measurements were performed on an F-4500 fluorescence spectrophotometer (Hitachi) using a micro quartz cuvette with 0.5 cm light path at room temperature. Spectra were acquired three times for each sample with excitation wavelength of 444 nm at a rate of 1200 nm/min.

Seed Preparation

Seeds were prepared by sonication of matured fibrils purified by centrifugation to remove peptide monomers. Matured K_3-TTR:E_3-TTR = 1:1 fibrils were purified three times by centrifugation at 21,600 × g for 30 min at 20ºC with Himac CF15R (Hitachi), followed by exchange of the 180 μl of supernatant to equivolume of 0.01 M HCl. Then, the purified fibrils were immediately sonicated with W-113 MK-II ultrasonic disperser (Honda Electronics) for 30 minutes. The seed solution was added to initial peptide solutions at 1% v/v.

Addition of K_3-TTR in the Middle of Kinetic Phase

Fibril formation was initiated in the presence of E_3-TTR at a concentration of 200 μM and of 0.5% v/v seed fibrils prepared as described above. After 8-hour incubation at 37ºC, the small amount of a peptide mixture of 1 mM K_3-TTR and 200 μM E_3-TTR was added to the fibrillation solution to give final K_3:E_3 ratio of 1:9. 10 μl aliquots were collected for every hour until 24 hours to prepare samples for AFM measurements to observe fibril structures.

3.4. Results

3.4.1. Unique Oligomerization Property of Mixed SCAPs Demonstrated by IM-MS

To characterize the effect of mixing multiple SCAPs on the enhancement of fibrillation, I analyzed the oligomerization process, which is the first step of self-assembly, by employing IM-MS (note that the term 'oligomer' here means only the species of associated peptide molecules and should be distinguished from cytotoxic oligomers). Figure 3-1 presents the ESI mass spectra of K_3-TTR, E_3-TTR, and their 1:1 mixture solutions. The most abundant peak for each sample has an $n/z = 1/2$ (where $n =$ oligomer number and $z =$ charge of the ion). The ^{13}C isotope separation of $\Delta(m/z) = 0.5$ for the double-charged $n/z = 1/2$ peak (Figure 3-1 insets of a–c) reveals that the dominant species in each sample must be the monomeric form ($n = 1$). However, it should be noted that there is a large difference between the oligomer distribution in the solution of the single peptides and that in the peptide mixture. The K_3-TTR and E_3-TTR data show oligomer peaks at $n/z = 2/3$, $3/5$, and/or $3/4$, whereas the 1:1 mixture data show multiple oligomer peaks that represent additional higher-order oligomers ($n/z = 4/5$ and $5/6$) and a much more intense $n/z = 2/3$ peak. In the high-resolution mass spectra, the $n/z = 2/3$ peak of the mixture is apparently in the middle of both homodimers (Figure 3-1d). A fit to the experimental spectrum of the mixture reveals the 1:20:5 abundance ratio of the K_3 homodimer to the heterodimer to the E_3 homodimer, whereas a 1:2:1 ratio is expected based on statistics. Therefore, dimers with a triple-charge state in mixed SCAPs obviously prefer heterodimer formation. Similarly, the $n/z = 3/4$, $3/5$, $4/5$, and $5/6$ species favorably formed heterooligomers, although the dominant ratios of K_3-TTR to E_3-TTR were not 1:1; rather, they were 1:2, 1:2, 1:3, and
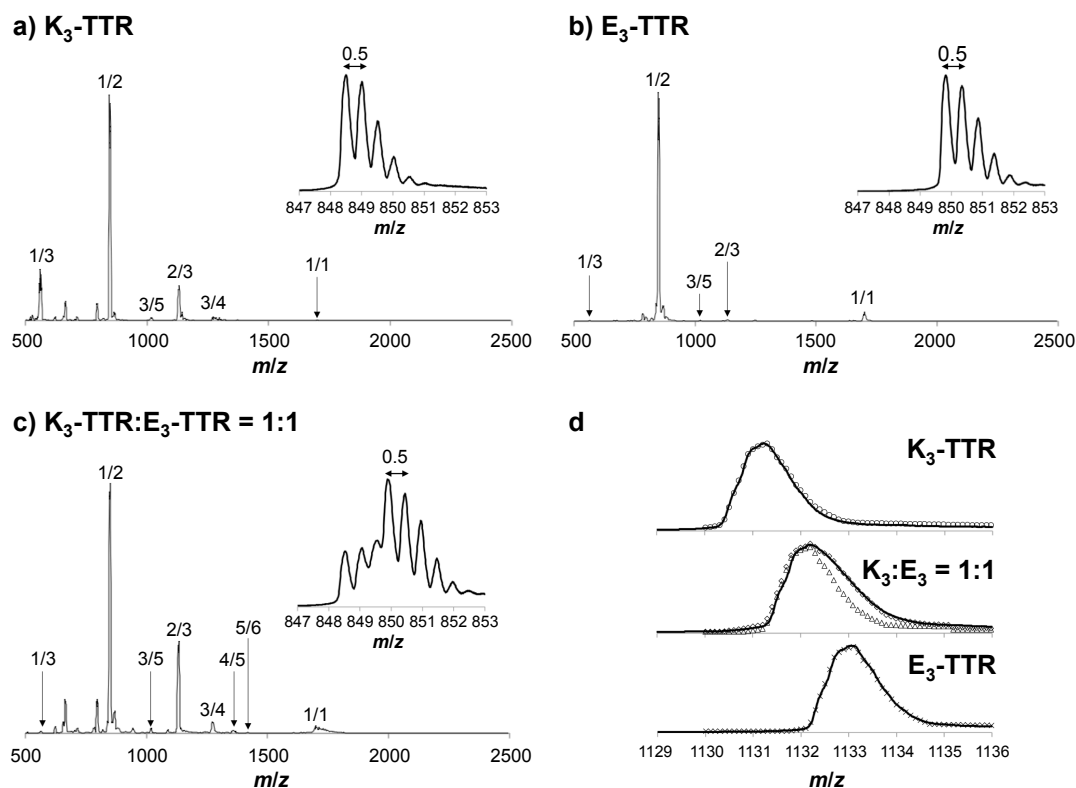
Figure 3-1. (a–c) ESI-Q mass spectra (positive ion mode) of (a) K_3-TTR, (b) E_3-TTR and a 1:1 mixture of (c) K_3-TTR and E_3-TTR. The peaks are labeled with the ratio of oligomer number n to charge z. The insets show high-resolution ^{13}C isotope patterns for the $n/z = 1/2$ peaks. The $n/z = 1/2$ peak shape of the 1:1 mixture shows an overlapped pattern of the K_3-TTR and E_3-TTR spectra. (d) High-resolution mass spectra of the $n/z = 2/3$ charge states for K_3-TTR (top), K_3-TTR:E_3-TTR = 1:1 (middle) and E_3-TTR (bottom). The symbols represent a fitting analysis for the abundance of each dimer species. Fits to K_3-TTR (○) and E_3-TTR (✕) spectra describe the spectrum patterns of the K_3 and E_3 homodimer, respectively. The triangle (△) is an average of both homodimers representing a pure heterodimer. A 1/20/5 ratio of the K_3 homodimer/heterodimer/E_3 homodimer (◇) gives the best fit to the experimental spectrum of the 1:1 mixture.

47

1:4, respectively (data not shown).

Figure 3-2 presents the arrival time distributions (ATDs) of the mass-selected ions corresponding to $n/z = 2/3$ at different peptide concentrations. The collision cross sections of the major peaks for K_3-TTR and E_3-TTR (544 and 510 Å^2, respectively) are about $2^{2/3}$ fold larger (yielding values of 538 and 519 Å^2, respectively) than the corresponding monomer cross sections, which indicates isotropic growth from the monomers to the dimers with globular structures in both cases. Interestingly, however, the $n/z = 2/3$ dimer of the 1:1 mixture has a cross section of 558 Å^2, which is ~ 6% larger than the expected isotropic dimer (525 Å^2), thus suggesting the formation of an extended fibrillar structure (Figure 3-2c). Moreover, the dimer cross section of the mixture increases to 574 Å^2 (~10% larger than the isotropic cross section) at higher concentrations, which was not the case for K_3-TTR or E_3-TTR. Similarly, this increase was also observed in the ATDs of the $n/z = 3/4$ and $3/5$ peaks (Figures 3-3 and 3-4). Thus, it is suggested that the extended parallel fibrillar structure is strongly stabilized when using the mixed-SCAP system. This assumption is further supported by the presence of $n/z = 4/5$ and $5/6$ peaks in the mixture only. The cross sections of the 4/5 and 5/6 ions follow the same linear correlation with oligomer number, n, as the dimer and trimer cross sections of the mixture (Figure 3-5 red line), which demonstrates that these oligomers grows linearly and not isotropically. Linear growth with n is expected for one-dimensional growth towards fibrillar structures (32). These results unambiguously show that mixed SCAPs possess a unique self-assembling property that enhances oligomer assembly accompanied by an extended fibrillar structure.

The minor $n/z = 1/1$ peak in the mixed SCAPs possesses an m/z value of ~1699, which is identical to that of E_3-TTR (Figure 3-6a). Collision cross section analysis
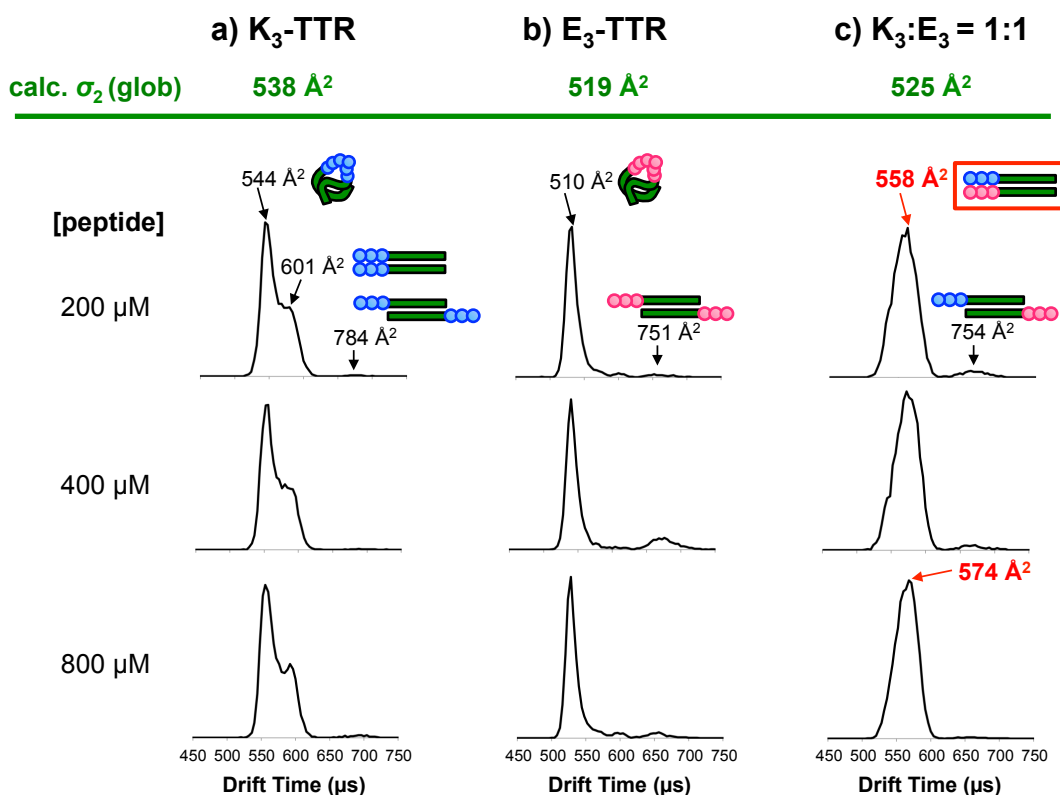
Figure 3-2. Arrival time distributions (ATDs) of (a) K_3-TTR, (b) E_3-TTR and (c) K_3-TTR:E_3-TTR = 1:1 for n/z = 2/3 charge states at three different peptide concentrations. The labels are the measured collision cross sections. The green numbers shown above the ATDs are the calculated collision cross sections expected for globular oligomers based on the cross section of each monomer (σ_1) and a theoretical equation of $\sigma_n = \sigma_1 \times n^{2/3}$ for isotropic oligomer growth mode. The weak peak with a cross section of 750-780 Å^2 could be an antiparallel β structure, in which the peptides are associating through the native TTR(105–115) region.
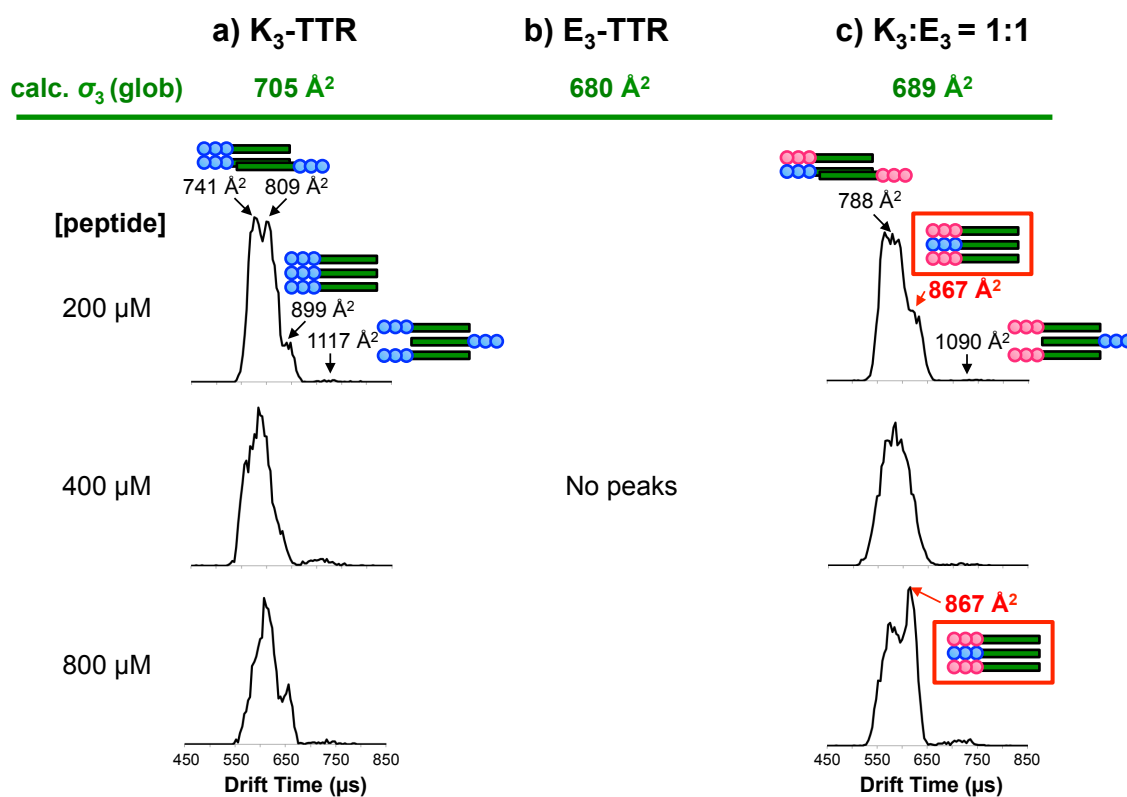
Figure 3-3. ATDs of (a) K_3-TTR, (b) E_3-TTR and (c) K_3-TTR:E_3-TTR = 1:1 for n/z = 3/4 charge states at three different peptide concentrations. No n/z = 3/4 peaks were detected in the E_3-TTR sample. The 1:1 mixture, but not the K_3-TTR, clearly showed concentration dependence of the enhancement of the extended structure. The peak labels indicate the collision cross sections for each species. The above numbers represent the calculated collision cross sections of the globular trimer.
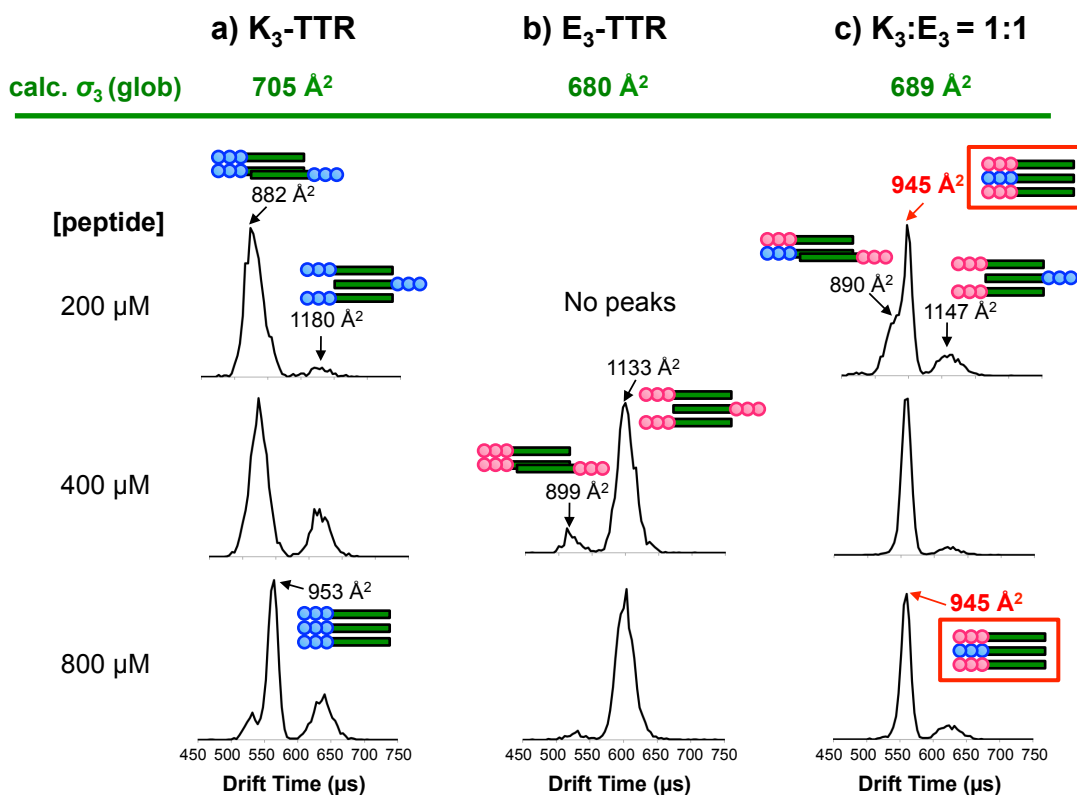
Figure 3-4. ATDs of (a) K_3-TTR, (b) E_3-TTR and (c) their 1:1 mixture for 3/5 charge states at three different concentrations. The $n/z = 3/5$ peak was not detected for E_3-TTR only at a concentration of 200 μM. The labels are the collision cross sections for each of the species. The peaks with the largest cross sections may be an antiparallel β structure. The 1:1 mixture prefers the parallel-extended structure over any other peptide structure. The antiparallel arrangement is likely to be favorable in E_3-TTR, but the intensity of the 3/5 peak was very weak (see Figure 3-1b), which suggests that it is a rare species. The numbers above represent calculated collision cross sections of a globular trimer.

a) n/z = 4/5

1127 Å²

923 Å²

450 550 650 750 850

Drift Time (µs)

b) n/z = 5/6

1418 Å²

1120 Å²

450 550 650 750 850

Drift Time (µs)

c)

major

rare

minor

σ (Å²)

1600
1400
1200
1000
800
600
400
200
0

globular (E₃-TTR)

0 1 2 3 4 5 6
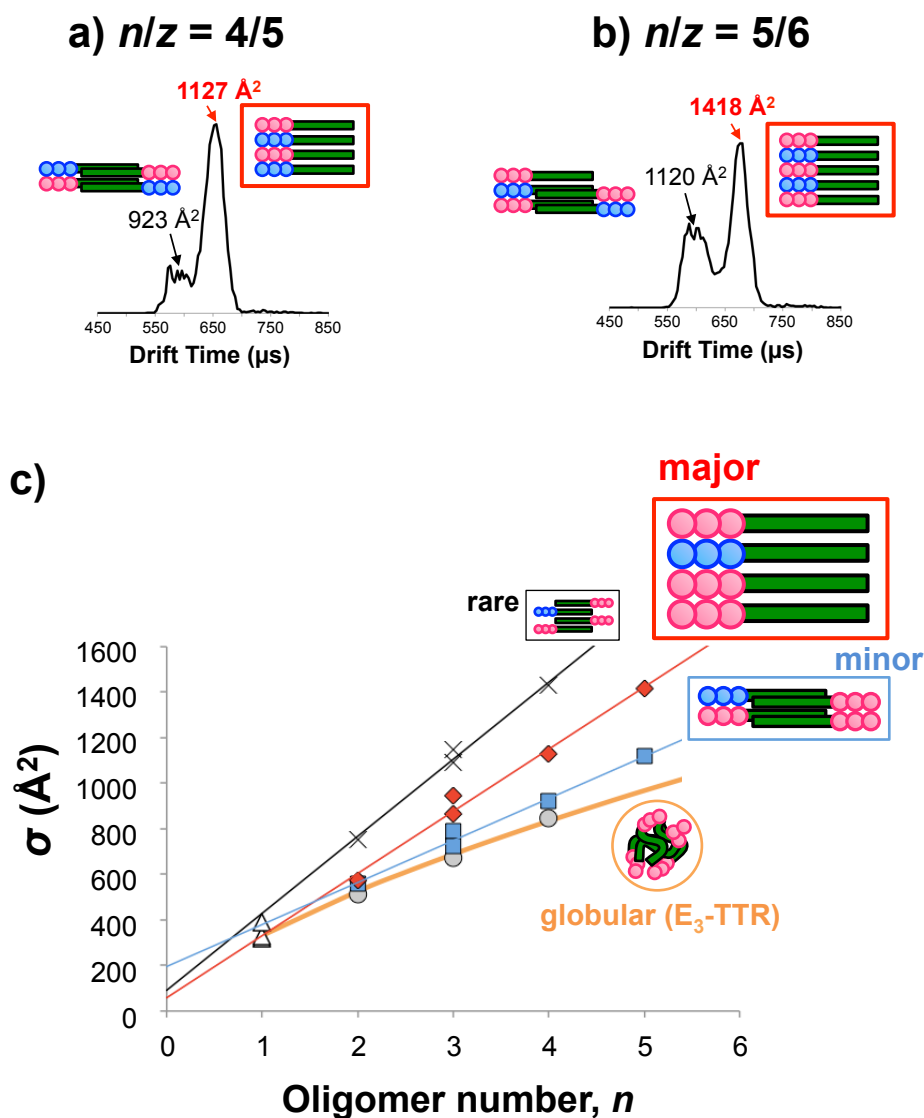
Oligomer number, n

Figure 3-5. ATDs of higher oligomer peaks, (a) n/z = 4/5 and (b) 5/6, detected in a 1:1 mixture of K_3-TTR and E_3-TTR. (c) Plot of collision cross sections as a function of oligomer number for the 1:1 mixture. The cross sections of the major species in these peaks follow the same linear correlation as those of other extended species (red◇), which clearly demonstrates that the peptides in the 4/5 and 5/6 charge states predominantly have the extended structure. Other cross sections correspond to major species in other peaks (○), minor (△), and very rare (✕) species. The yellow trace shows an increase of collision cross section calculated for isotropic oligomer growth.

a)

K$_3$:E$_3$ = 1:1

E$_3$-TTR

1694 1695 1696 1697 1698 1699 1700 1701

m/z

b)

calc. σ_2 (glob)	505 Å^2
calc. σ_3 (glob)	661 Å^2
calc. σ_4 (glob)	801 Å^2

671 Å^2 (3/3)   512 Å^2 (2/2)   318 Å^2 (1/1)

849 Å^2 (4/4)

500 600 700 800 900 1000

Drift Time (µs)
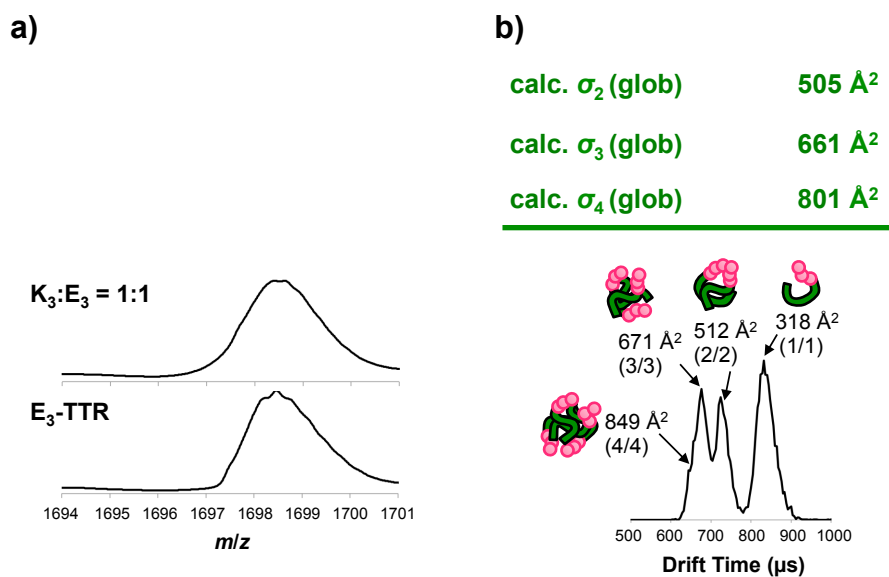
Figure 3-6. (a) High-resolution mass spectra of the *n/z* = 1/1 charge states for K$_3$-TTR:E$_3$-TTR = 1:1 (top) and E$_3$-TTR (bottom). (b) ATD of K$_3$-TTR:E$_3$-TTR = 1:1 for the 1/1 charge state. The labels are the collision cross sections for each of the species. The identical peak positions in (a) and the presence of globular oligomers in (b) demonstrate that homooligomerized E$_3$-TTR within the 1:1 mixture only possesses a globular structure, not an extended fibrillar structure.

showed this peak contains globular oligomers up to the tetramer, which is demonstrated by the isotropic, $n^{2/3}$-fold growth of their cross-section values (Figure 3-6d). These data suggest that a part of E_3-TTR within the mixture forms homooligomers, but which cannot possess the extended structure. Furthermore, another mixture of K_3-TTR:E_3-TTR = 1:9, which also produces long fibrils, showed a oligomerization feature quite similar to the 1:1 mixture of K_3-TTR:E_3-TTR (Figure 3-7). Therefore, formation of extended oligomers is unique property of the heterooligomerized mixed-SCAPs and must be related to the formation of extremely long fibrils.

3.4.2. Drastically Altered Elongation Process of Mixed SCAPs Revealed by Detailed AFM Analysis

To investigate the event occurring specifically during the elongation phase, seed fibrils were added to the initial peptide solution, which skips nucleation phase. Detailed observation of fibril structure was conducted by AFM. The fibrillation kinetics was simultaneously measured by ThT fluorescence. Figure 3-8 presents the ThT fluorescence as a function of time fitted with a following sigmoidal equation;

$$\text{Intensity} = 1/(1 + \exp(-k(t - t_{1/2}))) \tag{3}$$

where k is a rate constant, t is time, and $t_{1/2}$ is half time (Table 3-1). The sigmoidal profiles demonstrate the presence of secondary nucleation, which takes place during elongation phase because of, for example, fibril breakage and fibril-surface-catalyzed nucleation (40). The decrease in fluorescence after the maxima is presumably due to the reduced accessibility of ThT molecules resulting from agglomeration of fibrils (41).
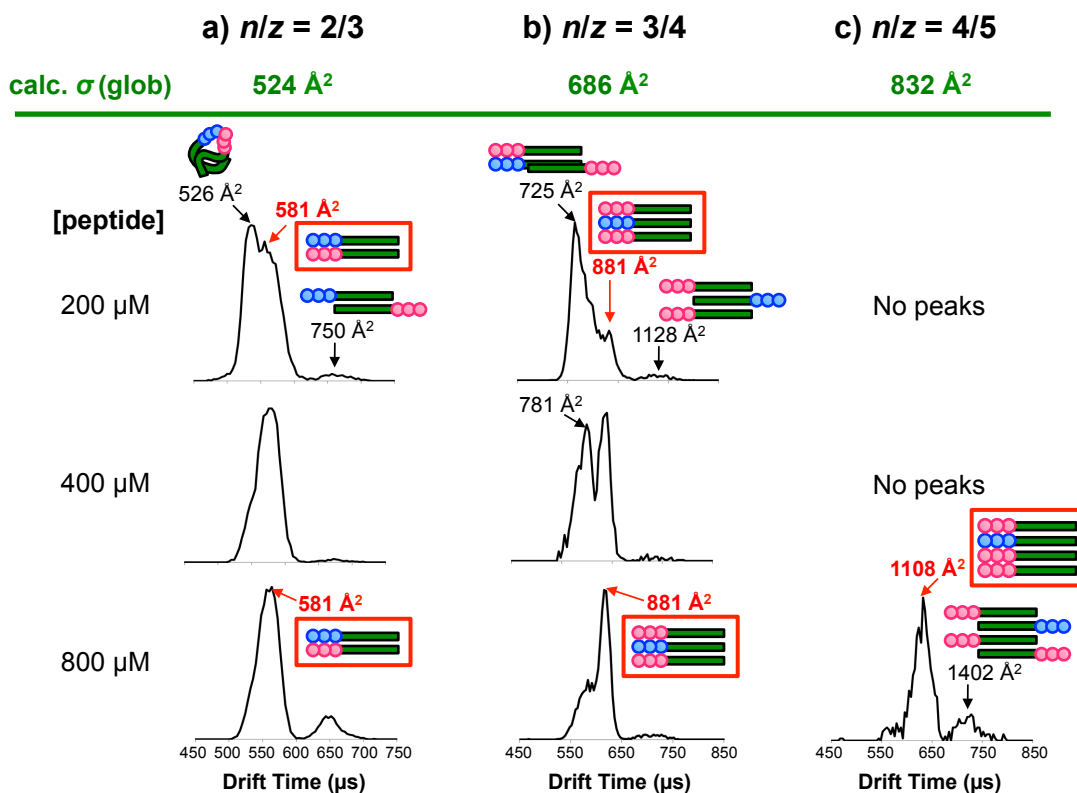
Figure 3-7. ATDs of the 1:9 mixture of K_3-TTR:E_3-TTR for n/z = (a) 2/3, 3/4, and 4/5 charge states at three different concentrations. The n/z = 4/5 peak was only detected at a concentration of 800 μM. The labels are the collision cross sections for each of the species.
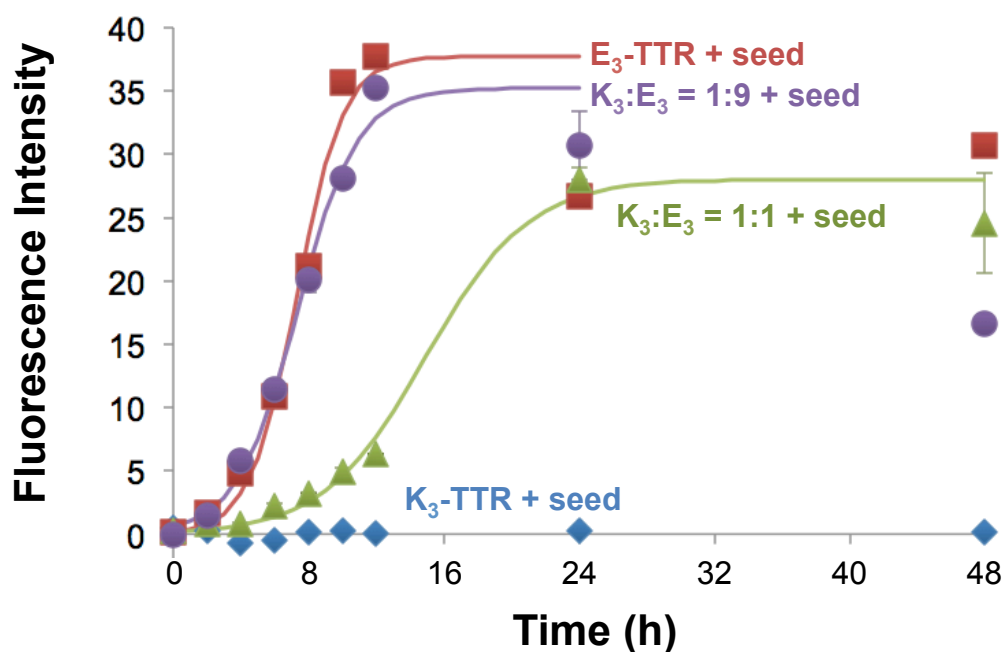
Figure 3-8. Measurements of seeded fibrillation kinetics of (◇) K_3-TTR, (□) E_3-TTR and the (△) 1:1 and (○) 1:9 mixtures of K_3-TTR:E_3-TTR based on ThT fluorescence. The excitation and emission wavelengths were 444 and 485 nm, respectively. The error bar represents the standard deviation of three scans. The curves fit an equation of $I_{obs} = I_{max}/(1 + \exp(-k(t - t_{1/2})))$, where I_{obs}: observed fluorescence intensity, I_{max}: maximum fluorescence intensity, k: rate constant, t: time and $t_{1/2}$: half time.

Table 3-1. Kinetic parameters acquired from the fits in Figure 3-9. An equation of I_{obs} $= I_{max}/(1 + \exp(-k(t - t_{1/2})))$ was used for fitting. I_{obs}: observed fluorescence intensity, I_{max}: maximum fluorescence intensity, k: rate constant, t: time and $t_{1/2}$: half time.

Sample	I_{max}	k (h^{-1})	$t_{1/2}$ (h)
E_3-TTR	37.7	0.72	7.3
K_3:E_3 = 1:1	28.0	0.33	15
K_3:E_3 = 1:9	35.2	0.56	7.3

E_3-TTR and the 1:9 mixture of K_3-TTR:E_3-TTR showed similar kinetic profiles, in which $t_{1/2}$ was the same and k was slightly different (Table 3-1). These parameters for the 1:1 mixture of K_3-TTR:E_3-TTR were approximately half of those for E_3 and the 1:9 mixture. K_3-TTR did not increase ThT fluorescence during the experiment in agreement with no fibril formation (data not shown).

Figures 3-9 represents the AFM images captured at the early (2 h), middle (8 and 12 h for E_3-TTR and K_3-TTR:E_3-TTR = 1:1, respectively), late (12 and 24 h for E_3-TTR and K_3-TTR:E_3-TTR = 1:1, respectively), and completely matured (48 h) kinetic phases based on ThT assay. During the elongation phase, E_3-TTR was always producing protofibrils (Figures 3-9 e-g), some of which were assembling into mature fibrils after the middle of kinetic phase (Figures 3-9 f and g). This phenomenon is a common feature of amyloid fibrillation. Finally, the protofibrils were no more observed after a 48-h incubation (Figure 3-9h) probably because they had all assembled into mature fibrils. Most fibrils were micrometers long as similar to the unseeded case although some long but broken fibrils were detected (Figure 3-9d). On the other hand, the fibrils of the mixed SCAPs in 1:1 K_3-TTR:E_3-TTR only possessed mature fibril structure regardless of the fibril length, and no protofibril species were detected at all (Figures 3-9 m-p). This suggests that protofibrils of the SCAP mixture can assemble into mature fibrils very rapidly or that the soluble peptides can directly be added to the fibril end without through protofibril intermediates. Furthermore, the end products were extremely long (Figures 3-9 k and l) that is the same case as the unseeded condition. Therefore, formation of the very long fibrils must result from the mechanism workingspecifically during elongation phase.

Seeding to the 1:9 mixture of K_3-TTR and E_3-TTR also showed increased fibril
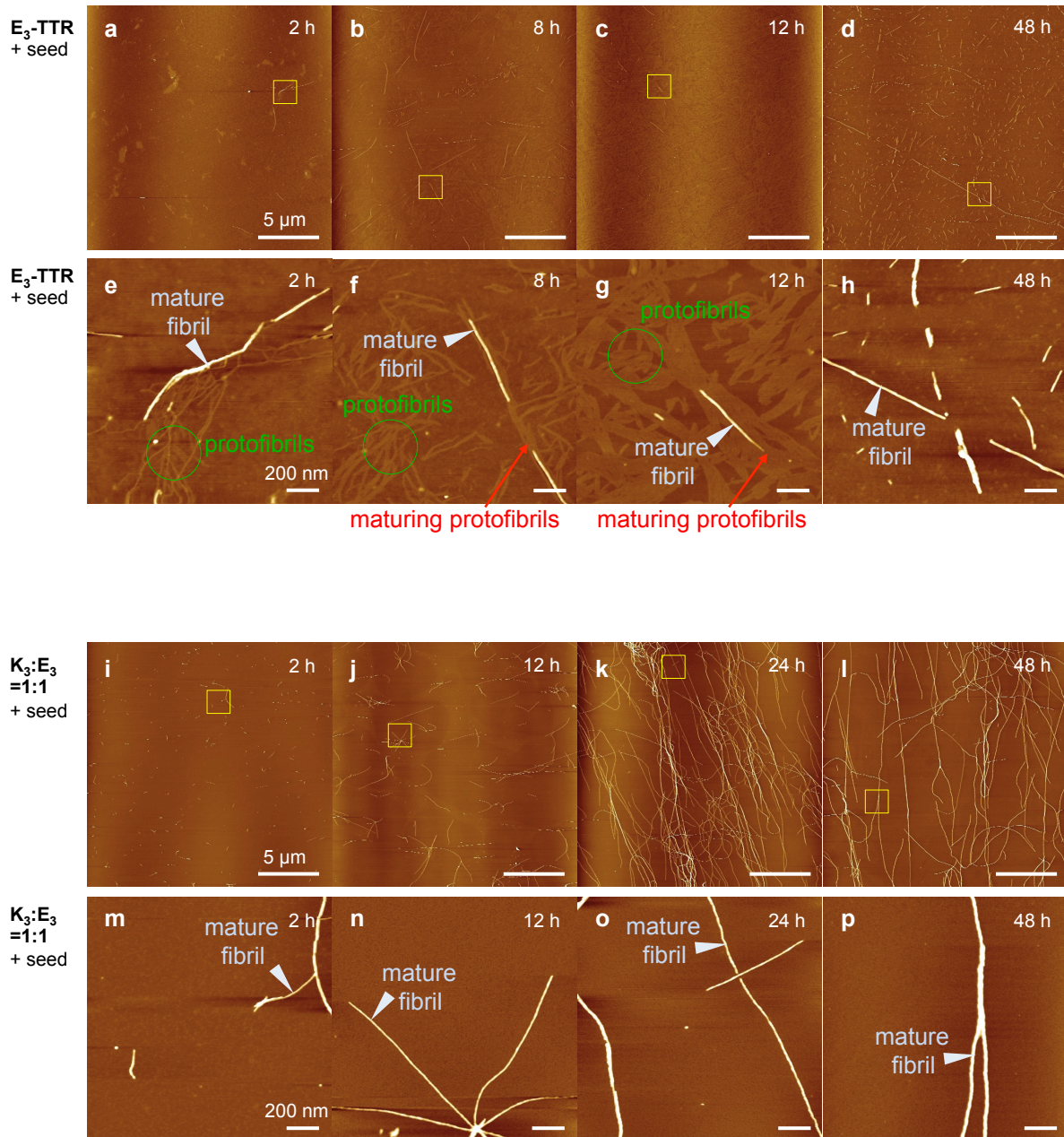
Figure 3-9. AFM images of elongating fibril structure of (a-h) E$_3$-TTR, and (i-p) K$_3$-TTR:E$_3$-TTR = 1:1 of captured at the early (a,e,i,m), middle (b,f,j,n), late (c,g,k,o), and completely matured (d,h,l,p) kinetic phase based on the ThT assay shown in Figure 3-8. The images (e-h,m-p) are the magnification of selected area as shown by the each yellow square. Scale bar represents 5 μm in (a-d,i-l) and 200 nm in (e-h,m-p).

length and no protofibril formation (Figures 3-10) as similar to the 1:1 mixed-SCAP condition.

3.4.3. Mixing of SCAPs during the Elongation Step Dramatically Accelerates Maturation Process

To investigate why no protofibrils were observed in the mixed SCAPs during the elongation phase, I changed the solution condition from E_3-TTR to K_3-TTR:E_3-TTR = 1:9 when protofibrils had already formed. After an 8-hour incubation of the seeded E_3-TTR solution (Figure 3-11 a and b), a small amount of high-concentration K_3-TTR solution was added to give the final molar ratio of K_3-TTR:E_3-TTR = 1:9. Interestingly, protofibrils had completely disappeared and all fibrils possessed mature structure with great length after 1 hour (Figure 3-11 c and d). This result clearly demonstrates that mixed SCAPs can accelerate maturation process of protofibrils, and that the accelerated maturation plays an important role in the formation of very long fibrils.
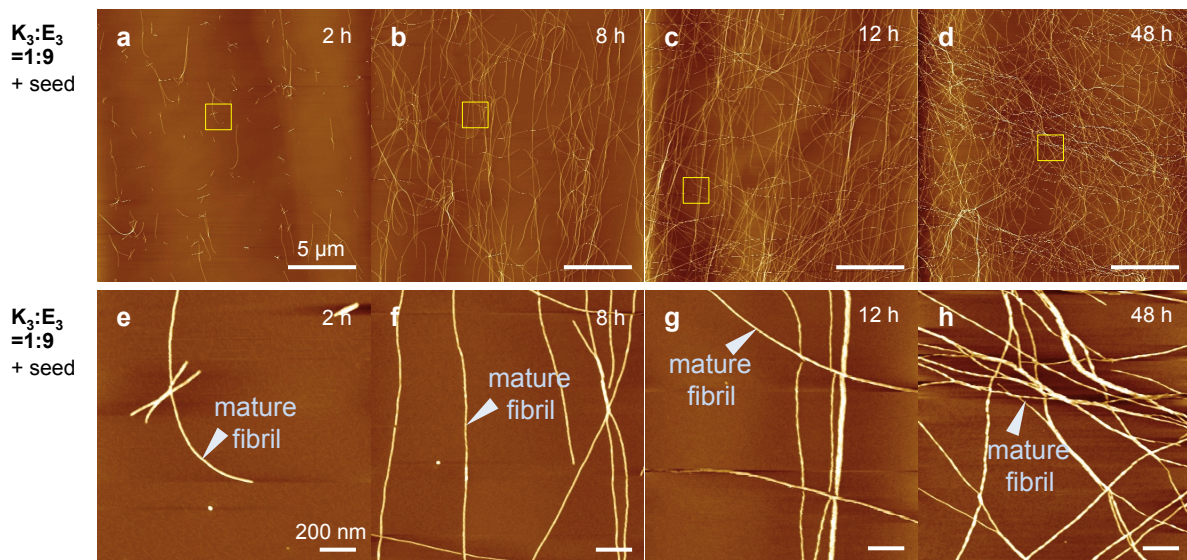
Figure 3-10. AFM images of elongating fibril structure of K_3-TTR:E_3-TTR = 1:9 of captured at the early (a,e), middle (b,f), late (c,g), and completely matured (d,h) kinetic phase based on the ThT assay shown in Figure 3-8. The images (e-h) are the magnification of selected area as shown by the each yellow square. Scale bar represents 5 μm in (a-d) and 200 nm in (e-h).
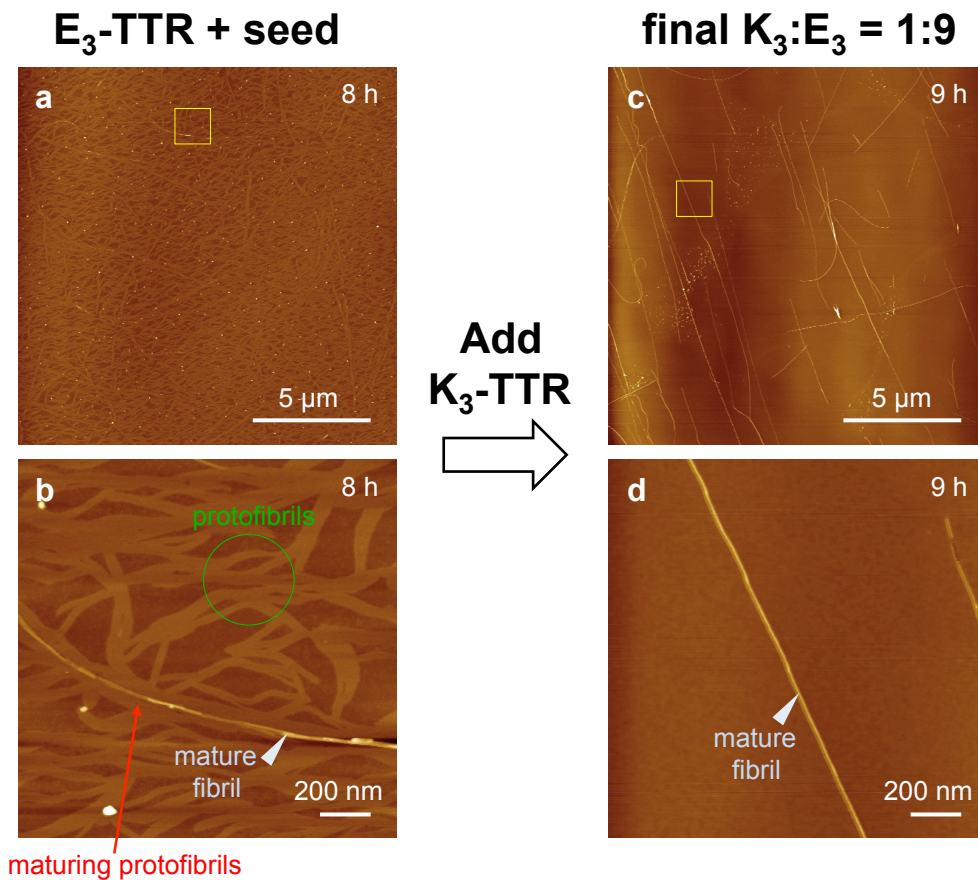
Figure 3-11. The effect of adding K_3-TTR to the solution of the preformed protofibrils using E_3-TTR. (a,b) AFM images of seeded E_3-TTR incubated for 8 h. K_3-TTR was added to the growing E_3-TTR solution after removal of aliquots for the AFM shown in (a,b). The final ratio of K_3-TTR:E_3-TTR was 1:9. (c,d) AFM images of the mixture incubated for 1 h after addition of K_3-TTR. The bottom panels (b,d) are magnified AFM images corresponding to the selected areas shown as the yellow squares in (a,c). Scale bar represents 5 μm in (a,c) and 200 nm in (b,d).

3.5. Discussion

I presented in the current study that the unique oligomerization property of mixed SCAPs controls fibrillation over the elongation phase and finally produces extremely long fibrils. Very few studies about modulation of fibril length have been reported (12,14). And, this work is the first demonstration that fibril length can be altered by elongation-specific mechanism.

A very interesting finding in the IM-MS study is that the self-assembly conditions that lead reproducibly to the extremely long fibrils (1:1 and 1:9 mixtures of K_3 and E_3-based TTR peptides) also lead to the formation of a higher number of oligomers with a remarkably extended peptide conformation arranged in parallel. By contrast, E_3-TTR, which forms short fibrils, primarily assumes oligomers with globular states. Oligomers observed by IM-MS under mixed-SCAP conditions are dimers through pentamers and the data indicate a non-isotropic one-dimensional growth from monomer to dimer up to the pentamer. This finding shows that a fibril-like arrangement of the peptide units is already present at the oligomer stage. The parallel fibrillar arrangement is known to be the structural element responsible for the fibrils of not only the native TTR(105-115) peptide but also various modified versions (42-50), thus indicating the existence of the same structural element in fibrils formed under our SCAP conditions. Hence, it is possible that the unique oligomerization property of mixed SCAPs affects the assembling process of soluble peptides into fibrils. Perhaps the interaction of the E_3 and K_3 units with one another mediates an appropriate binding mode among the core TTR(105-115) sequences to form the parallel extended arrangement. Several studies have reported that electrostatic interactions within the core sequences stabilize

intermolecular arrangement of peptides (51-53). In our mixed-SCAP system, things are likely to be more complicated because nearly all (~99%) of the carboxyl groups should theoretically be protonated at pH 2 although the presence of multiple successive carboxyl groups may lead to the local deprotonation which allows electrostatic interactions between the K_3 and E_3 units. Another possible interaction is ionic hydrogen bonding, which plays an important role in condensed phase chemistry such as crystallization and protein folding (54). Because amyloid fibrillation also takes place in condensed phase and involves some mechanistic similarities to crystallization and protein folding, ionic hydrogen bonding between Lys protonated ammonium and Glu carbonyl groups may underlie the association mechanism of mixed SCAPs.

Over the elongation phase, mixed SCAPs showed no protofibrils, and all of the fibrils adopted a mature structure regardless of their length. This completely differs from the case of E_3-TTR or general amyloid systems (24,26-29), which produced many protofibril intermediates. Ban *et al*. reported that no protofibril formation occurred in seeded fibrillation (55), but that a secondary nucleation pathway similar to the pathway in our system can form protofibrils (56-58). Furthermore, I observed no protofibril formation in non-seeded fibrillization of mixed SCAPs (Figure 3-12). Moreover, addition of K_3-TTR into the protofibril solution of E_3-TTR readily altered the morphology to the matured form (Figure 3-11). Therefore, the rapid maturation process must be a unique mechanism underlying mixed-SCAP systems, possibly resulting from the unique oligomerization of mixed SCAPs.

It is reported that cytotoxic globular oligomers are composed of β barrel-like structure, named cylindrin, in which the number and pattern of hydrogen bonding are different from those in mature amyloid fibrils (59,60). Generally, nuclei are generated

E₃-TTR non-seeded **K₃:E₃ = 1:1 non-seeded**
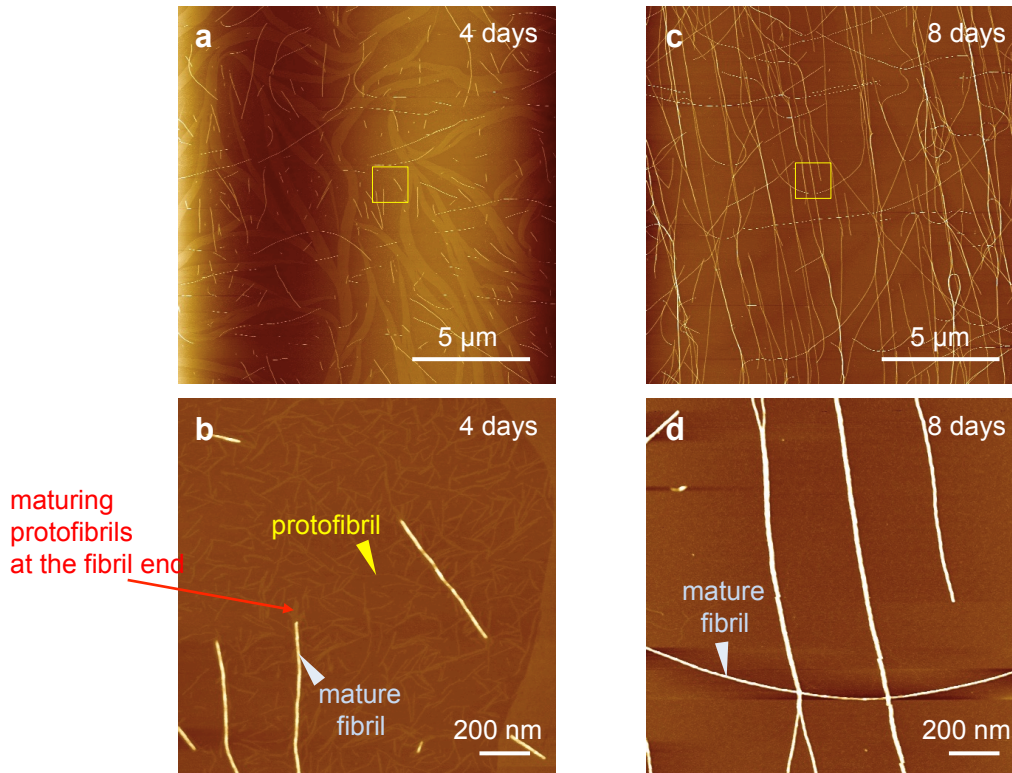
Figure 3-12. AFM images of E_3-TTR (a,b) and K_3-TTR:E_3-TTR = 1:1 (c,d) incubated for 4 and 8 days, respectively, without seeding. The bottoms (b,d) are magnified AFM images corresponding to the selected areas shown as the yellow squares in (a,c). Scale bar represents 5 μm in (a,c) and 200 nm in (b,d).

from the globular oligomer species (cytotoxic oligomers), and protofibrils subsequently emerge by addition of monomer peptides, not oligomers, onto the nuclei (61,62) (see also Figure 1-1). Therefore, peptides in nuclei and protofibrils have a less-structured β conformation with different hydrogen-bond arrangement (63,64), and conformational reorganization is required during the maturation process, making maturation a slow and rate-limiting step in elongation phase (63). This pathway can explain the fibrillation of E_3-TTR since it forms globular oligomers and protofibrils (Figure 3-13a). However, the unique oligomerization property of mixed SCAPs, which can stabilize an extended peptide structure within small oligomers, could alter the elongation mechanism (Figure 3-13b). Because of the unique oligomerization property, mixed SCAPs must form extended protofibrils. And, these protofibrils possibly readily assemble into fibrils with a mature structure since very small conformational rearrangement for maturation should be required. Furthermore, the presence of the stable extended oligomers may allow peptides to be added as an oligomer unit. This should be a great advantage for long fibril formation because addition of the extended oligomers to the fibril end is possible even when monomer peptides cannot be added due to, for example, reduced catalytic activity of fibril end for conformational conversion of monomers to fit to the β structure. These two possible aspects, oligomer addition and rapid maturation, allow the formation of extremely long fibrils (Figure 3-13b).

The traditional model of elongation kinetics defines elongation step as only the addition of a monomer peptide to the fibril end (65,66). My data suggest that at least two steps have to be separately considered: addition of soluble peptide and maturation of protofibrils. Furthermore, oligomer addition mechanism may be taken into account in addition to monomer addition. Quantitative analyses of the kinetics and thermodynam-
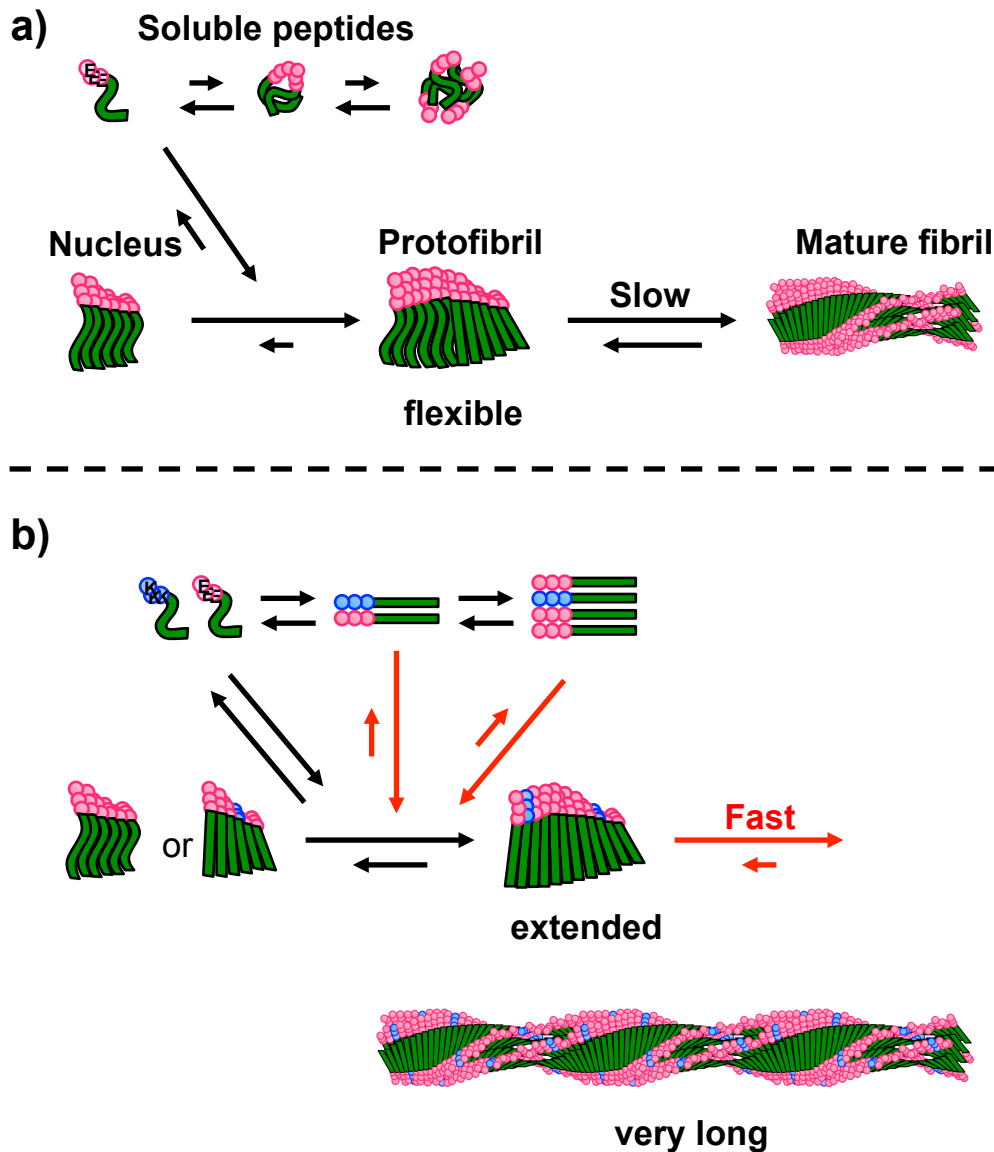
Figure 3-13. A model for explaining the mechanism of very long fibril formation by mixing SCAPs. In the elongation phase, E_3-TTR or typical amyloid peptide (a) is added to the nucleus as a monomer and produces protofibrils. Because of their flexible structure, the protofibrils require further conformational optimization to assemble into mature fibrils, making the maturation a slow process. Mixed SCAPs (b) can form extended protofibrils due to their unique oligomerization property. This type of protofibrils needs very small conformational conversion to assemble into mature fibrils, resulting in the fast maturation process. Furthermore, protofibril growth can also take place by addition of the extended oligomers, allowing the continuous growth of mature fibrils to the great length.

ics based on this mechanism may allow precise control of fibril length. The lack of reports in the literature regarding approaches to adjust fibril length highlights the importance of the mechanism of mixed-SCAP fibrillization. In addition, recent studies have demonstrated that cytotoxic species are protofibrils (and globular oligomers) and not mature fibrils (67). Traditional therapeutic strategies targeting inhibitors of oligomer and protofibril formation have not developed effective cure for amyloidosis-related diseases, and there is an emerging strategy promoting fibril formation to reduce cytotoxic species (68,69). Therefore, the presented result regarding the maturation process may provide rational approach for the strategy.

My data also suggest that the conformation of peptides in the oligomerization process could be a major determinant of the resulting fibril structure. Because the mixing of SCAPs can effectively alter oligomer formation, the use of other SCAPs with different three amino-acid-residue caps to provide novel binding modes could allow further tuning of oligomerization property. Such tuning may introduce opportunities for controlling or tailoring the macroscopic fibrillar assembly, which is one of the key steps for the development of functional nanomaterials and nanodevices. IM-MS may be a good approach for analyses of oligomerization properties in such a mixed peptide system. Identifying the relationships between oligomerization and macroscopic fibril structure would allow the development of practical approaches for precise control of fibril architecture.

4. Development of Fibril-Patterning Methods for the Creation of Functional Nanocircuitry

4.1. Abstract

The patterning of self-assembled nanowires is a key process for creating nanocircuitry and nanodevices using these bottom-up nanomaterials. The current study presents two simple methods for directional and positional control of our SCAP-based functional nanowires. An easily preparable water flow system with a thickness of 0.2 mm thickness, width of 1 mm width and lengths of 10–20 mm was applied to our functionalized or probed nanowires yielded by mixing SCAPs with F/P-SCAPs, which allowed the alignment of these nanowires along the flow direction. Probe-specific functional materials could also be conjugated to the aligned probed nanowires. It was possible to control the initiation position of the fibrils by targeting gold nanoparticles present on the substrate surface with specific α-lipoyl fibril seeds with subsequent incubation of the mixed-SCAP solution with the seeded nanoparticles. The resulting individual fibrils were formed from one nanoparticle. This is the first demonstration of positional control of each fibril among amyloid systems. These two methods together with other techniques such as nanolithography could open up new approaches for precise patterning or integration of our bottom-up functionalized nanowires.

4.2. Introduction

The advantages of functionalized nanowires derived from the one-dimensional geometry with tunable functional properties make them essential components in various nanodevices including chemo- and bio-sensors (1), light-emitting diodes (2-4), photodiodes (5,6), and field effect transistors (7,8). Although a top-down approach based on lithographic techniques (9) has widely been developed to manufacture commercial nanodevices, it is facing fundamental physical and economic limitations (10). By contrast, a bottom-up approach on the basis of molecular self-assembly has been developed to address these physical and economic issues (11,12). This is because the bottom-up methods allow the formation of nanowires much more effectively than top-down methods, which is promising for the development of next-generation nanoelectronic devices if integrated circuits are realized using the bottom-up nanowires. Our SCAP strategy should garner attention among bottom-up methods because of its ability to confer diverse and arbitrary functions to nanowires as described in Chapter 2 (13).

Patterning nanowires is a key process to construct functional nanocircuitry and use them in electronic devices (14,15). However, the bottom-up approach still involves a considerable challenge in controlling the placement and orientation of nanowires. The Langmuir-Blodgett (LB) technique is one of the most common approaches for preparation of nanowire arrays (16-18). However, the LB method requires modification of nanowires with hydrophobic groups. Other approaches using magnetic force (19), dielectrophoresis (20), microfluidics (19,21,22), and equipment for direct manipulation of individual nanowires (23) have been developed, but they depend on particular

properties of nanowires or need specific instruments that make it difficult or costly to achieve nanowire patterning at a large scale. Furthermore, these methods cannot be applied to our functionalized nanowires formed from peptide building blocks.

In the present study I show two approaches to control the direction and position of nanowires. A simple water flow system allowed the alignment of functionalized or probed nanowires preformed by our SCAP-mixing method. The aligned probed nanowires can also be functionalized with specific molecules. In addition, I demonstrate that seeding gold nanoparticles present on the surface with gold-specific sonicated fibrils is effective for initiation of fibril formation from a single nanoparticle and is thus useful for controlling the initial position of the nanowires.

4.3. Experimental Procedures

Peptide Synthesis

Peptides were synthesized with a standard Fmoc-chemistry on Rink amide resin automatically with an Applied Biosystems 433A peptide synthesizer (Applied Biosystems Inc., Foster City, CA) or manually. All N-terminal modifications, biotin, maleimide, tetramethylrhodamine, and fluorescein were carried out on the resins. Biotin or α-lipoic acid was coupled by the use of 10 eq. D-Biotin (Sigma) or DL-α-lipoic acid (Watanabe Chem.), 10 eq. HBTU/HOBt, and 20 eq. DIEA in NMP for 1 h or 30 min, respectively. Maleimide coupling was performed with a mixture of 2 eq. 3-maleimidopropionic acid (*N*-maleoyl-β-alanine, Aldrich), and 1 eq. WSCI in DMF/DCM = 1/1, for 1 h. For fluorescent modifications, the N-terminal-free peptide resins were washed once using 2 M DIEA/NMP and twice with NMP prior to coupling. Fluorescein and tetramethylrhodamine were coupled with 1.2 eq. NHS-Fluorescein (Pierce) and NHS-Rhodamine (Pierce) for 12 h, respectively. The peptides, except for one modified with maleimide, were then deprotected and cleaved with reagent K (TFA/H_2O/phenol/thioanisole/ethaneditiol = 82.5/5/5/5/2.5) over two-hour incubation to yield crude peptide materials. The cleavage of maleimide peptides were performed with TFA/H_2O = 95/5 for 2 h. All crude materials were subsequently purified using a reverse-phase HPLC (SCL-10A, SPD-10A, DGU-12A, LC-6AD, Shimadzu) with a C-8 column (22 x 250 mm, Cat. No. 208TP1022, Vydac) eluted with a linear gradient of water and acetonitrile containing 0.05 and 0.04% TFA, respectively. The peptides were obtained in ≥95% purity determined by reverse-phase HPLC (PU-980, UV-970, HG-980-31, DG-980-50, Jasco) with a C8 column (4.6 x 250 mm, Cat. No. 208TP104,

Vydac), and were identified by MALDI-TOF-MS (voyager System 6171, Applied Biosystems, in Stractural Chemistry Laboratory or at the OPEN FACILITY in Sousei Hall).

Fibril Formation

The 8 mM stock solutions of each peptide and mixture were diluted by a factor of 40 in aqueous solution at pH 2.0 (adjusted by HCl), and incubated in plastic tubes at 37 °C. UVmini-1240 spectrophotometer (Shimadzu) was utilized for measurements of stock solution concentration. The extinction coefficient of $\varepsilon_{276} = 2900$ $M^{-1}cm^{-1}$, derived from the two tyrosine residues at 100 mM sodium phosphate (pH 7.0) in the presence of 6 M guanidine hydrochloride (Ref), were used for calculation.

Alignment of Fibrils by Water Flow

To prepare water flow path a sample substrate, mica (Cat. No. 990066, Nilako, Japan) for AFM or a cover glass (Micro Cover Glass 18 × 18 mm, Cat. No. C018181, Matsunami Glass, Osaka, Japan) for fluorescence microscopy, was spaced from a large cover glass (NEO Microscope Cover Glass 24 × 40 mm, Cat. No. C024451, Matsunami Glass) with vinyl tapes of 0.2 mm thick (Cat. No. 200-19, Yamato, Japan). The width of the flow path was adjusted to ca. 1 mm by sight. The final dimension of the flow path was 0.2 mm thick, 1 mm wide, and 10~20 mm long (depending on the size of sample substrates). 10 µl suspension of preformed fibrils was introduced into the flow path from one side and simultaneously absorbed with filter paper on the other side to generate water flow. The sample substrate surface was subsequently washed three times with 10 µl of ultra-pure water, then by immersion in a plethora of water for 15 seconds.

Modification of Probed Nanowires with Functional Materials

For modification of biotin-probed nanowires, 10 µl suspension of 5-fold diluted avidin magnetic beads (MACS, Cat. No. 130-048-102, Miltenyi Biotec) was incubated for 15 min on a shaker immediately after adsorption of the biotinylated nanowires. Maleimide-probed nanowires were functionalized with 10 µM F-TBP-Cys aqueous solution buffered by 10 mM phosphate (pH 7.4) for 10 min. After incubation the sample substrates were dipped in copious water for 15 seconds to wash the surface and dried in air.

Exchanging the Ligand of Gold Nanoparticles

BSPP was utilized as an alternative ligand of gold nanoparticles stabilized by citrate (Colloidal gold/SC ϕ = 40 nm, Lot No. A070629-1F, Tanaka Kikinzoku Kogyo, Japan). The gold colloid particles were centrifuged at 14,000 × g for 15 min at room temperature with MiniSpin Plus (Eppendorf, Germany) and the supernatant was substituted by fleshly prepared BSPP aqueous solution at a concentration of 1 mg/mL. This mixture of BSPP and gold particles was then incubated overnight at room temperature. After incubation, the nanoparticles were washed twice with 1 mg/mL BSPP by centrifugation at the same condition as above and exchange of the supernatant. The obtained BSPP-stabilized gold nanoparticle suspension was kept at 4ºC for experiments.

Control of Initiation Position of Fibrils with a Gold Nanoparticle

To immobilize gold nanoparticles on mica, the surface was precoated with PLL (M_W = 15-30 k, Cat. No. P7890, Sigma) by incubation at a concentration of 1 mg/mL

for 1 min and by subsequent wash with ultra-pure water (1 mL × 3) and dry in air. 10-fold diluted suspension of gold nanoparticles was incubated on the PLL-coated mica surface for 5 min and the surface was washed and dried similarly. PLL was employed again by the same procedure for recoating the surface. The immobilized gold nanoparticles were then modified with seed fibrils with α-lipoyl groups, prepared by sonication of preformed fibrils formed from a mixture of K_3-TTR:Lip-E_3-TTR:E_3-TTR = 1:1:8 with W-113 MK-II ultrasonic disperser (Honda Electronics, Aichi, Japan) for 30 min, by incubation of the seed suspension diluted with 0.01 M HCl by a factor of three on the surface for 5 min. After the surface was washed, dried and measured by AFM, 8 µl of a peptide solution of K_3-TTR:E_3-TTR = 1:1 at a total peptide concentration of 200 µM was incubated in a double-stacked silicon chamber (CultureWell multiwell chambered coverslip, 3 mm diameter and 1 mm depth, 3-10 µl, Cat. No. CW-50R-1.0, Grace Bio-Labs, Oregon, USA), mounted on the surface and sealed with a cover glass (Round Micro Cover Glass 15 mm dia., Cat. No. C015001, Matsunami Glass, Osaka, Japan), at 37ºC for 12 hours. Subsequently, the surface was washed and dried in air.

Atomic Force Microscopy

AFM measurements were performed using a Nanoscope IIIa system (Digital Instruments, Santa Barbara, CA) with a standard silicon cantilever (OMCL-AC240TS, Olympus). Images were captured at 512 × 512 pixel resolution at a scan rate of 0.25 Hz with a typical condition of 60-80 kHz of drive frequency, and 1.6-1.8 V of amplitude set point.

Fluorescence Microscopy

Fluorescence microscopy was performed using a BIOREVO BZ-9000 confocal microscope (Keyence) with a GFP-BP filter (excitation, 470±40 nm; emission, 520±35 nm; dichroic, 495 nm long pass), or a TRITC filter (excitation, 540±25 nm; emission, 605±55 nm; dichroic, 565 nm long pass). Shutter speed was set at 3.5 sec for green, and 1.0 sec for red fluorescence observation.

4.4. Results

4.4.1. Directional Control of Functionalized Nanowires by Water Flow

We developed a system to control the directional alignment of nanofibrils by water flow. Figure 4-1 represents a schematic representation of this system involving a narrow flow path with a thickness of 0.2 mm, a width of 1 mm, and an arbitrary length, ranging from 10 to 20 mm in this study, developed manually between a cover glass and a substrate surface. Water flow can be generated by coincident injection and absorption of water from one side with a micropipette to the other side with a sheet of filter paper. Fibrils can be adsorbed to the substrate surface under the influence of the flow. Hence, applying this system to our remarkably long functionalized nanowires created from SCAP mixtures allows construction of long-range arrangements of functional molecules in a particular direction on the surface. Fibrils of a 1:1 K_3-TTR:E_3-TTR mixture were first employed and successfully aligned in line with the flow direction, as measured by AFM (Figure 4-2a). Similarly, fibrils functionalized with tetramethylrhodamine molecules (K_3-TTR:TMR-E_3-TTR:E_3-TTR = 1:1:8 fibrils) were subjected to flow, and a clear alignment of the red fluorescence over 60 μm was observed (Figure 4-2b), which indicates that this flow method in conjunction with our mixed-SCAP fibrils can create long-scale alignment of functional molecules in a desired direction. This system was also applied to nanowires probed with biotin or maleimide groups formed from K_3-TTR:Bio-E_3-TTR:E_3-TTR = 1:1:8 or K_3-TTR:Mal-E_3-TTR:E_3-TTR = 5:1:4, respectively. Specific functional materials, i.e., avidin magnetic beads or the functional peptide F-TBP-Cys (Fluorescein-G-RKLPDA-GG-C-amide), were subsequently incubated with the fibrils on the surface. AFM and fluorescence microscopy depicted
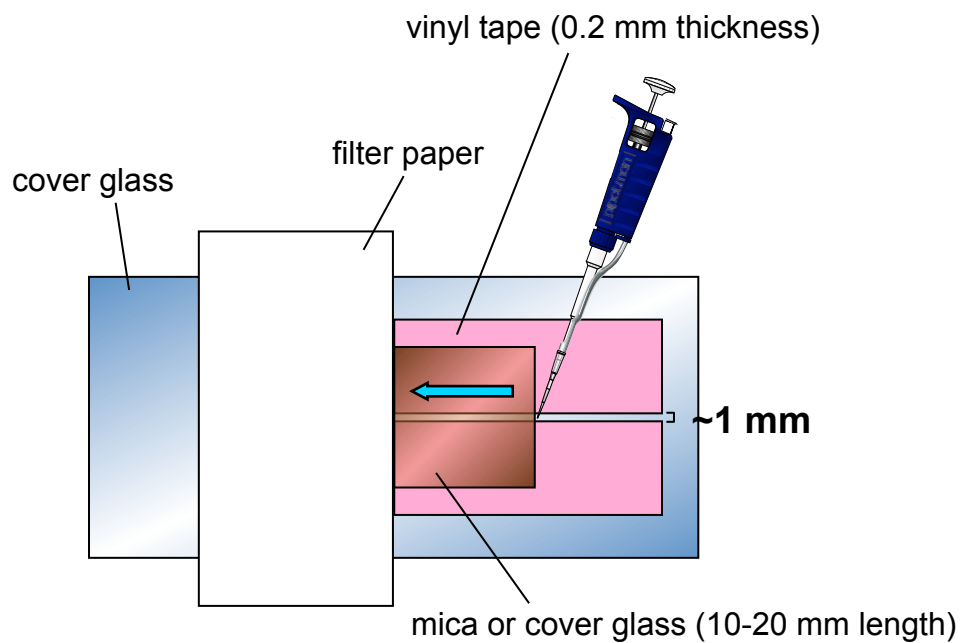
Figure 4-1. Schematic representation of a flow system. The flow path is composed of two substrates and a vinyl tape spacer, yielding the dimensions of 1 mm width, 0.2 mm height and 10-20 mm length. The fibril suspension is injected from one side and the flow is generated by absorption of the injected sample suspension from the other side. Thus, fibrils can be adsorbed on the substrate surface under the influence of water flow.
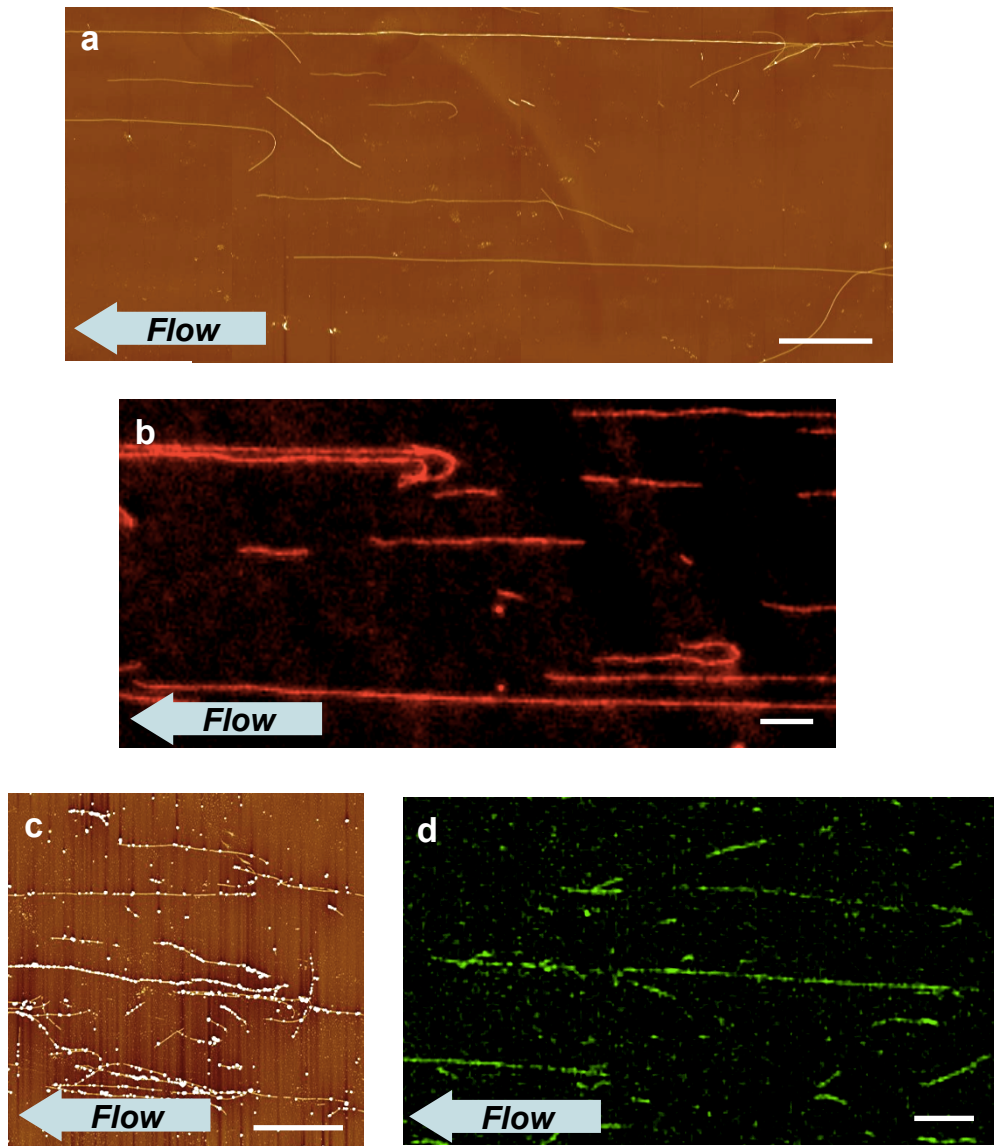
Figure 4-2. Directional control of functionalized nanowires by the flow system displayed in Figure 4-1. Alignment of (a) mixed-SCAP fibrils, (b) F-SCAP-functionalized nanowires and (c,d) P-SCAP-functionalized fibrils. (a) K_3-TTR:E_3-TTR = 1:1, (b) K_3-TTR:TMR-E_3-TTR:E_3-TTR = 1:1:8, (c) avidin magnetic bead array on K_3-TTR:Bio-E_3-TTR:E_3-TTR = 1:1:8, and (d) F-TBP-Cys-functionalized K_3-TTR:Mal-E_3-TTR:E_3-TTR = 5:1:4 fibrils. The probe-specific functional materials were conjugated after fibril alignment. Scale bars are 5 μm.

the arrangement of these materials onto the aligned fibrils (Figures 4-2 c and d). Therefore, specific modification of patterned fibrils has been demonstrated to be possible. These data obviously show the usefulness of the flow system for directional control of various functional nanowires and nanomaterials.

4.4.2. Control of the Initiation Position of Fibrils Using a Gold Nanoparticle

The strategy for controlling the initiation position of fibrils is schematically shown in Figure 4-3, where seed fibrils are specifically attached to surface-immobilized gold nanoparticles, followed by elongation of fibrils by incubation with a SCAP mixture. Gold-specific seeds were prepared by sonicating α-lipoyl-probed fibrils formed from a SCAPs mixture of K_3-TTR:Lip-E_3-TTR:E_3-TTR = 1:1:8 (Figure 4-4). To achieve the highly dispersed adsorption of gold nanoparticles, the gold ligand was exchanged from the originally used citrate to bis(p-sulfonatophenyl)phenylphosphine (BSPP). BSPP has a phosphine backbone with a high affinity for gold and two benzylsulfonate groups with a very low pKa of -2.8 (24), and it has been widely utilized in systems for modifying gold nanoparticles with biomolecules (25). Use of the BSPP stabilizer led to more dispersion of immobilized gold nanoparticles relative to citrate as indicated by an AFM study of the PLL-coated mica surface after incubation of the two types of gold nanoparticles (Figures 4-5 a and b). After the surface was recoated with PLL, which can block nonspecific (electrostatic) adsorption of fibrils (26), the α-lipoyl seeds were incubated with the fixed gold nanoparticles. AFM shows that the seeds were attached to the gold nanoparticles (Figures 4-5 e–i) but mainly not on the surface (Figure 4-5c), which suggests specific conjugation of the seeds with the gold nanoparticles.

Gold nanoparticle　　**α-lipoyl seed**

Mica surface

(1) Nanoparticle immobilization

(2) Seed attachment

(3) Nanowire formation
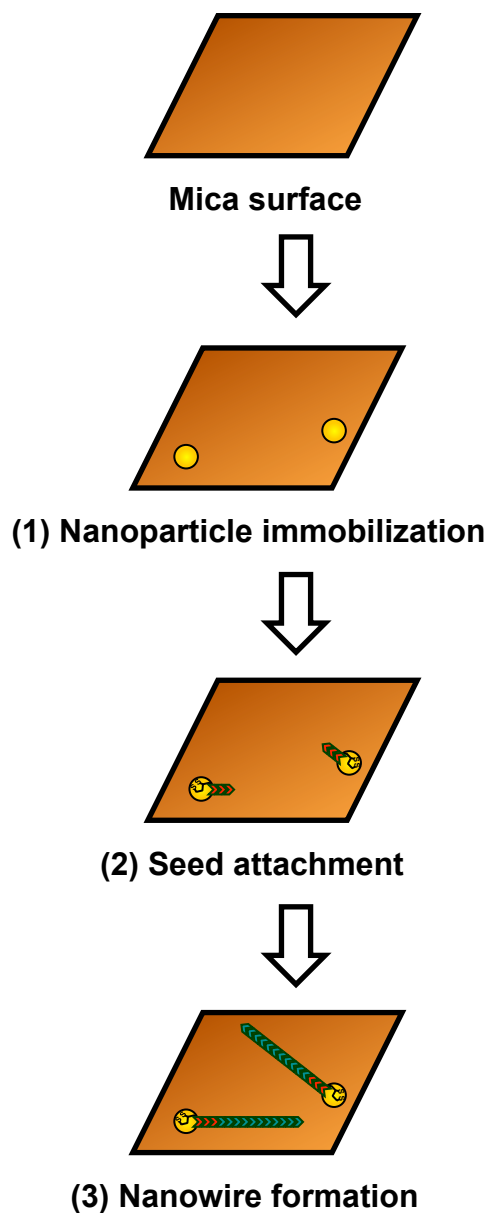
Figure 4-3. A schematic illustration of controlling the initiation position of fibrils using a gold nanoparticle. This strategy includes three steps: (1) gold nanoparticles are immobilized on a mica surface with high dispersity, (2) the nanoparticles are seeded with gold-specific sonicated fibrils with α-lipoyl groups, and (3) nanowire formation is initiated from each nanoparticle through incubation with peptide solutions.
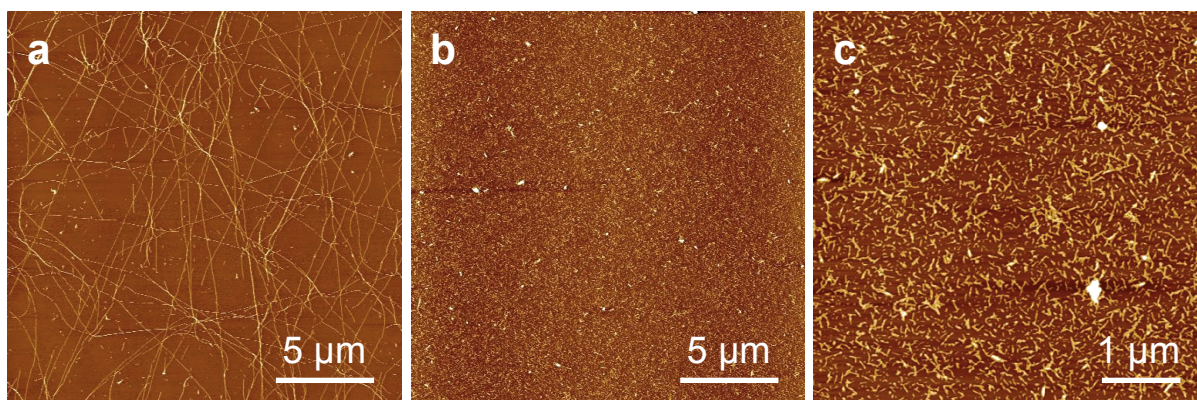
Figure 4-4. Preparation of gold-specific seeds. AFM images of (a) gold-specific fibrils formed from a mixture of K_3-TTR:Lip-E_3-TTR:E_3-TTR = 1:1:8 and (b,c) sonicated α-lipoyl fibrils with an average length of 45 ± 20 nm. The scale bars represent 5 μm in (a,b) and 1 μm in (c).
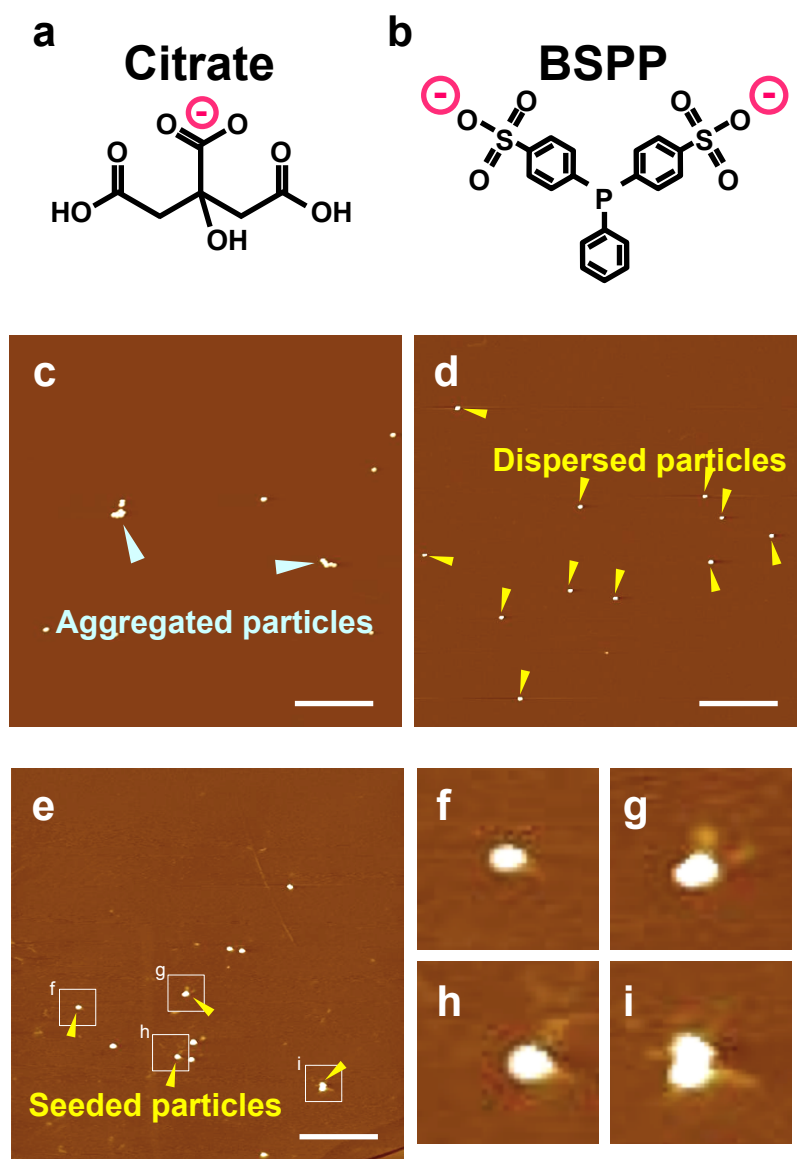
Figure 4-5. (a,b) Chemical structure of gold ligands: (a) citrate and (b) BSPP. (c,d) Effects of ligands on particle dispersity: (c) citrate-stabilized and (d) BSPP-stabilized gold nanoparticles immobilized on PLL-coated mica surface. (e-i) Seeding to BSPP-stabilized gold nanoparticles: (e) AFM image after seeding, and (f-i) digital zoom images of seeded nanoparticles corresponding to the selected areas in (e). Scale bar shows 1 μm.

To initiate fibril formation from these seeded particles, a solution of the 1:1 K_3-TTR:E_3-TTR mixture was incubated on the surface for 12 h. Consequently, fibrils initiated from a gold nanoparticle were successfully observed (Figures 4-6 a and b). This is the first demonstration of positionally controlled amyloid initiation. Statistic analysis of the fibrils and nanoparticles revealed that 75% of the total fibrils appeared to be initiated from nanoparticles, thus showing the efficacy of this method. In contrast, incubation of the 1:1 mixture with non-seeded nanoparticles on surface resulted in no fibril formation (Figure 4-6c), confirming that the fibrils formed from the seeded nanoparticles. Thus, our method using seeded gold nanoparticles is very useful for controlling the initiation position and for patterning amyloid nanowires.
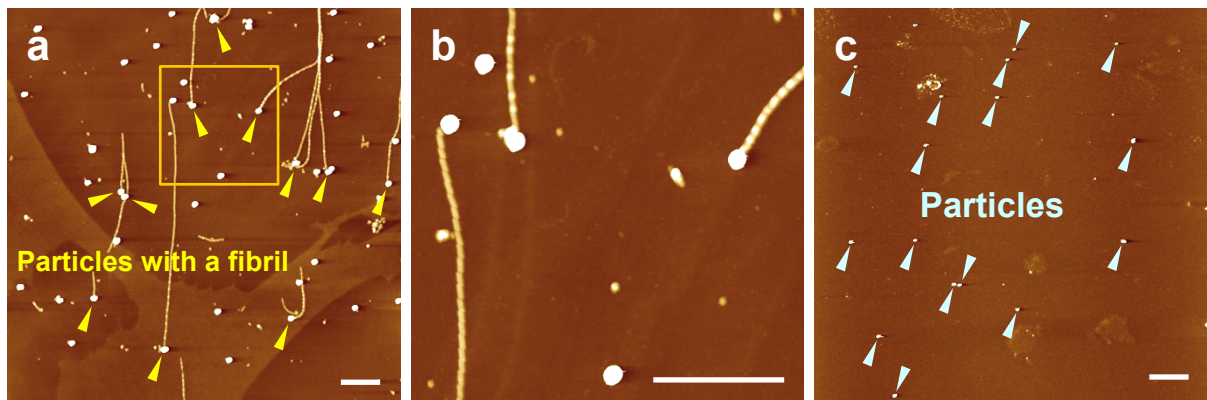
Figure 4-6. (a) K_3-TTR:E_3-TTR = 1:1 fibrils initiated from a gold nanoparticle and (b) magnified image of the selected region in (a). (c) An AMF image of unseeded gold nanoparticles after incubation with a 1:1 mixture of K_3-TTR to E_3-TTR under the same condition used for (a,b). The lack of fibril formation indicates selectively successful fibril formation from seeded nanoparticles. Scale bar shows 1 μm.

4.5. Discussion

The current study presents two approaches for patterning our extremely long mixed-SCAP nanowires: directional and positional control. Patterning of one-dimensional structures is a promising way to develop nano-scale compartments, thus creating functional nanocircuitry. These approaches, together with the ability of our SCAP-mixing method to control the structure function of fibrils, could make our SCAP strategy practical for developing next-generation nanodevices.

The flow method enables the control of fibril orientation in any desired direction, thus making it possible to adjust the relative angle between fibrils or between a fibril and another object. This capability may find use, for example, in wiring nanoelectrodes perpendicularly to the flow direction or creating a crossed-fibril pattern, which is one of the useful structures for nanodevice fabrication (27). A nanoelectrode-nanoelectrode interconnection can also be fabricated on parallel-aligned nanowires with subsequent photolithographic procedures (15). Therefore, flow-induced alignment of nanowires with various biological or molecular recognition properties imparted by our SCAP method could have great utility for developing chemical and biological sensors. Other studies focused on the use of aligned fibrils, especially collagen fibers, for control of cell culture and movement (21). Alignment of our fibrils modified with biological molecules is probably useful for such bio-nanotechnological applications.

Several approaches for orientation control of nanowires and nanofibrils, such as the LB method and flow systems using microfluidics, have been widely utilized to date (16-19,21,22). Compared with those approaches, the advantages of our method involve a simple setup that is applicable for various substrates at relatively large scale and

requires no other reagents. Furthermore, the ability of our SCAP method to form extremely long nanowires allows this flow system to create long-range parallel alignment of functional nanomaterials.

I, for the first time, presented the control of the initiation position of amyloid fibrils by using a gold nanoparticle and gold-specific seed modified with α-lipoyl groups. Positional control of nanowires and fibrils remains challenging although it is one of the most important processes for developing nanodevices (14). The fact that very few studies have achieved this to date (20,22) highlights the importance of our study. The method targeting gold nanoparticles present on the surface could also be applied to a gold nanostructure array constructed by photolithographic techniques. Hence, this approach may have practical use in the development of top down-bottom up hybrid methods through interconnection of gold nanoelectrodes.

In summary, I have developed two distinct ways to control the direction or initiation position of nanowires on a substrate surface. The use of these two approaches mixed together or with mechanistic controls of fibrillation would be useful to achieve highly ordered nanowire patterns and construct functional nanocircuitry.

5. Conclusions

In this study, I presented a novel methodology for controlling amyloid fibrillation based on mixing multiple SCAPs. This strategy allowed effective formation of various modified amyloid fibrils and also modulation of fibril architectures. Because these two aspects are of great importance to create functionalized nanowires, mixing of SCAPs should be a promising methodology for developing nanowire-based materials and devices. For example, the ability to form diverse functionalized nanowires makes it possible to obtain nanowires with various sensing capabilities based on the materials attached to the fibrils. The hybrid method with biomineralization enables the application of these nanowires in nanoelectronic devices. Because of their peptidic nature, our nanowires could find applications in the field of bionanotechnology.

I demonstrated an impressive fibril growth mechanism: oligomerization property alters the elongation process and determines the final architecture of fibrils. IM-MS successfully revealed the unique oligomerization property of mixed SCAPs, through which mixed oligomers adopt an extended structure with a high oligomer number. This property presumably alters two mechanisms of elongation: one of which is that the extended oligomers can possibly be added to the growing end as a unit, and the other is that the unique oligomerization property also induces an extended structure of protofibrils which makes maturation process very fast. These two mechanisms can explain the entire elongation mechanism of mixed SCAPs. This insight may find use in tailoring fibril architecture, which is one of the most important procedures to develop bottom-up nanowire-based devices. Alteration of oligomerization properties by, for example, adding another SCAP with a different unit may provide further control of

fibril structure. The mechanism of acceleration of maturation process could also be applied to the development of rational therapeutic approaches against amyloidosis. Therefore, further mechanistic study of mixed-SCAP fibrillation has to be proceeded. Mixing of SCAPs must affect the nucleation process as well because mixed SCAPs enabled fibril formation of modified SCAPs, which did not self-assemble by themselves or when mixed with E_3-TTR. This mechanism also has to be elucidated.

Finally, I demonstrated very simple methods for controlling the orientation and initiation position of nanowires. These methods could be used for interconnection of two or more nanoelectrodes to implant them into functional nanocircuitry.

In summary, the presented methods and discoveries regarding the effective functionalization, control of fibril architecture, and patterning shed new light on the fields of nanotechnology, nanobiotechnology, and therapeutics.

References

Chapter 1

[1] Zheng, G., Lu, W., Jin, S., Lieber, C. M. (2004) Synthesis and fabrication of high-performance n-type silicon nanowire transistors. *Adv. Mater.* **16**, 1890-1893.

[2] Yang, C., Zhong, Z., Lieber, C. M. (2005) Encoding electronic properties by synthesis of axial modulation-doped silicon nanowires. *Science* **310**, 1304-1307.

[3] Bryllert, T., Wernersson, L.-E., Fröberg, L. E., Samuelson, L. (2006) Vertical high-mobility wrap-gated InAs nanowire transistor. *IEEE Elect. Dev. Lett.* **27**, 323-325.

[4] Xiang, J., Lu, W., Hu, Y., Wu, Y., Yan, H., Lieber, C. M. (2006) Ge/Si nanowire heterostructures as high-performance field-effect transistors. *Nature* **441**, 489-493.

[5] Lee, P., Lee, J., Lee, H., Yeo, J., Hong, S., Nam, K. H., Lee, D., Lee, S. S., Ko, S. H. (2012) Highly stretchable and highly conductive metal electrode by very long metal nanowire percolation network. *Adv. Mater.* **24**, 3326-3332.

[6] Patolsky, F., Zheng, G., Hayden, O., Lakadamyali, M., Zhuang, X., Lieber, C. M. (2004) Electrical detection of single viruses. *Proc. Natl. Acad. Sci. USA* **101**, 14017-14022.

[7] Liu, H., Kameoka, J., Czaplewski, D. A., Craighead, H. G. (2004) Polymeric nanowire chemical sensor. *Nano Lett.* **4**, 671-675.

[8] Wang, X., Zhou, J., Song, J., Liu, J., Xu, N., Wang, Z. L. (2006) Piezoelectric field effect transistor and nanoforce sensor based on a single ZnO nanowire. *Nano Lett.* **6**, 2768-2772.

[9] Kuang, Q., Lao, C., Wang, Z. L., Xie, Z., Zheng, L. (2007) High-sensitivity

humidity sensor based on a single SnO$_2$ nanowire. *J. Am. Chem.* Soc. **129**, 6070-6071.

[10] Zheng, G., Gao, X. P. A., Lieber, C. M. (2010) Frequency domain detection of biomolecules using silicon nanowire biosensors. *Nano Lett.* **10**, 3179-3183.

[11] Su, S., Wei, X., Zhong, Y., Guo, Y., Su, Y., Huang, Q., Lee, S.-T., Fan, C., He, Y. (2012) Silicon nanowire-based molecular beacons for high-sensitivity and sequence-specific DNA multiplexed analysis. *ACS Nano* **6**, 2582-2590.

[12] Hu, H., Shao, M., Zhang, W., Lu, L., Wang, H., Wang, S. (2007) Synthesis of layer-deposited silicon nanowires, modification with Pd nanoparticles and their excellent catalytic activity and stability in the reduction of methylene blue. *J. Phys. Chem. C* **111**, 3467-3470.

[13] Formo, E., Lee, E., Campbell, D., Xia, Y. (2008) Functionalization of electrospun TiO$_2$ nanofibers with Pt nanoparticles and nanowires for catalytic applications. *Nano Lett.* **8**, 66-672.

[14] Ge, D., Hu, L., Wang, J., Li, X., Qi, F., Xu, J., Cao, X., Gu, H. (2013) Reversible hyadrogenation-oxidation dehydrogenation of quinolones over a highly active Pt nanowire catalyst under mild conditions. *ChamCatChem* **5**, 1-4.

[15] Liao, L., Zhang, Yan, B., Zheng, Z., Bao, Q. L., Wu, T., Li, C. M., Shen, Z. X., Zhang, J. X., Gong, H., Li, J. C., Yu, T. (2009) Multifunctional CuO nanowire devices: p-type field effect transistors and CO gas sensors. *Nanotechnology* **20**, 085203.

[16] Zhang, X., Zhang, T., Ng, J., Sun, D. D. (2009) High-performance multifunctional TiO$_2$ nanowire ultrafiltration membrane with a hierarchical layer structure for water treatment. *Adv. Funct. Mater.* **19**, 3731-3736.

[17] Menzel, A., Subannajui, K, Güder, F., Moser, D., Paul, O., Zacharias, M. (2011) Multifunctional ZnO-nanowire-based sensor. *Adv. Funct. Mater.* **21**, 4342-4348.

[18] Ates, E. S., Unalan, H. E. (2012) Zinc oxide nanowire enhanced multifunctional coatings for cotton fabrics. *Thin Solid Films* **520**, 4658-4661.

[19] Dehon, A. (2005) Nanowire-based programmable architectures. *ACM J. Emer. Technol. Comput. Syst.* **1**, 109-162.

[20] Zhong, Z., Wang, D., Cui, Y., Bockrath, M. W., Lieber, C. M. (2003) Nanowire crossbar arrays as address decoder for integrated nanosystems. *Science* **302**, 1377-1379.

[21] Lu, W., Lieber, C. M. (2007) Nanoelectronics from the bottom up. *Nature Mater.* **6**, 841-850.

[22] Fischer, K. E., Alemán, B. J., Tao, S. L., Daniels, R. H., Li, E. M., Bünger, M. D., Nagaraj, G., Singh, P., Zetti, A., Desai, T. A. (2009) Biomimetic nanowire coatings for next generation adhesive drug delivery. *Nano Lett.* **9**, 716-720.

[23] Uskoković, V., Lee, P. P., Walsh, L. A., Fischer, K. E., Desai, T. A. (2012) PEGylated silicon nanowire coated silica microparticles for drug delivery across intestinal epithelium. *Biomaterials* **33**, 1663-1672.

[24] Licht, M., Uchugonove, A., König K., Straub, M. (2012) Sub-15 fs mutiphoton lithography of three-dimensional structures for live cell applications. *J. Opt.* **14**, 065601.

[25] Bhattacharya, M., Malinen, M. M., Lauren, P., Lou, Y.-R., Kuisma, S. W., Kanninen, L., Lille, M., Corlu, A., GuGuen-Guillouzo, C., Ikkala, O., Laukkanen, A., Urtti, A., Yliperttula, M. (2012) Nanofibrillar cellulose hydrogel promotes three-dimensional liver cell culture. *J. Cont. Rel.* **164**, 291-298.

[26] Zhang, S. (2003) Fabrication of novel biomaterials through molecular self-assembly. *Nat. Biotechnol.* **21**, 1171-1178.

[27] Lim, Y.-b., Moon, K.-S., Lee, M. (2009) Recent advances in functional supramolecular nanostructures assembled from bioactive building blocks. *Chem. Soc. Rev.* **38**, 925-934.

[28] Lieber, C. M., Wang, Z. L. (2007) Functional nanowires. *MRS Bulletin* **32**, 99-108.

[29] Patolsky, F., Timko, B. P., Zheng, G., Lieber, C. M. (2007) Nanowire-based nanoelectronic devices in the life sciences. *MRS Bulletin* **32**, 142-149.

[30] Duan, X., Lieber, C. M. (2000) General synthesis of compound semiconductor nanowires. *Adv. Mater.* **12**, 298-302.

[31] Cui, Y., Duan, X., Hu, J., Lieber, C. M. (2000) Doping and electrical transport in silicon nanowires. *J. Phys. Chem. B* **104**, 5213-5216.

[32] Duan, X., Huang, Y., Cui, Y., Wang, J., Lieber, C. M. (2000) Indium phosphide nanowire as building blocks for nanoscale electronic and optoelectronic devices. *Nature* **409**, 66-69.

[33] Cui, Y., Lieber, C. M. (2001) Functional nanoscale electronic devices assembled using silicon nanowire building blocks. *Science* **291**, 851-853.

[34] Tian, B., Zheng, X., Kempa, T. J., Fang. Y., Yu, N., Yu, G., Huang, J., Lieber, C. M. (2007) Coaxial silicon nanowires as solar cells and nanoelectronic power sources. *Nature* **449**, 885-889.

[35] Kempa, T. J., Tian, B., Kim, D. R., Hu, J., Zheng, X., Lieber, C. M. (2008) Single and tandem axial p-i-n nanowire photovoltaic devices. *Nano Lett.* **8**, 3456-3460.

[36] Jiang, X., Tian, B., Xiang, J., Qian, F., Zheng, G., Wang, H., Mai, L., Lieber, C. M. (2011) Rational growth of branched nanowire heterostructures with synthetically

encoded properties and function. *Proc. Natl. Acad. Sci. USA* **108**, 12212-12216.

[37] Gudiksen, M. S., Lauhon, L. J., Wang, J., Smith, D. C., Lieber, C. M. (2002) Growth of nanowire superlattice structures for nanoscale photonics and electronics. *Nature* **415**, 617-620.

[38] Huang, Y., Duan, X., Lieber, C. M. (2005) Nanowires for integrated multicolor nanophotonics. *Small* **1**, 142-147.

[39] Park, H.-G., Barrelet, C. J., Wu, Y., Tian, B., Qian, F., Lieber, C. M. (2008) A wavelength-selective photonic-crystal waveguide coupled to a nanowire light source. *Nature Photon.* **2**, 622-626.

[40] Cui, Y., Wei, O., Park, H., Lieber, C. M. (2001) Nanowire nanosensors for highly sensitive and selective detection of biological and chemical species. *Science* **293**, 1289-1292.

[41] Briseno, A. L., Mannsfeld, S. C. B., Lu, X., Xiong, Y., Jenekhe, S. A., Bao, Z., Xia, Y. (2007) Fabrication of field-effect transistors from hexathiapentacene single-crystal nanowires. *Nano Lett.* **7**, 668-675.

[42] Wakayama, Y., Hayakawa, R., Chikyow, T., Machida, S., Nakayama, T., Egger, S., de Oteyza, D. G., Dosch, H., Kobayashi, K. (2008) Self-assembled molecular nanowires of 6,13-bis(methylthio)pentacene: growth, electrical properties, and applications. *Nano Lett.* **8**, 3273-3277.

[43] Hill, J. P., Jin, W., Kosaka, A., Fukushima, T., Ichihara, H., Shimomura, T., Ito, K., Hashizume, T., Ishii, N., Aida, T. (2004) Self-assembled hexa-peri-hexabenzocoronene graphitic nanotube. *Science* **304**, 1481-1483.

[44] Yamamoto, Y., Fukushima, T., Suna, Y., Ishii, N., Saeki, A., Seki, S., Tagawa, S., Taniguchi, M., Kawai, T., Aida, T. (2006) Photoconductive coaxial nanotubes of

molecularly connected electron donor and acceptor layers. *Science* **314**, 1761-1764.

[45] Aida, T., Fukushima, T. (2007) Soft materials with graphitic nanostructures. *Phil. Trans. R. Soc. A* **365**, 1539-1552.

[46] Zhang, W., Jin, W., Fukushima, T., Saeki, A., Seki, S., Aida, T. (2011) Supramolecular linear heterojunction composed of graphite-like semiconducting nanotubular segments. *Science* **334**, 340-343.

[47] Ghadiri, M. R., Granja, J. R., Milligan, R. A., McRee, D. E., Khazanovich, N. (1993) Self-assembling organic nanotubes based on a cyclic peptide architecture. *Nature* **366**, 324-327.

[48] Clark, T. D., Buehler, L. K., Ghadiri, M. R. (1998) Self-assembling cyclic β-peptide nanotubes as artificial transmembrane ion channels. *J. Am. Chem. Soc.* **120**, 651-656.

[49] Hartgerink, J. D., Beniash, E., Stupp, S. I. (2001) Self-assembly and mineralization of peptide-amphiphile nanofibers. *Science* **294**, 1684-1688.

[50] Hartgerink, J. D., Beniash, E., Stupp, S. I. (2002) Peptide-amphiphile nanofibers: a versatile scaffold for the preparation of self-assembling materials. *Proc. Natl. Acad. Sci. USA* **99**, 5133-5138.

[51] Hamley, I. W. (2007) Peptide fibrillization. *Angew. Chem. Int. Ed.* 46, 8128-8147.

[52] Cherny, I., Gazit, E. (2008) Amyloids: not only pathological agents but also ordered nanomaterials. *Angew. Chem. Int. Ed.* **47**, 4062-4069.

[53] Meindl, J. D., Chen, Q., Davis, J. A. (2001) Limits on silicon nanoelectronics for terascale integration. *Science* **293**, 2044-2049.

[54] Tao, A., Kim, F., Hess, C., Goldberger, J., He, R., Sun, Y., Xia, Y., Yang, P.

(2003) Langmuir-Blodgett silver nanowire monolayers for molecular sensing using surface-enhanced raman spectroscopy. *Nano Lett.* **3**, 1229-1233.

[55] Cao, Y., Liu, W., Sun, J., Han, Y., Zhang, J., Liu, S., Sun, H., Guo, J. (2006) A technique for controlling the alignment of silver nanowire with an electric field. *Nanotechnology* **17**, 2378-2380.

[56] Guo. C., Kaufman, L. J. (2007) Flow and magnetic field induced collagen alignment. *Biomaterials* **28**, 1105-1114.

[57] Li, Y., Wu, Y. (2009) Coassembly of graphene oxide and nanowires for large-area nanowire alignment. *J. Am. Chem. Soc.* **131**, 5851-5857.

[58] Raychaudhuri, S., Dayeh, S. A., Wang, D., Yu, E. T. (2009) Precise semiconductor nanowire placement through dielectrophoresis. *Nano Lett.* **9**, 2260-2266.

[59] Mathai, P. P., Carmichael. P. T., Shapiro, B. A., Liddle, J. A. (2013) Simultaneous positioning and orientation of single nano-wires using flow control. *RSC Adv*. **3**, 2677-2682.

[60] Chiti, F., Dobson, C. M. (2006) Protein misfolding, functional amyloid and human disease. *Annu. Rev. Biochem.* **75**, 333-366.

[61] Jiménez J. L., Nettleton, E. J., Bouchard, M., Robinson, C. V., Dobson, C. M. (2002) The protofilament structure of insulin amyloid fibrils. *Proc. Natl. Acad. Sci. USA* **99**, 9196-9201.

[62] Makin, O. S., Serpell, L. C. (2005) Structures for amyloid fibrils. *FEBS J.* **272**, 5950-5961.

[63] Sipe, J. D. (1992) Amyloidosis. *Annu. Rev. Biochem.* **61**, 947-975.

[64] Gustavsson, Å., Engström, U., Westermark, P. (1991) Normal transthyretin and synthetic transthyretin fragments form amyloid-like fibrils *in vitro*. *Biochem.*

Biophys. Res. Commun. **175**, 1159-1164.

[65] Sunde, M., Serpell, L. C., Bartlam, M., Fraser, P. E., Pepys, M. B., Blake, C. C. F. (1997) Common core structure of amyloid fibrils by synchrotron X-ray diffraction. *J. Mol. Biol.* **273**, 729-739.

[66] Knowles, T. P. J., Smith, J. F., Craig, A., Dobson, C. M., Welland, M. E. (2006) Spatial persistence of angular correlations in amyloid fibrils. *Phys. Rev. Lett.* **96**, 238301.

[67] Smith, J. F., Knowles, T. P. J., Dobson, C. M., MacPhee, C. E., Welland, M. E. (2006) Characterization of the nanoscale properties of individual amyloid fibrils. *Proc. Natl. Acad. Sci. USA* **103**, 15806-15811.

[68] Sawaya, M. R., Sambashiva, S., Nelson, R., Ivanova, M. L., Sievers, S. A., Apostol, M. I., Thompson, M. J. Balbirnie, M., Wiltzius, J. J. W., McFarlane, H. T., Madsen, A. Ø., Riekel, C., Eisenberg, D. (2007) Atomic structures of amyloid cross-β spines reveal varied steric zippers. *Nature* **447**, 453-457.

[69] Knowles, T. P. Fitzpatrick, A. W., Meehan, S., Mott, H. R., Vendruscolo, M., Dobson, C. M., Welland, M. E. (2007) Role of intermolecular forces in defining material properties of protein nanofibrils. *Science* **318**, 1900-1903.

[70] Baldwin, A. J., Knowles, T. P. J., Tartaglia, G. G., Fitzpatrick, A. W., Devlin, G. L., Shammas, S. L., Waudby, C. A., Mossuto, M. F., Meehan, S., Gras, S. L., Christodoulou, J., Anthony-Cahill, S. J., Barker, P. D., Vendruscolo, M., Dobson, C. M. (2011) Metastability of native proteins and the phenomenon of amyloid formation. *J. Am. Chem. Soc.* **133**, 14160-14163.

[71] Lesné S., Koh, M. T., Kotilinek, L., Kayed, R., Glabe, C. G., Yang, A., Michela, G., Ashe, K. H. (2006) A specific amyloid-β protein assembly in the brain impairs

memory. *Nature* **440**, 352-357.

[72] Bernstein, S. L., Dupuis, N. F., Lazo, N. D., Wyttenbach, T., Condron, M. M., Bitan, G., Teplow, D. B., Shea, J.-E., Ruotolo, B. T., Robinson, C. V., Bowers, M. T. (2009) Amyloid-β protein oligomerization and the importance of tetramers and dodecamers in the aetiology of Alzheimer's disease. *Nature Chem.* **1**, 326-331.

[73] Kheterpal, I., Chen, M., Cook, K. D., Wetzel, R. (2006) Structural differences in Aβ amyloid protofibrils and fibrils mapped by hydrogen exchange − mass spectrometry with on-line proteolytic fragmentation. *J. Mol. Biol.* **361**, 785-795.

[74] Sakono, M., Zako, T. (2010) Amyloid oligomers: formation and toxicity of Aβ oligomers. *FEBS J.* **277**, 1348-1358.

[75] Caughey, B., Lansbury, P. T. (2003) Protofibrils, pores, fibrils, and neurodegeneration: separating the responsible protein aggregates from the innocent bystanders. *Annu. Rev. Neurosci.* **26**, 267-298.

[76] Harper, J. D., Lieber, C. M., Lansbury, P. T. Jr. (1997) Atomic force microscopic imaging of seeded fibril formation and fibril branching by the Alzheimer's disease amyloid-β protein. *Chem. Biol.* **4**, 951-959.

[77] Petkova, A. T., Leapma, R. D., Guo, Z., Yau, W.-M., Mattson, M. P., Tycko, R. (2005) Self-propagating, molecular-level polymorphism in Alzheimer's β amyloid fibrils. *Science* **307**, 262-265.

[78] Andersen, C. B., Yagi, H., Manno, M., Martorana, V., Ban, T., Christiansen, G., Otzen, D. E., Goto, Y., Rischel, C. (2009) Branching in amyloid fibril growth. *Biophys. J.* **96**, 1529-1536.

[79] Wu, J. W., Breydo, L., Isas, J. M., Lee, J., Kuznetsov, Y. G., Langen, R., Glabe, C. (2010) Fibrillar oligomers nucleate the oligomerization of monomeric amyloid β

but do not seed fibril formation. *J. Biol. Chem.* **285**, 6071-6079.

[80] Cohen, S. I., Vendruscolo, M., Dobson, C. M. Knowles, T. P. (2012) From macroscopic measurements to microscopic mechanisms of protein aggregation. *J. Mol. Biol.* **421**, 160-171.

[81] Kebarle, P., Hogg, A. M. (1965) Mass-spectrometric study of ions at atmospheric pressures. I. The ionic polymerization of ethylene. *J. Chem. Phys.* **42**, 668.

[82] Hogg, A. M., Kebarle, P. (1965) Mass-spectrometric study of ions at near-atmospheric pressure. II. Ammonium ions produced by the alpha radiolysis of ammonia and their solvation in the gas phase by ammonia and water molecules. *J. Chem. Phys.* **43**, 449.

[83] Wyttenbach, T., Kemper, P. R., Bowers, M. T. (2001) Design of a new electrospray ion mobility mass spectrometer. *Int. J. Mass Spectrom.* **212**, 13-23.

[84] Smith, D. P., Radford, S. E., Ashcroft, A. E. (2009) Elongated oligomers in β_2-microglobulin amyloid assembly revealed by ion mobility spectrometry-mass spectrometry. *Proc. Natl. Acad. Sci. USA* **107**, 6794-6798.

[85] Cole, H. L., Kalapothakis, J. M. D., Bennett, G., Barran, P. E., MacPhee, C. E. (2010) Characterizing early aggregates formed by an amyloidogenic peptide by mass spectrometry. *Angew. Chem. Int. Ed.* **49**, 9448-9451.

[86] Bleiholder, C., Dupuis, N. F., Wyttenbach, T., Bowers, M. T. (2011) Ion mobility-mass spectrometry reveals a conformational conversion from random assembly to β-sheet in amyloid fibril formation. *Nature Chem.* **3**, 172-177.

[87] Seo, Y., Andaya, A., Bleiholder, C., Leary, J. A. (2013) Differentiation of CC vs CXC chemokine dimers with GAG octasaccharide binding partners: an ion mobility mass spectrometry approach. *J. Am. Chem. Soc.* **135**, 4325-4332.

[88] Bleiholder, C., Dupuis, N. F., Bowers, M. T. (2013) Dimerization of chirally mutated encephalin neurotransmitters: implications for peptide and protein aggregation mechanisms. *J. Phys. Chem. B* **117**, 1770-1779.

[89] Wyttenbach, T., Bowers, M. T. (2011) Structural stability from solution to the gas phase: native solution structure of ubiquitin survives analysis in a solvent-free ion mobility-mass spectrometry environment. *J. Phys. Chem. B* **115**, 12266-12275.

[90] Bernstein, S. L., Wyttenbach, T., Baumketner, A., Shea, J.-E., Bitan, G., Teplow, D. B., Bowers, M. T. (2005) Amyloid β-protein: monomer structure and early aggregation states of Aβ42 and its Pro[19] alloform. *J. Am. Chem. Soc*. **127**, 2075-2084.

[91] Murray, M. M., Bernstein, S. L., Nyugen, V., Condron, M. M., Teplow, D. B., Bowers, M. T. (2009) Amyloid β protein: Aβ40 inhibits Aβ42 oligomerization. *J. Am. Chem. Soc*. **131**, 6316-6317.

[92] Dupuis, N. F., Wu, C., Shea, J.-E., Bowers, M. T. (2009) Human islet amyloid polypeptide monomers form ordered β-hairpins: a possible direct amyloidogenic precursor. *J. Am. Chem. Soc.* **131**, 18283-18292.

[93] Grabenauer, M., Wu, C., Soto, P., Shea, J.-E., Bowers, M. T. (2010) Oligomers of the prion protein fragment 106-126 are likely assembled from β-hairpins in solution, and methionine oxidation inhibits assembly without altering the peptide's monomeric conformation. *J. Am. Chem. Soc.* **132**, 532-539.

[94] Zheng, X., Gessel, M. M., Wisniewski, M. L., Viswanathan, K., Wright, D. L., Bahr, B. A., Bowers, M. T. (2012) Z-Phe-Ala-diazomethylketone (PADK) disrupts and remodels early oligomer states of the Alzheimer disease Aβ42 protein. *J. Biol. Chem.* **287**, 6084-6088.

[95] Yan, L., Zhang, S., Chen, P., Liu, H., Yin, H. and Li, H. (2012) Magnetotactic bacteria, magnetosomes and their application. *Microbiol. Res.* **167**, 507-519.

[96] Hildebrand, M. (2008) Diatoms, biomineralization, processes and genomics. *Chem. Rev.* **108**, 4855-4874.

[97] Weiss, I. (2012) Species-specific shells: Chitin synthases and cell mechanics in molluscs. *Z. Kristallogr.* **227**, 723-728.

[98] Sarikaya, M., Tamerler, C., Jen, A. K.-Y., Schulten, K., Baneyx, F. (2003) Molecular biomimetics: nanotechnology through biology. *Nature Mater.* **2**, 577-585.

[99] Sano, K., Sasaki, H., Shiba, K. (2005) Specificity and biomineralization activities of Ti-binding peptide-1 (TBP-1). *Langmuir* **21**, 3090–3095.

[100]   Coppage, R., Slocik, J. M., Briggs, B. D., Frenkel, A. I., Heinz, H., Naik, R. R., Knecht, M. R. (2011) Crystallographic recognition controls peptide binding for bio-based nanomaterials. *J. Am. Chem. Soc*. **133**, 12346-12349.

Chapter 2

[1]   Dehon, A. (2008) Nanowire-based progmmable architectures. *ACM J. Emer. Technol. Comput. Syst*. **1**, 109–162.

[2]   Lu, W., Lieber, C. M. (2007) Nanoelectronics from the bottom up. *Nature Mater.* **6**, 841–850.

[3]   Agarwal, R., Lieber, C. M. (2006) Semiconductor nanowires: optics and optoelectronics. *Appl. Phys. A: Mater. Sci. Proc.* **85**, 209–215.

[4]   Thelander, C., Agarwal, P., Brongersma, S., Eymery, J., Feiner, L. F., Forchel, A., Scheffler, M., Riess, W., Ohlsson, B. J., Gösele, U., Samuelson, L. (2006) Nanowire-based one-dimensional electronics. *Mater. Today* **9**, 28–35.

[5] Zhang, S. (2003) Fabrication of novel biomaterials through molecular self-Assembly. *Nat. Biotechnol.* **21**, 1171–1178.

[6] Börner, H. G., Schlaad, H. (2007) Bioinspired functional block copolymers. *Soft Matter* **3**, 394–408.

[7] Lim, Y.-b., Moon, K.-S., Lee, M. (2009) Recent advances in functional supramolecular nanostructures assembled from bioactive building blocks. *Chem. Soc. Rev.* **38**, 925–934.

[8] Aida, T., Fukushima, T. (2007) Soft materials with graphitic nanostructures. *Phil. Trans. R. Soc. A* **365**, 1539–1552.

[9] Hartgerink, J. D., Beniash, E., Stupp, S. I. (2001) Self-assembly and mineralization of peptide-amphiphile nanofibers. *Science* **294**, 1684-1688.

[10] Hamley, I. W. (2007) Peptide fibrillization. *Angew. Chem. Int. Ed.* **46**, 8128–8147.

[11] Cherny, I., Gazit, E. (2008) Amyloids: not only pathological agents but also ordered nanomaterials. *Angew. Chem. Int. Ed*. **47**, 4062–4069.

[12] Makin, O. S., Serpell, L. C. (2005) Structures for amyloid fibrils. *FEBS J.* **272**, 5950–5961.

[13] Sunde, M., Serpell, L. C., Bartlam, M., Fraser, P. E., Pepys, M. B., Blake, C. C. F. (1997) Common core structure of amyloid fibrils by synchrotron X-ray diffraction. *J. Mol. Biol.* **273**, 729–739.

[14] Knowles, T. P. J., Smith, J. F., Craig, A., Dobson, C. M., Welland, M. E. (2006) Spatial persistence of angular correlations in amyloid fibrils. *Phys. Rev. Lett.* **96**, 238301.

[15] Sawaya, M. R., Sambashivan, S., Nelson, R., Ivanova, M. I., Sievers, S. A., Apostol, M. I., Thompson, M. J., Balbirnie, M., Wiltzius, J. J. W., McFarlane, H. T.

Madsen, A. Ø., Riekel, C., Eisenberg, D. (2007) Atomic structures of amyloid cross-β spines reveal varied steric zippers. *Nature* **447**, 453–457.

[16] Knowles, T. P., Fitzpatrick, A. W., Meehan, S., Mott, H. R., Vendruscolo, M., Dobson, C. M., Welland, M. E. (2007) Role of Intermolecular Forces in Defining Material Properties of Protein Nanofibrils. *Science* **318**, 1900–1903.

[17] Sipe, J. D. (1992) Amyloidosis. *Annu. Rev. Biochem. 61*, 947–975.

[18] Chiti, F., Dobson, C. M. (2006) Protein misfolding, functional amyloid, and human disease. *Annu. Rev. Biochem.* **75**, 333–366.

[19] Fändrich, M. (2007) On the structural definition of amyloid fibrils and other polypeptide aggregates. *Cell. Mol. Life Sci.* **64**, 2066–2078.

[20] Takahashi, Y., Ueno, A., Mihara, H. (2001) Heterogeneous assembly of complementary peptide pairs into amyloid fibrils with α - β structural transition. *ChemBioChem* **1**, 75.

[21] Channon, K. J., Devlin, G. L., Magennis, S. W., Finlayson, C. E., Tickler, A. K., Silva, C., MacPhee, C. E. (2008) Modification of fluorophore photophysics through peptide-driven self-assembly. *J. Am. Chem. Soc.* **130**, 5487–5491.

[22] Asanomi, Y., Kobayashi, Y., Sakai, H., Masuda, T., Chen, X., Chuman, Y., Uosaki, K., Sakaguchi, K. (2010) Drastic effects on fibril formation of amyloid-β peptide by the addition of amino acid residue units to the termini. *Protein Pept. Lett.* **17**, 458–463.

[23] Sakai, H., Watanabe, K., Asanomi, Y., Kobayashi, Y., Chuman, Y., Shi, L., Masuda, T., Wyttenbach, T., Bowers, M. T., Uosaki, K., Sakaguchi, K. (2013) Formation of functionalized nanowires by control of self-assembly using multiple modified amyloid peptides. *Adv. Funct. Mater.* 2013 in press.

[24] Gustavsson, Å., Engström, U., Westermark, P. (1991) Normal transthyretin and synthetic transthyretin fragments form amyloid-like fibrils *in vitro*. *Biochem. Biophys. Res. Commun.* **175**, 1159–1164.

[25] Jaroniec, C. P., MacPhee, C. E., Astof, N. S., Dobson, C. M., Griffin, R. G. (2002) Molecular conformation of a peptide fragment of transthyretin in anamyloid fibril. *Proc. Natl. Acad. Sci. U.S.A.* **99**, 16748–16753.

[26] Caporini, M. A., Bajaj. V. S., Veshtort, M., Fitzpatrick, A., MacPhee, C. E., Vendruscolo, M., Dobson, C. M., Griffin, R. G. (2010) Accurate determination of interstrand distances and alignment in amyloid fibrils by magic angle spinning NMR. *J. Phys. Chem. B* **114**, 13555–13561.

[27] Jaroniec, C. P., MacPhee, C. E., Bajaj, V. S., McMahon, M. T., Dobson, C. M., Griffin, R. G. (2004) High-resolution molecular structure of a peptide in an amyloid fibril determined by magic angle spinning NMR spectroscopy. *Proc. Natl. Acad. Sci. U.S.A.* **101**, 711–716.

[28] Sano, K., Shiba, K. (2003) A hexapeptide motif that electrostatically binds to the surface of titanium. *J. Am. Chem. Soc.* **125**, 14234–14235.

[29] Sano, K., Sasaki, H., Shiba, K. (2005) Specificity and biomineralization activities of Ti-binding peptide-1 (TBP-1). *Langmuir* **21**, 3090–3095.

[30] Inoue, M., Hirata, A., Tainaka, K., Morii, T., Konno, T. (2008) Charge-paring mechanism of phosphorylation effect upon amyloid fibrillation of human tau core peptide. Biochemistry **47**, 11847-11857.

[31] MacPhee, C. E., Dobson, C. M. (2000) Formation of mixed fibrils demonstrates the generic nature and potential utility of amyloid nanostructures. *J. Am. Chem. Soc*. **122**, 12707–12713.

[32] Kodama, H., Matsumura, S., Yamashita, T., Mihara, H. (2004) Construction of a protein array on amyloid-like fibrils using co-assembly of designed peptides. *Chem. Commun.* 2876–2877.

[33] Liang, Y., Guo, P., Pingali, S. V., Pabit, S., Thiyagarajan, P., Berland, K. M., Lynn, D. G. (2008) Light harvesting antenna on an amyloid scaffold. *Chem. Commun.* 6522–6524.

[34] Scheibel, T., Parthasarathy, R., Sawicki, G., Lin, X.-M., Jaeger, H., Lindquist, S. L. (2003) Conducting nanowires built by controlled self-Assembly of amyloid fibers and selective metal deposition. *Proc. Natl. Acad. Sci. U.S.A.* **100**, 4527–4532.

[35] Carny, O., Shalev, D. E., Gazit, E. (2006) Fabrication of coaxial metal nanocables using a self-assembled peptide nanotubes scaffold. *Nano Lett.* **6**, 1594–1597.

[36] Kasotakis, E., Mossou, E., Adler-Abramovich, L., Mitchell, E. P., Forsyth, V. T., Gazit, E., Mitraki, A. (2009) Design of metal-binding sites onto self-assembled peptide fibrils. *Pept. Sci.* **92**, 164–172.

[37] Jayawarna, V., Ali, M., Jowitt, T. A., Miller, A. F., Saiani, A., Gough, J. E., Ulijn, R. V. (2006) Nanostructured hydrogels for three-dimensional cell culture through self-assembly of fluorenylmethoxycarbonyl-dipeptides. *Adv. Mater.* **18**, 611–614.

[38] Yang, Z., Gu, H., Fu, D., Gao, P., Lam, J. K., Xu, B. (2004) Enzymatic formation of supramolecular hydrogels. *Adv. Mater.* **16**, 1440–1444.

[39] Zhang, Y., Gu, H., Yang, Z., Xu B. (2003) Supramolecular hydrogels respond to ligand-receptor interaction. *J. Am. Chem. Soc.* **125**, 13680–1368.

[40] Channon, K. J., Devlin, G. L., MacPhee, C. E. (2009) Efficient energy transfer within self-assembling peptide fibers: a route to light-harvesting nanomaterials. *J. Am. Chem. Soc.* **131**, 12520–12521.

[41] Sarikaya, M., Tamerler, C., Jen, A. K.-Y., Schulten, K., Baneyx, F. (2003) Molecular biomimetics: nanotechnology through biology. *Nature Mater.* **2**, 577−585.

[42] Dickerson, M. B., Sandhage, K. H., Naik, R. R. (2008) Protein- and peptide-directed syntheses of inorganic materials. *Chem. Rev.* **108**, 4935−4978.

[43] Chen, C.-L., Rosi, N. L. (2010) Peptide-based methods for the preparation of nanostructured inorganic materials. *Angew. Chem. Int. Ed.* **49**, 2−21.

[44] Scheibel, T., Kowal, A. S., Bloom, J. D., Lindquist, S. L. (2001) Bidirectional amyloid fiber growth for a yeast prion determinant. *Curr. Biol.* **11**, 366−369.

[45] Inoue, Y., Kishimoto, A., Hirao, J., Yoshida, M., Taguchi, H. (2001) Strong growth polarity of yeast prion fiber revealed by single fiber imaging. *J. Biol. Chem.* **276**, 35227−35230.

Chaper 3

[1] Jiménez J. L., Nettleton, E. J., Bouchard, M., Robinson, C. V., Dobson, C. M. (2002) The protofilament structure of insulin amyloid fibrils. *Proc. Natl. Acad. Sci. USA* **99**, 9196-9201.

[2] Makin, O. S., Serpell, L. C. (2005) Structures for amyloid fibrils. *FEBS J.* **272**, 5950-5961.

[3] Sunde, M., Serpell, L. C., Bartlam, M., Fraser, P. E., Pepys, M. B., Blake, C. C. F. (1997) Common core structure of amyloid fibrils by synchrotron X-ray diffraction. *J. Mol. Biol.* **273**, 729-739.

[4] Chiti, F., Dobson, C. M. (2006) Protein misfolding, functional amyloid and human disease. *Annu. Rev. Biochem.* **75**, 333-366.

[5]   Sipe, J. D. (1992) Amyloidosis. *Annu. Rev. Biochem.* **61**, 947-975.

[6]   Hamley, I. W. (2007) Peptide fibrillization. *Angew. Chem. Int. Ed.* **46**, 8128-8147.

[7]   Knowles, T. P. J., Smith, J. F., Craig, A., Dobson, C. M., Welland, M. E. (2006) Spatial persistence of angular correlations in amyloid fibrils. *Phys. Rev. Lett.* **96**, 238301.

[8]   Smith, J. F., Knowles, T. P. J., Dobson, C. M., MacPhee, C. E., Welland, M. E. (2006) Characterization of the nanoscale properties of individual amyloid fibrils. *Proc. Natl. Acad. Sci. USA* **103**, 15806-15811.

[9]   Sawaya, M. R., Sambashiva, S., Nelson, R., Ivanova, M. L., Sievers, S. A., Apostol, M. I., Thompson, M. J. Balbirnie, M., Wiltzius, J. J. W., McFarlane, H. T., Madsen, A. Ø., Riekel, C., Eisenberg, D. (2007) Atomic structures of amyloid cross-β spines reveal varied steric zippers. *Nature* **447**, 453-457.

[10] Knowles, T. P. Fitzpatrick, A. W., Meehan, S., Mott, H. R., Vendruscolo, M., Dobson, C. M., Welland, M. E. (2007) Role of intermolecular forces in defining material properties of protein nanofibrils. *Science* **318**, 1900-1903.

[11] Baldwin, A. J., Knowles, T. P. J., Tartaglia, G. G., Fitzpatrick, A. W., Devlin, G. L., Shammas, S. L., Waudby, C. A., Mossuto, M. F., Meehan, S., Gras, S. L., Christodoulou, J., Anthony-Cahill, S. J., Barker, P. D., Vendruscolo, M., Dobson, C. M. (2011) Metastability of native proteins and the phenomenon of amyloid formation. *J. Am. Chem. Soc.* **133**, 14160-14163.

[12] Scheibel, T., Parthasarathy, R., Sawicki, G., Lin, X.-M., Jaeger, H., Lindquist, S. L. (2003) Conducting nanowires built by controlled self-Assembly of amyloid fibers and selective metal deposition. *Proc. Natl. Acad. Sci. U.S.A.* **100**, 4527–4532.

[13] Hamedi, M., Herland, A., Karlsson, R., and Inganas, O. (2008) Electrochemical

devices made from conducting nanowire networks self-assembled from amyloid fibrils and alkoxysulfonate PEDOT, *Nano Lett.* **8**, 1736-1740.

[14] Domigan, L. J., Healy, J. P., Meade, S. J., Blaikie, R. J., Gerrard, J. A. (2011) Controlling the dimensions of amyloid fibrils: toward homogeneous components for bionanotechnology. *Biopolymers* **97**, 123-133.

[15] Carny, O., Shalev, D. E., Gazit, E. (2006) Fabrication of coaxial metal nanocables using a self-assembled peptide nanotubes scaffold. *Nano Lett.* **6**, 1594–1597.

[16] Juárez, J., Cambón, A., Goy-López, S., Topete, A., Taboada, P., Mosquera, V. (2010) Obtention of metallic nanowires by protein biotemplating and their catalytic application. *Phys. Chem. Lett.* **1**, 2680-2687.

[17] Jayawarna, V., Ali, M., Jowitt, T. A., Miller, A. F., Saiani, A., Gough, J. E., Ulijn, R. V. (2006) Nanostructured hydrogels for three-dimensional cell culture through self-assembly of fluorenylmethoxycarbonyl-dipeptides. *Adv. Mater.* **18**, 611–614.

[18] Yang, Z., Gu, H., Fu, D., Gao, P., Lam, J. K., Xu, B. (2004) Enzymatic formation of supramolecular hydrogels. *Adv. Mater.* **16**, 1440–1444.

[19] Zhang, Y., Gu, H., Yang, Z., Xu B. (2003) Supramolecular hydrogels respond to ligand-receptor interaction. *J. Am. Chem. Soc.* **125**, 13680–1368.

[20] Asanomi, Y., Kobayashi, Y., Sakai, H., Masuda, T., Chen, X., Chuman, Y., Uosaki, K., Sakaguchi, K. (2010) Drastic effects on fibril formation of amyloid-β peptide by the addition of amino acid residue units to the termini. *Protein Pept. Lett.* **17**, 458–463.

[21] Sakai, H., Watanabe, K., Asanomi, Y., Kobayashi, Y., Chuman, Y., Shi, L., Masuda, T., Wyttenbach, T., Bowers, M. T., Uosaki, K., Sakaguchi, K. (2013)

Formation of functionalized nanowires by control of self-assembly using multiple modified amyloid peptides. *Adv. Funct. Mater.* 2013 in press.

[22] Baskakov, I. V., Legname, G., Baldwin, M. A., Prusiner, S. B., Cohen, F. E. (2002) Pathway complexity of prion protein assembly into amyloid. *J. Biol. Chem.* **277**, 21140-21148.

[23] Eichner, T., Radford, S. E. (2011) A diversity of assembly mechanism of a generic amyloid fold. Mol. Cell 43, 8-18.

[24] Harper, J. D., Wong, S. S., Lieber, C. M., Lansbury, P. T. Jr. (1997) Observation of metastable Aβ amyloid protofibrils by atomic force microscopy. *Chem. Biol.* **4**, 119-125.

[25] Harper, J. D., Lieber, C. M., Lansbury, P. T. Jr. (1997) Atomic force microscopic imaging of seeded fibril formation and fibril branching by the Alzheimer's disease amyloid-β protein. *Chem. Biol.* **4**, 951-959.

[26] Goldsbury, C., Kistler J., Aebi, U., Arvinte, T., Cooper, G. J. (1999) Watching amyloid fibrils grow by time-lapse atomic force microscopy. *J. Mol. Biol.* **285**, 33-39.

[27] Jansen, R., Dzwolak, W., Winter, R. (2005) Amyloidogenic self-assembly of insulin aggregates probed by high resolution atomic force microscopy. *Biophys. J.* **88**, 1344-1353.

[28] Adamcik, J., Castelletto, V., Bolisetty, S., Hamley, I. W., Mezzenga, R. (2011) Direct observation of time-resolved polymorphic states in the self-assembly of end-capped heptapeptides. *Angew. Chem. Int. Ed.* **50**, 5495-5498.

[29] Zhang, S., Andreasen, M., Nielsen, J. T., Liu, L., Nielsen, E. H., Song, J., Ji, G., Sun, F., Skrydstrup, T., Besenbacher, F., Nielsen, N. C., Otzen, D. E., Dong, M.

(2013) Coexistence of ribbon and helical fibrils originating from $hIAPP_{20-29}$ revealed by quantitative nanomechanical atomic force microscopy. *Proc. Natl. Acad. Sci. USA* **110**, 2798-2803.

[30] Bernstein, S. L., Dupuis, N. F., Lazo, N. D., Wyttenbach, T., Condron, M. M., Bitan, G., Teplow, D. B., Shea, J.-E., Ruotolo, B. T., Robinson, C. V., Bowers, M. T. (2009) Amyloid-β protein oligomerization and the importance of tetramers and dodecamers in the aetiology of Alzheimer's disease. *Nature Chem.* **1**, 326-331.

[31] Murray, M. M., Bernstein, S. L., Nyugen, V., Condron, M. M., Teplow, D. B., Bowers, M. T. (2009) Amyloid β protein: Aβ40 inhibits Aβ42 oligomerization. *J. Am. Chem. Soc*. **131**, 6316-6317.

[32] Bleiholder, C., Dupuis, N. F., Wyttenbach, T., Bowers, M. T. (2011) Ion mobility-mass spectrometry reveals a conformational conversion from random assembly to β-sheet in amyloid fibril formation. *Nature Chem*. **3**, 172-177.

[33] Kuperstein, I., Broersen, K., Benilova, I., Rozenski, J., Jonckheere, W., Debulpaep, M., Vandersteen, A., Segers-Nolten, I., Werf, K. V. D., Subramaniam, V., Braeken, D., Callewaert, G., Bartic, C., D'Hooge, R., Martins, I. C., Rousseau, F., Schymkowitz, J., Strooper, B. D. (2010) Neurotoxicity of Alzheimer's disease Aβ peptides is induced by small changes in the $Aβ_{42}$ to $Aβ_{40}$ ratio. *EMBO J.* **29**, 3408-3420.

[34] Barghorn, S., Nimmrich, V., Striebinger, A., Krantz, C., Keller, P., Janson, B., Bahr, M., Schmidt, M., Bitner, R. S., Harlan, J., Barlow, E., Ebert, U., Hillen, H. (2005) Globular amyloid $β-peptide_{1-42}$ oligomer – a homogeneous and stable neuropathological protein in Alzheimer's disease. *J. Neurochem.* **95**, 834-847.

[35] Wyttenbach, T., Kemper P. R., Bowers, M. T. (2001) Design of a new electrospray ion mobility mass spectrometer. *Int. J. Mass Spectrom.* **212**, 13-23.

[36] Brandts, J. F., Kaplan, L. J. (1973) Derivative spectroscopy applied to tyrosyl chromophores. Ribonuclease, lima bean inhibitors, insulin and pancreatic trypsin inhibitor. *Biochemistry* **12**, 2011-2024.

[37] Mason, E. A., McDaniel, E. W. (1988) *Transport properties of ions in gases*, Wiley: New York.

[38] Gidden, J., Baker, E. S., Ferzoco, A., Bowers, M. T. (2005) Structural motifs of DNA complexes in the gas phase *Int. J. Mass Spectrom.* **240**, 183-193.

[39] Pringle, S. D., Giles, K., Wildgoose, J. L., Williams, J. P., Slade, S. E., Thalassinos, K., Bateman, R. H., Bowers, M. T., Scrivens, J. H. (2007) An Investigation of the Mobility Separation of Some Peptide and Protein Ions Using a New Hybrid Quadrupole/Travelling Wave IMS/oa-ToF Instrument *Int. J. Mass Spectrom.* **2007**, *261*, 1–12.

[40] Cohen, S. I., Vendruscolo, M., Dobson, C. M. Knowles, T. P. (2012) From macroscopic measurements to microscopic mechanisms of protein aggregation. *J. Mol. Biol.* **421**, 160-171.

[41] Loksztejn, A., Dzwolak, W. (2010) Vortex-induced formation of insulin amyloid superstructures probed by time-lapse atomic force microscopy and circular dichroism spectroscopy. *J. Mol. Biol.* **395**, 643-655.

[42] Jarvis, J. A., Craik, D. J., Wilce M. C. J. (1993) X-ray diffraction studies of fibrils formed from peptide fragments of transthyretin. *Biochem. Biophys. Res. Commun.* **192**, 991-998.

[43] Deng, W., Cao, A., Lai, L. (2007) Detecting the inter-peptide arrangement and

maturation process of transthyretin (105-115) amyloid fibril using a FRET pair with short Förster distance. *Biochem. Biophys. Res. Commun.* **362**, 689-694.

[44] Channon, K. J., Devlin, G. L., Magennis, S. W., Finlayson, C. E., Tickler, A. K., Silva, C., MacPhee, C. E. (2008) Modification of fluorophore photophysics through peptide-driven self-assembly. *J. Am. Chem. Soc.* **130**, 5487-5491.

[45] Gras, S. L., Tickler, A. K., Squires, A. M., Devlin, G. L., Horton, M. A., Dobson, C. M., MacPhee, C. E. (2008) Functionalised amyloid fibrils for roles in cell adhesion. *Biomaterials* **29**, 1553-1562.

[46] Caporini, M. A., Bajaj, V. S., Veshtort, M., Fitzpatrick, A., MacPhee, C. E., Vendruscolo, M., Dobson, C. M., Griffin, R. G. (2010) Accurate determination of interstrand distances and alignment in amyloid fibrils by magic angle spinning NMR. *J Phys. Chem. B* **114**, 13555-13561.

[47] Bongiovanni, M. N., Scanlon, D. B., Gras, S. L. (2011) Functional fibrils derived from the peptide TTR1-cycloRGDfK that target cell adhesion and spreading. *Biomaterials* **32**, 6099-6110.

[48] Bongiovanni, M. N., Puri D., Goldie, K. N., Gras, S. L. (2012) Noncore Residues Influence the Kinetics of Functional TTR$_{105-115}$-based amyloid fibril assembly. *J. Mol. Biol.* **421**, 256-269.

[49] Rodríguez-Pérez, J. C., Hamley, I. W., Gras, S. L., Squires, A. M. (2012) Local orientation disorder in peptide fibrils probed by a combination of residue-specific 13C-18O labelling, polarised infrared spectroscopy and molecular combing. *Chem. Commun.* **48**, 11835-11837.

[50] Bongiovanni, M. N., Caruso, F., Gras, S. L. (2013) Lysine functionalised amyloid fibrils: the design and assembly of a TTR1-based peptide. *Soft Matter* **9**,

3315-3330.

[51] Takahashi, Y., Ueno, A., Mihara, H. (2001) Heterogeneous assembly of complementary peptide pairs into amyloid fibrils with α - β structural transition. *ChemBioChem* **1**, 75.

[52] Inoue, M., Hirata, A., Tainaka, K., Morii, T., Konno, T. (2008) Charge-paring mechanism of phosphorylation effect upon amyloid fibrillation of human tau core peptide. Biochemistry **47**, 11847-11857.

[53] Inoue, M., Konno, T., Tainaka, K., Nakata, E., Yoshida, H., Morii, T. (2012) Positional effects of phosphorylation on the stability and morphology of tau-related amyloid fibrils. *Biochemistry* **51**, 396-1406.

[54] Meot-Ner, M. (2005) The ionic hydrogen bond. *Chem. Rev.* **105**, 213-284.

[55] Ban, T., Hamada, D., Hsegawa, K., Naiki, H., Goto, Y. (2003) Direct observation of amyloid fibril growth monitored by thioflavin T fluorescence. *J. Biol. Chem.* **278**, 16462-16465.

[56] Andersen, C. B., Yagi, H., Manno, M., Martorana, V., Ban, T., Christiansen, G., Otzen, D. E., Goto, Y., Rischel, C. (2009) Branching in amyloid fibril growth. *Biophys. J.* **96**, 1529-1536.

[57] Wu, J. W., Breydo, L., Isas, J. M., Lee, J., Kuznetsov, Y. G., Langen, R., Glabe, C. (2010) Fibrillar oligomers nucleate the oligomerization of monomeric amyloid β but do not seed fibril formation. *J. Biol. Chem.* **285**, 6071-6079.

[58] Jeong, J. S., Ansaloni, A., Mezzenga, R., Lashuel, H. A., Dietler, G. (2013) Novel mechanistic insight into the molecular basis of amhyloid polymorphism and secondary nucleation during amyloid formation. *J. Mol. Biol.* **425**, 1765-1781.

[59] Laganowsky, A., Liu, C., Sawaya, M. R., Whitelegge, J. P., Park, J., Zhao, M., Pensalfini, A., Soriaga, A. B., Landau, M., Teng, P. K., Cascio, D., Glabe, C., Eisenberg, D. (2012) Atomic view of a toxic amyloid small oligomer. *Science* **335**, 1228-1231.

[60] Liu, C., Zhao, M., Jiang, L., Cheng, P.-N., Park, J., Sawaya, M. R., Pensalfini, A., Gou, D., Berk, A. J., Glabe, C. G., Nowick, J., Eisenberg, D. (2012) Out-of-register β-sheets suggest a pathway to toxic amyloid aggregates. *Proc. Natl. Acad. Sci. USA* **109**, 20913-20918.

[61] Serio, T. R., Cashikar A. G., Kowal, A. S., Sawicki, G. J., Moslehi, J. J., Serpell, L., Arnsdorf, M. F. and Lindquist, S. L. (2000) Nucleated conformational conversion and the replication of conformational information by a prion determinant. *Science* **289**, 1317-1321.

[62] Rochet, J.-C., Lansbury, P. T. Jr. (2000) Amyloid fibrillogenesis: themes and variations. *Curr. Opin. Struct. Biol.* **10**, 60-68.

[63] Kheterpal, I., Chen, M., Cook, K. D., Wetzel, R. (2006) Structural differences in Aβ amyloid protofibrils and fibrils mapped by hydrogen exchange − mass spectrometry with on-line proteolytic fragmentation. *J. Mol. Biol.* **361**, 785-795.

[64] Scheidt, H. A., Morgado, I., Rothemund, S., Huster, D., Fändrich, M. (2011) *Angew. Chem. Int. Ed.* **50**, 2837-2840.

[65] Knowles, T. P. J., Waudby, C. A., Devlin, G. L., Cohen, S. I. A., Aguzzi, A., Vendruscolo, M., Terentjev, E. M., Welland, M. E., Dobson, C. M. (2009) An analytical solution to the kinetics of breakable filament assembly. *Science* **326**, 1553-1537.

[66] Kusumoto, Y., Lomakin, A., Teplow, D. B., Benedek, G. B. (1998) Temperature

dependence of amyloid β-protein fibrillization. *Proc. Natl. Acad. Sci. USA* **95**, 12277-12282.

[67] Caughey, B., Lansbury, P. T. (2003) Protofibrils, pores, fibrils, and neurodegeneration: separating the responsible protein aggregates from the innocent bystanders. *Annu. Rev. Neurosci.* **26**, 267-298.

[68] Planchard, M. S., Samel, M. A., Kumar, A., Rangachari, V. (2012) The natural product betulinic acid rapidly promotes amyloid-β fibril formation at the expense of soluble oligomers. *ACS Chem. Neurosci.* **3**, 900-908.

[69] D'Amico, M., Carlo, M. G. D., Groenning, M., Militello, V., Vetri, V., Leone, M. (2012) Thioflavin T promotes Aβ(10-40) amyloid fibrils formation. *Phys. Chem. Lett.* **3**, 1596-1601.

Chapter 4

[1] Cui, Y., Wei, O., Park, H., Lieber, C. M. (2001) Nanowire nanosensors for highly sensitive and selective detection of biological and chemical species. *Science* **293**, 1289-1292.

[2] Gudiksen, M. S., Lauhon, L. J., Wang, J., Smith, D. C., Lieber, C. M. (2002) Growth of nanowire superlattice structures for nanoscale photonics and electronics. *Nature* **415**, 617-620.

[3] Huang, Y., Duan, X., Lieber, C. M. (2005) Nanowires for integrated multicolor nanophotonics. *Small* **1**, 142-147.

[4] Park, H.-G., Barrelet, C. J., Wu, Y., Tian, B., Qian, F., Lieber, C. M. (2008) A wavelength-selective photonic-crystal waveguide coupled to a nanowire light source. *Nature Photon.* **2**, 622-626.

[5] Hayden, O., Agarwal, R., Lieber, C. M. (2006) Nanoscale avalanche photodiodes for highly sensitive and spatially resolved photon detection. *Nature Mater.* **5**, 352-356.

[6] Novotny, C. J., Yu, E. T., Yu, P. K. L. (2007) InP nanowire/polymer hybrid photodiode. *Nano Lett.* **8**, 775-779.

[7] Duan, X., Huang, Y., Cui, Y., Wang, J., Lieber, C. M. (2000) Indium phosphide nanowire as building blocks for nanoscale electronic and optoelectronic devices. *Nature* **409**, 66-69.

[8] Cui, Y., Lieber, C. M. (2001) Functional nanoscale electronic devices assembled using silicon nanowire building blocks. *Science* **291**, 851-853.

[9] Melosh, N. A., Boukai, A., Diana, F., Gerardot, B., Badolato, A., Petroff, P. M., Heath, J. R. (2003) Ultrahigh-density nanowire lattices and circuits. *Science* **300**, 112-115.

[10] Meindl, J. D., Chen, Q., Davis, J. A. (2001) Limits on silicon nanoelectronics for terascale integration. *Science* **293**, 2044-2049.

[11] Zhang, S. (2003) Fabrication of novel biomaterials through molecular self-assembly. *Nat. Biotechnol.* **21**, 1171-1178.

[12] Lim, Y.-b., Moon, K.-S., Lee, M. (2009) Recent advances in functional supramolecular nanostructures assembled from bioactive building blocks. *Chem. Soc. Rev.* **38**, 925-934.

[13] Sakai, H., Watanabe, K., Asanomi, Y., Kobayashi, Y., Chuman, Y., Shi, L., Masuda, T., Wyttenbach, T., Bowers, M. T., Uosaki, K., Sakaguchi, K. (2013) Formation of functionalized nanowires by control of self-assembly using multiple modified amyloid peptides. *Adv. Funct. Mater.* 2013 in press.

[14] Lieber, C. M., Wang, Z. L. (2007) Functional nanowires. *MRS Bulletin* **32**, 99-108.

[15] Patolsky, F., Timko, B. P., Zheng, G., Lieber, C. M. (2007) Nanowire-based nanoelectronic devices in the life sciences. MRS Bulletin 32, 142-149.

[16] Tao, A., Kim, F., Hess, C., Goldberger, J., He, R., Sun, Y., Xia, Y., Yang, P. (2003) Langmuir-Blodgett silver nanowire monolayers for molecular sensing using surface-enhanced raman spectroscopy. *Nano Lett.* **3**, 1229-1233.

[17] Whang, D., Jin, S., Wu, Y., Lieber, C. M. (2003) Large-scale hierarchical organization of nanowire arrays for integrated nanosystems. Nano Lett. 3, 1255-1259.

[18] Acharya, S., Panda, A. B., Belman, N., Efrima, S., Golan, Y. (2006) A semiconductor-nanowire assembly of ultrahigh junction density by the Langmuir-Blodgett technique. Adv. Mater. 18, 210-213.

[19] Guo. C., Kaufman, L. J. (2007) Flow and magnetic field induced collagen alignment. *Biomaterials* **28**, 1105-1114.

[20] Raychaudhuri, S., Dayeh, S. A., Wang, D., Yu, E. T. (2009) Precise semiconductor nanowire placement through dielectrophoresis. *Nano Lett.* **9**, 2260-2266.

[21] Lanfer, B., Freudenberg, U., Zimmermann, R., Stamov, D., Körber, V., Werner, C. (2008) Aligned fibrillar collagen matrices obtained by shear flow deposition. *Biomaterials* **29**, 3888-3895.

[22] Mathai, P. P., Carmichael. P. T., Shapiro, B. A., Liddle, J. A. (2013) Simultaneous positioning and orientation of single nano-wires using flow control. *RSC Adv*. **3**, 2677-2682.

[23] Li, Q., Koo, S.-M., Richter, C. A., Edelstein, M. D., Bonevich, J. E., Kopanski, J. J., Suehle, J. S., Vogel, E. M. (2007) Precise alignment of single nanowires and

fabrication of nanoelectromechanical switch and other test structures. *IEEE Trans, Nanotechnol.* **6**, 256-262.

[24] Guthrie, J. P. (1978) Hydrolysis of esters of oxy acids: pK_a values for strong acids; Brønsted relationship for attack of water at methyl; free energies of hydrolysis of esters of oxy acids; and a linear relationship between free energy of hydrolysis and pK_a holding over a range of 20 pK units. *Can. J. Chem.* **56**, 2342.

[25] Suzuki, K., Hosokawa, K., Maeda, M. (2009) Controlling the number and positions of oligonucleotides on gold nanoparticle surface. *J. Am. Chem. Soc.* **131**, 7518-7519.

[26] Mesquida, P., Ammann, D. L., MacPhee, C. E., McKendry, R. A. (2005) Microarrays of peptide fibrils created by electrostatically controlled deposition. *Adv. Mater.* **17**, 893-897.

[27] Zhong, Z., Wang, D., Cui, Y., Bockrath, M. W., Lieber, C. M. (2003) Nanowire crossbar arrays as address decoder for integrated nanosystems. *Science* **302**, 1377-1379.

Acknowledgments

I would never have been able to finish my doctoral thesis without the help and support of the kind people around me, only some of whom have been acknowledged here.

Foremost, I would like to express my sincere gratitude to my supervisor, Prof. Kazuyasu Sakaguchi, for providing me excellent research experiences and guidance. He has always taught me deep understanding that has made me become a better future scientist.

I would like to acknowledge Prof. Kohei Uosaki with much appreciation for his tremendous support to my research interest. I would also like to gratefully thank Prof. Michael T. Bowers who let me have great opportunities to perform ion-mobility studies in his laboratory at UC Santa Barbara.

I am grateful to the rest of my thesis committee: Prof. Yota Murakami, Prof. Koichiro Ishimori, Prof. Seiichi Taguchi, and Dr. Toshiaki Imagawa. Their encouragement and insightful comments were highly appreciated.

I really appreciate the assistance of my colleagues Dr. Yuya Asanomi, Yumiko Kobayashi, Ken Watanabe, and Katsuya Takayama who worked on the same research project. The time I shared with them made my research life enjoyable literally and scientifically. I would like to thank Dr. Yoshiro Chuman for his kind help and

encouragement for my thesis even at midnight. I would also like to appreciate to Dr. Takuya Masuda for his dedicated support to my research and a plethora of advice. I would like to thank Dr. Thomas Wyttenbach and Dr. Christian Bleiholder. They provided me with extensive living and experimental support during my stay in the US. Many thanks to Jose Isagani Janairo and Lussier-Price Mathieu for their linguistic help and giving me a lot of fun.

Finally, I would like to thank my mother. She has been raising me by herself with plenty of love since I was a very small child. She has allowed me, for a long time, to study in Hokkaido University until I become a scientist.